

Determination of adsorption and activation volumes and apparent transfer coefficients by pressure and potential modulation

Dissertation

zur

Erlangung des Doktorgrades (Dr. rer.nat)

der

Mathematisch-Naturwissenschaftlichen Fakultät

der

Rheinischen Friedrich-Wilhelms-Universität Bonn

vorgelegt von

Hanchun Wang

aus

Lichuan, Hubei Province, China

Bonn, 2009

Angefertigt mit Genehmigung der Mathematisch-Naturwissenschaftlichen Fakultät der
Rheinischen Friedrich-Wilhelms-Universität Bonn

Promotionskommission

Erster Gutachter: Prof. Dr. Helmut Baltruschat

Zweiter Gutachter: Prof. Dr. Klaus Wandelt

Fachnaher Gutachter: Prof. Dr. Siegfried Waldvogel

Fachfremder Gutachter: Prof. Dr. Karl Maier

Tag der mündlichen Prüfung:

16.03.2010

Erscheinungsjahr: 2010

Ich versichere, dass ich diese Arbeit selbständig verfasst und keine anderen als die angegebenen Quellen
und Hilfsmittel benutzt sowie die Zitate kenntlich gemacht habe.

Bonn, 23.12.2009

Hanchun Wang

For my parents, my wife and my son
献给我的父母、妻子和儿子！

Contents

1	Introduction.....	1
1.1	Fundamentals.....	1
1.1.1	Potential sweep method and potential step method.....	1
1.1.2	Electrochemical impedance spectroscopy.....	3
1.1.3	Method of ac voltammetry.....	5
1.1.4	Single crystals.....	6
1.1.5	Charge transfer coefficient and Tafel plot.....	11
1.2	Introduction to fuel cells and CO oxidation.....	13
1.2.1	Introduction to Fuel cell.....	13
1.2.2	CO oxidation mechanism.....	19
1.2.3	The determination of the Tafel slope or apparent transfer coefficient for CO oxidation on Pt and the contradiction in literature.....	20
1.3	Volume measurement and surface volume excess.....	23
1.3.1	Basic volume measurement.....	23
1.3.2	Partial molar volume in solution, especially H ⁺	24
1.3.3	Reaction volume.....	27
1.3.4	Activation volume.....	27
1.3.5	Surface volume excess and adsorption volume.....	28
2	Materials, instruments and methods.....	33
2.1	Chemicals.....	33
2.2	Glassware.....	33
2.3	Electrochemical instrumentation.....	34
2.3.1	Potentiostat and Lock-in Amplifier.....	34
2.3.2	The cells.....	34
2.3.3	The setup for pressure modulation.....	35
2.4	Experimental procedures.....	36
2.4.1	Preparation of the single crystal electrodes.....	36
2.4.2	Preparation of reference electrodes: RHE and Ag/AgCl.....	37
2.4.3	CO oxidation experiment.....	38
2.4.4	Pressure modulation experiment.....	38
2.4.5	Calibration of the force sensor Pressure modulation experiment.....	38
3	Determination of the apparent charge transfer coefficient for CO oxidation on various Pt surfaces.....	41
3.1	Principles and calculations.....	41
3.1.1	Principles.....	41
3.1.2	Correction for slow ion adsorption.....	41
3.2	Polycrystalline platinum.....	46
3.2.1	Cyclic voltammetry (CV) and electrochemical impedance spectroscopy (EIS).....	46
3.2.2	Potential sweep measurement.....	48
3.2.3	Potential step experiments.....	51
3.3	Pt(111).....	59
3.3.1	CV and EIS.....	59

3.3.2	Potential sweep measurement.....	61
3.3.3	Potential step measurement.....	61
3.4	Pt(665)	65
3.4.1	CV and EIS.....	65
3.4.2	Potential sweep measurement.....	67
3.5	Pt(332)	71
3.5.1	CV	71
3.5.2	Potential sweep experiment.....	71
3.5.3	Potential step measurements	73
3.6	General discussion for the mechanism of CO oxidation on Pt	76
3.6.1	General review of our results	76
3.6.2	About the contradiction in Tafel slope in literature.....	78
3.6.3	About the chemical step as the rds and the detection of COOHad in literature.....	80
3.6.4	About the origin of the prepeak.....	81
3.6.5	About the potential dependence of Tafel slope for CO oxidation in alkaline solution...	82
3.7	The stepped Pt surfaces modified by Ru and Sn.....	83
3.7.1	α' for CO oxidation on Ru step decorated Pt(665)	83
3.7.2	α' for CO oxidation on Sn step decorated Pt(332)	85
3.8	Summary.....	88
4	The surface volume excess of hydrogen adsorption on polycrystalline Pt and the effect of cations	91
4.1	Volume change for $\text{Fe}(\text{CN})_6^{3-} + e^- \leftrightarrow \text{Fe}(\text{CN})_6^{4-}$: a test experiment.....	92
4.1.1	Principles for measuring reaction volume by the method of Pressure modulation.....	92
4.1.2	Results and discussion.....	93
4.2	Principles and calculations for surface volume excess measurements.....	94
4.2.1	Principles.....	94
4.2.2	Corrections for the pressure dependence of the reference electrode.....	97
4.3	Results and discussion.....	100
4.3.1	Cyclic voltammetry.....	100
4.3.2	The measurement of ac voltammetry.....	103
4.3.3	The ac current arising from pressure modulation	104
4.3.4	Molar volume of adsorbed hydrogen on polycrystalline Pt	105
4.3.5	The effect of cations on hydrogen adsorption	107
4.4	Summary.....	110
5	Activation volume for CO oxidation on polycrystalline Platinum	113
5.1	Principles.....	113
5.2	Results and discussion.....	114
5.2.1	Activation volume for CO oxidation on Pt(poly)	114
5.2.2	Explanation for the activation volume.....	117
5.3	Summary.....	119
	Conclusions.....	120

Notations

i	current	Q	CO oxidation charge
\bar{i}	current phasor	C	Capacitance
i_{dc}	dc current	q	surface charge
i_{ac}	ac current	f	Frequency
i_{ac-re}	real part of the ac current	V	Volume
i_{ct}	charge transfer current	ΔV	volume change
i_{ad}	adsorption current	ΔV^\ddagger	activation Volume
i_{max}	maximum current or peak current	ΔV_{ad}	adsorption volume
j	current density	v_i	partial molar volume of species "i"
\dot{j}	$\sqrt{-1}$	v	potential sweep rate
α	transfer coefficient	v_m	mean molar volume
α'	apparent transfer coefficient	a_{ox}	chemical activities of oxidized species
k	rate constant	a_{red}	chemical activities of reduced species
k'	apparent rate constant	t	Time
K	equilibrium constant	t_{max}	time elapsed at current maximum
θ_i	fractional coverage of species i	c	Concentration
Γ_i	the amount of adsorbed species i	r	Radius
Γ_s	surface excess of entropy	d	Diameter
Γ_V	surface excess of volume	η	Overpotential
φ	Phase angle between ac current and voltage	G	Gibbs energy
b	Tafel slope, $b = 2.303RT/cnF$	ΔG^\ddagger	activation free energy
n	The number of electrons transferred Mole number	R	gas constant, $8.314 \text{ J}\cdot\text{K}^{-1}\cdot\text{mol}^{-1}$ resistance
F	Faraday constant, $96485 \text{ C}\cdot\text{mol}^{-1}$	H	Enthalpy
E	potential	S	Entropy
U_{ac}	ac voltage	x_B	mole fraction of species B
\vec{u}_{ac}	ac voltage in phasor notation	γ	interfacial tension of electrode
T	absolute temperature	μ	chemical potential
Z	impedance	p	Pressure
Z_{re}	the real part of the impedance	CPE	constant phase element
Z_{im}	the imaginary part of the impedance	ω	angular velocity

Abbreviations

CV	Cyclic voltammetry	FCs	Fuel cells
LSV	Linear sweep voltammetry	AFC	alkaline fuel cell
fcc	face centered cubic	PEMFC	polymer electrolyte membrane fuel cell, Proton exchange membrane fuel cell
bcc	body centered cubic	PAFC	phosphoric acid fuel cell
hcp	hexagonal close packed	MCFC	molten carbonate fuel cell
STM	scanning tunneling microscope	SOFC	solid oxide fuel cell
EIS	electrochemical impedance spectroscopy	ORR	Oxygen reduction reaction
RE	Reference electrode	L-H	Langmuir-Hinshelwood
WE	Working electrode	E-R	Eley-Rideal
CE	Counter electrode	PM	Pressure modulation

Abstract

In this thesis the following investigations were carried out on Pt or Pt based electrodes: the determination of the apparent transfer coefficient (α') for CO oxidation using an ac method, the determination of the molar adsorption volume of hydrogen and the effect of cations thereupon combining the methods of pressure modulation and ac voltammetry, and the determination of the activation volume for CO oxidation by pressure modulation.

The ac method for the determination of apparent transfer coefficients or Tafel slopes has been developed in this thesis; it's used here for CO oxidation on noble metals. This method involves a sinusoidal modulation of the potential and the simultaneous recording of the ac and the dc current. It allows to record α' quasi continuously as a function of potential or time (i.e., in cyclic voltammetry or in potentiostatic experiments), with the reaction rate varying with time, much more accurately than the traditional method that can only measure the transfer coefficient or Tafel slope over a large range of potentials. Since the mechanism for CO oxidation on noble metals is in the focus of electrocatalytic research in recent years, I applied this ac method to the determination of the apparent transfer coefficient for the oxidation of pre-adsorbed CO at Pt electrodes in sulfuric acid. Electrodes of polycrystalline platinum and single crystalline Pt(111), Pt(665) and Pt(332) were investigated using either potential sweeps or potential steps while superimposing an ac voltage. The apparent transfer coefficients were measured and the transition of values from 1.5 to 0.5 with potential increase, which had been predicted in a simulation by Koper et al., was clearly observed experimentally for the first time. Some assumptions on the mechanism of CO oxidation on Pt by other authors could thus be rejected. The measurement of the apparent transfer coefficient by the ac method is also extended to CO oxidation on Ru and Sn decorated Pt and contributes to the understanding of those processes, as well. The ac method for the determination of the apparent transfer coefficient, which I used here, will be of great help also in many other cases, especially under steady state conditions, where the major limitations of the method are avoided.

The volume of adsorbed hydrogen on Pt and the cation effects on it were investigated combining pressure modulation method and ac voltammetry. The pressure modulation method has been developed in our group by Loewe et al for the measurement of reaction and adsorption volumes and was further improved in this work. Instead of the traditional way of using high pressure in a complicated device, modulation by less than 1 bar is sufficient for the measurement of pressure dependences. The adsorption of hydrogen on noble metal surfaces is important for many other reactions, the partial molar volume of adsorbed hydrogen is of fundamental interest. In this thesis, the molar adsorption volume of hydrogen is measured to be $3.3 \pm 1 \text{ cm}^3 \cdot \text{mol}^{-1}$ on polycrystalline Pt in sulphuric acid. Cation were observed to largely influence the molar volume of adsorbed hydrogen in Li^+ , K^+ and Cs^+ containing electrolytes. A preliminary explanation for these cation effects is proposed. This work will be of importance in understanding the surface structure of the double layer in the hydrogen adsorption region and the involvement of cations in the interface.

The pressure modulation method has been extended in this work to the determination of the activation

volume for CO oxidation. Activation volume is one of the few parameters that can be measured for the activated complex. Instead of the traditional way of using complicated high pressure method, in this thesis I introduced the pressure modulation method to the measurement of the activation volume of the oxidation of adsorbed CO on polycrystalline Pt. Reasonable values are obtained at low sweep rates and low step potentials with an average of $-18.2 \text{ cm}^3 \cdot \text{mol}^{-1}$. A preliminary structure for this activated complex is put forward. The applicability of pressure modulation method for measuring the activation volume of electrochemical processes is thus demonstrated.

1 Introduction

1.1 Fundamentals

1.1.1 Potential sweep method and potential step method

Potential sweep method

The potential sweep method is one of the most basic and popular techniques applied in the investigation of electrochemistry. Normally the potential is varied linearly with time, which is known as *linear sweep voltammetry* (LSV). In many cases, the potential is cycled continuously with constant sweep rate in a limited potential range, e.g., 0.05~1.55 V for polycrystalline platinum. This so called *cyclic voltammetry* (CV) is a useful technique in obtaining some primary information of an electrochemical system. A schematic plot for the cyclic potential sweep and i - E curve are displayed in Figure 1-1.

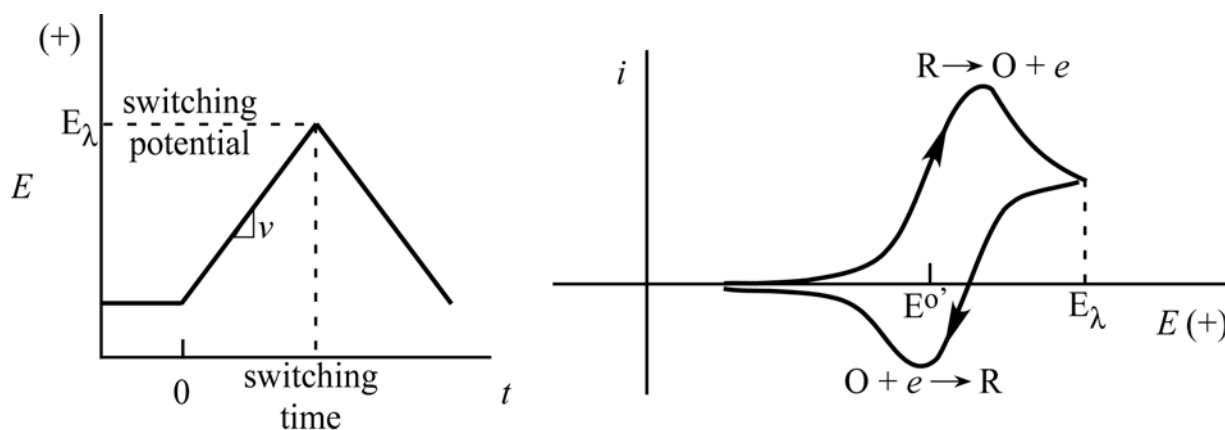


Figure 1-1. Cyclic potential sweep and the resulting cyclic voltammogram for species in solution.

For reversible systems, the reaction at the electrode surface is fast and the concentrations of reactant (R) and oxidant (O) are adjusted to the ratio according to Nernst equation:

$$E = E^{\ominus} + \frac{RT}{nF} \ln \frac{a_{\text{ox}}}{a_{\text{red}}} \quad (1-1)$$

Here E^{\ominus} is the standard potential with the chemical activities of both oxidant and reductant (a_{ox} and a_{red}) equal to 1. R is the gas constant, $8.314 \text{ J}\cdot\text{K}^{-1}\cdot\text{mol}^{-1}$; T represents the absolute temperature; F is the Faraday constant ($F = 96485 \text{ C}\cdot\text{mol}^{-1}$), and n the number of electrons transferred. At room temperature, i.e., $25 \text{ }^{\circ}\text{C}$, eq. (1-1) is frequently expressed in common logarithms rather than natural logarithms:

$$E = E^{\ominus} + \frac{0.05916 \text{ V}}{n} \lg \frac{a_{\text{ox}}}{a_{\text{red}}} \quad (1-2)$$

Under Nernst conditions, the following characteristics can be obtained: $j_{pa} = j_{pc}$ regardless of the sweep rate; the separation of peak potentials for anodic and cathodic processes, $E_{pa} - E_{pc}$, always closes to $2.3RT/nF$ (or $59/n$ mV at 25°C) and is slightly dependent on the switching potential; the peak current is proportional to $v^{1/2}$.

In many of the cases, the electroactive species, including organic and inorganic molecules and some anions, can be strongly adsorbed on the electrodes made of noble metals. In this case, the voltametric response is controlled by surface adsorption and desorption process and the contribution of species from solution can be ignorable to some extent.

In pure adsorption process, as with a linear potential sweep, the current density j is given by

$$\frac{j}{nF} = \frac{\partial \Gamma_i}{\partial t} = \frac{\partial \Gamma_i}{\partial E} \cdot \frac{\partial E}{\partial t} = \left(\frac{\partial \Gamma_i}{\partial E} \right) \cdot v$$

Here Γ_i is the amount of adsorbed species i per unit area and v is the sweep rate. To describe the voltammetric behavior theoretically, an appropriate adsorption isotherm is needed to interpret the coverage dependence of species i on it's concentration in solution and the electrode potential. If a langmuir adsorption isotherm is assumed, a symmetrical shape, as shown in Figure 1-2, will be obtained with the following features: 1) The current peaks for anodic and cathodic process locate at the same potential, $E_{pa} = E_{pc}$; 2) the peak current is directly proportional to the sweep rate v ; 3) the total charge is the charge required for the full reduction or oxidation of the adsorbed layer, independent of v ; 4) the full width at half-height of the peak is 90.6 mV at 25°C .

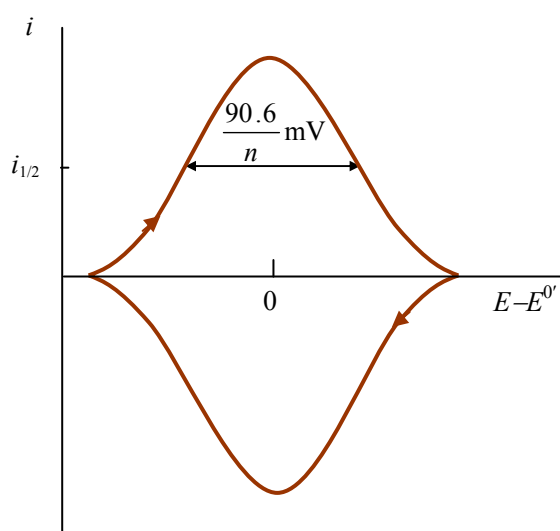


Figure 1-2. Typical CV for the oxidation and reduction of an adsorbed species under the assumption of a Langmuir isotherm.

Potential step methods

Chronoamperometry is the most often used potential step method, in which the potential is kept constant and the current is recorded as a function of time, as shown in Figure 1-3.

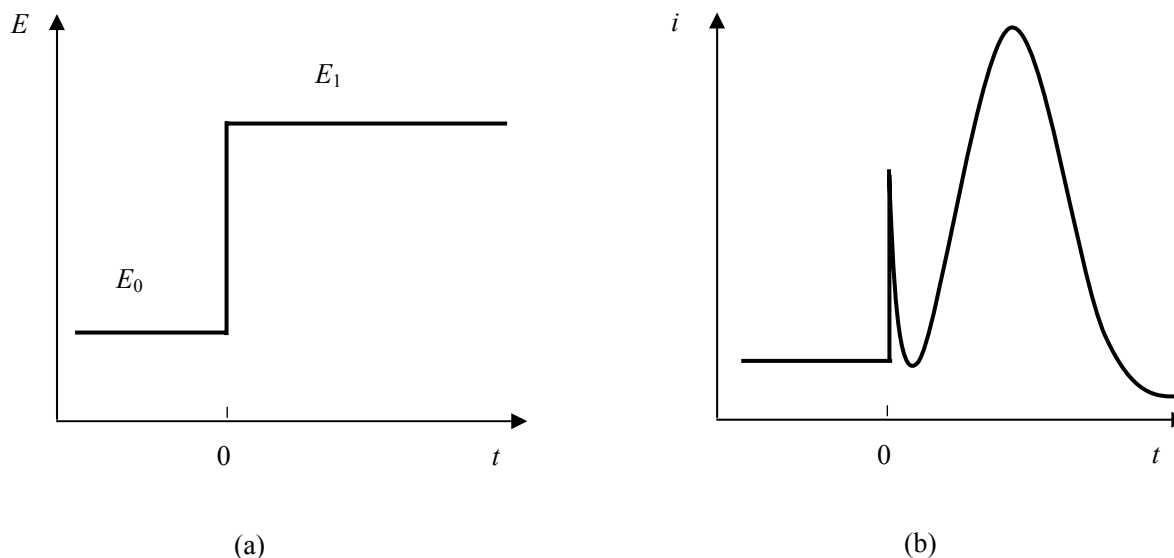


Figure 1-3. (a) Waveform of a potential step experiment. (b) The corresponding current for the oxidation of an adsorbed species.

1.1.2 Electrochemical impedance spectroscopy

The electrochemical system can be characterized by measuring the impedance (Z) over a range of frequencies (f) and the spectroscopy is denoted as *electrochemical impedance spectroscopy* (EIS). The variation of the impedance with frequency is often displayed in different ways: a *Nyquist plot* displays the imaginary part (Z_{Im}) of impedance versus real part of impedance (Z_{Re}) at various frequencies, as shown in Figure 1-4a, and an alternative representation, the *Bode plot* with both the logarithm of impedance and phase plotted versus the logarithm of frequency, see Figure 1-4b, c. An electrochemical system is often more complicated than the simple model. However, in many cases, the electrochemical process can be simulated with some equivalent circuit. A 3-electrode electrochemical cell can be interpreted as the equivalent circuit shown in Figure 1-5, in which the working electrode is interpreted as an electrolyte resistance in series with the combination of double layer capacitance and faradaic impedance in parallel. To investigate the faradaic process, the electrolyte resistance should be as small as possible.

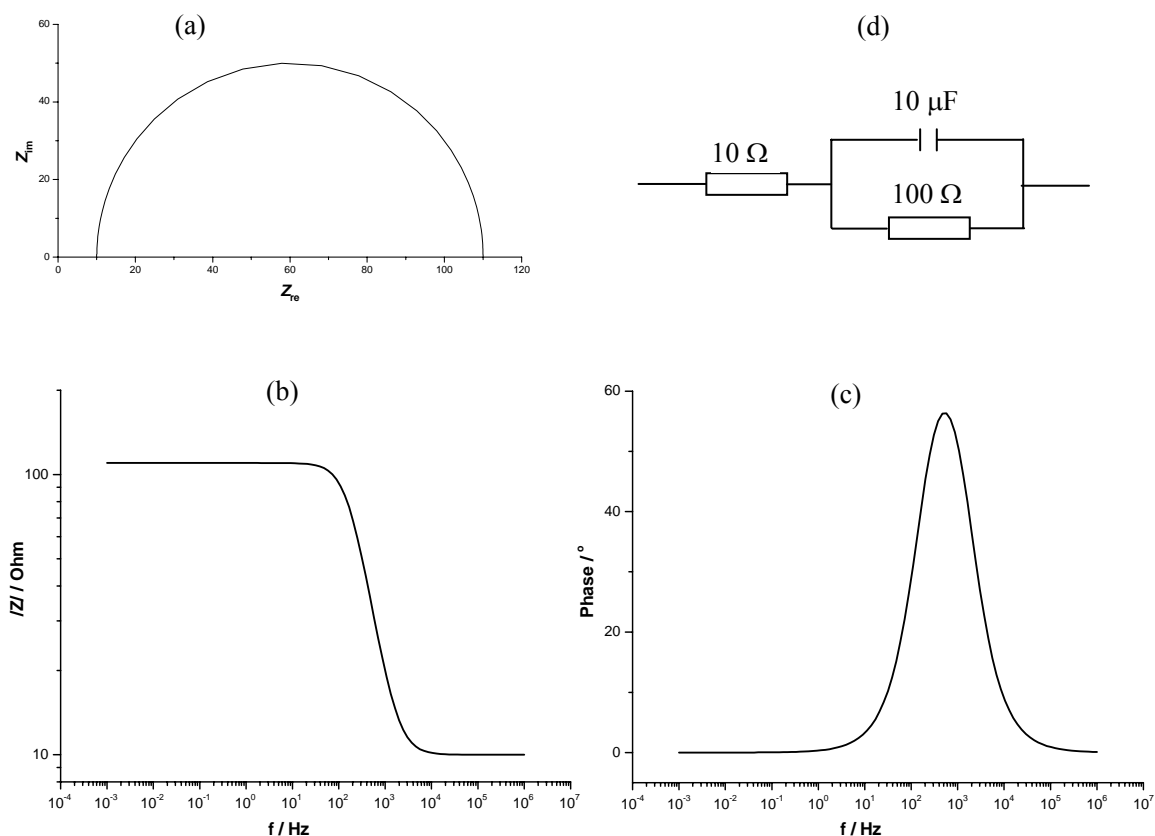


Figure 1-4. Nyquist plot, (a), and Bode plot, (b) and (c), for the circuit in (d).

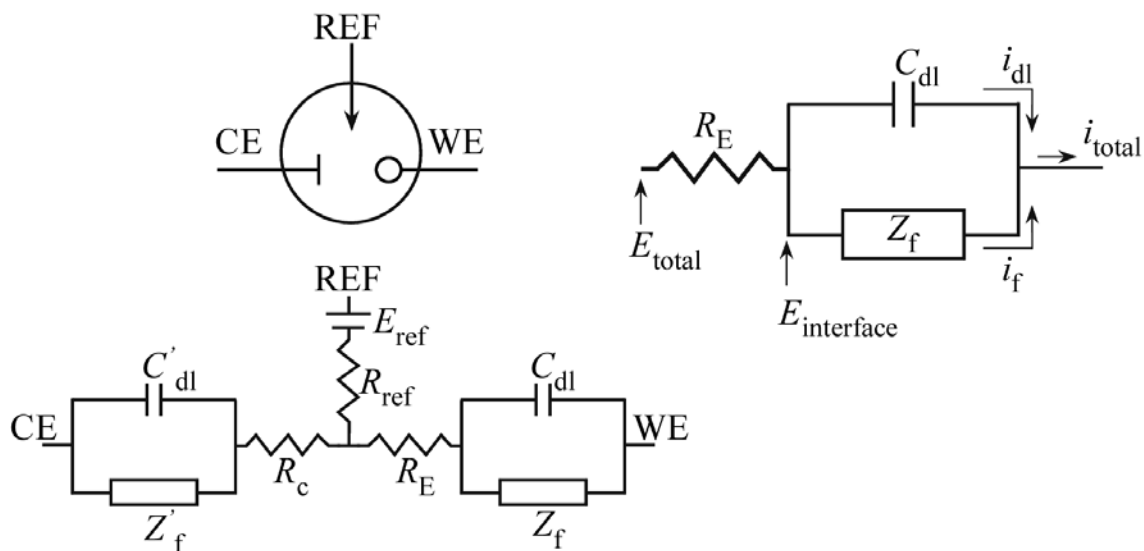


Figure 1-5. Representation of a three-electrode electrochemical cell and its equivalent circuit. The equivalent circuit for the working electrode interface is shown on the right. Adapted from [1].

1.1.3 Method of ac voltammetry

In the experiment of ac voltammetry, a small ac voltage, E_{ac} , is superimposed to the dc potential during the normal voltammetric process. The ac current thus generated is recorded at the same frequency of E_{ac} and as well as the phase with respect to that of E_{ac} . A schematic diagram of ac voltammetric experiment is shown in Figure 1-6. The method of ac voltammetry is very useful in determining the impedance features of a system in a whole potential range, and also for the determination of the i - E relationship for electrochemical process, such as rate constant.

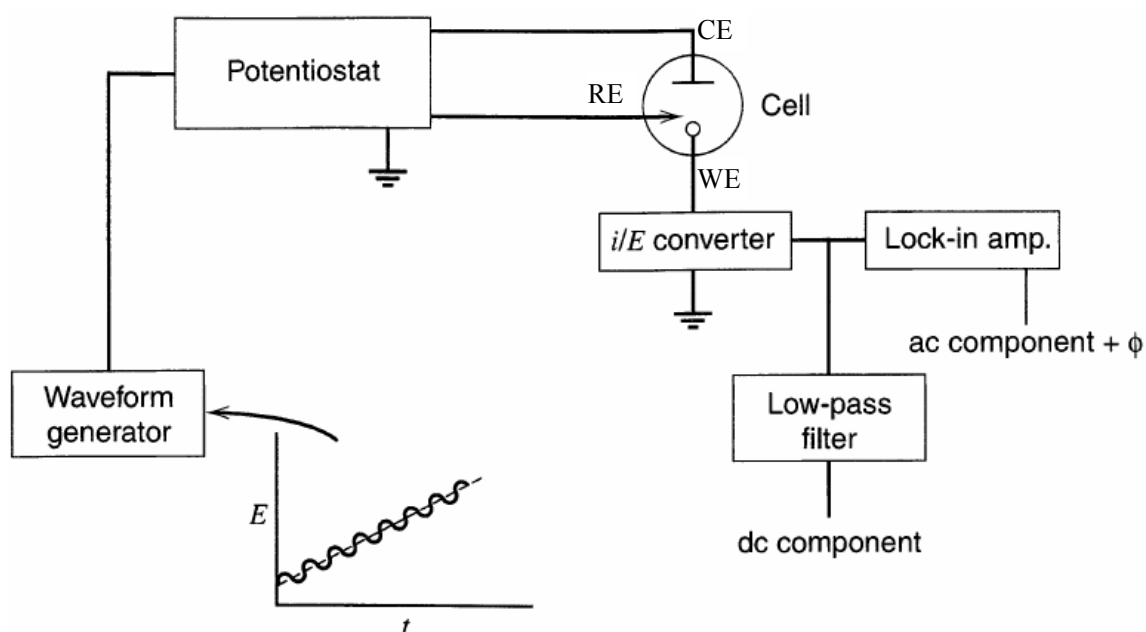


Figure 1-6. Schematic diagram of an ac voltammetric experiment.

1.1.4 Single crystals

Single crystals are very useful model electrodes for the electrochemical investigations due to their simple, ordered structure on the surface. An ideal crystal is built by infinite repetitions of an identical structural unit, which is called the *base* of the crystal or *unit cell*, in three-dimensional space and follows a certain pattern called the crystalline *lattice*. Any crystal structure in three-dimensional space can be described in a unique way by its basis and one of the 14 different fundamental lattices [2]. The most common metallic crystal structures are the following three types: face centered cubic (fcc), body centered cubic (bcc) and hexagonal close packed (hcp), as shown in Figure 1-7.

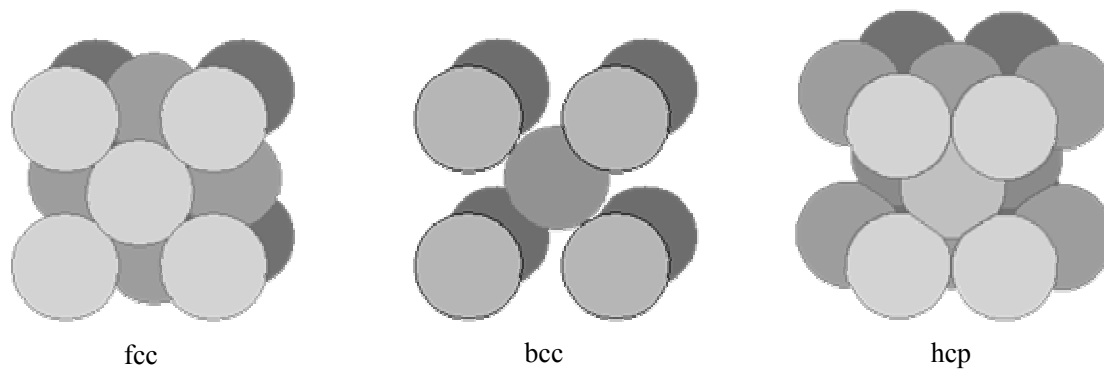


Figure 1-7. Models of fcc, bcc and hcp metallic crystal 3-D structure.

However, the surface of real crystals are actually far from being perfect and can show a broad spectrum of defects, like vacancies, adatoms, islands, steps, dislocations, etc. Some of these are depicted in Figure 1-8.

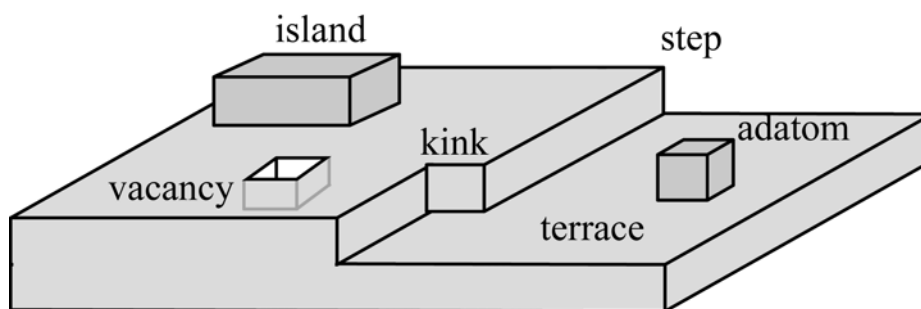


Figure 1-8. Model of a real solid surface, showing different surface sites.

The faces of a single crystal are usually characterized by Miller indices (hkl), which represent the reciprocal of the intercepts of the plane under consideration with the x-, y- and z-axes, as shown in Figure 1-9. Conventionally, small integer numbers are used so that parallel planes have identical indices. Negative intercepts are indicated with a bar above the respective indices.

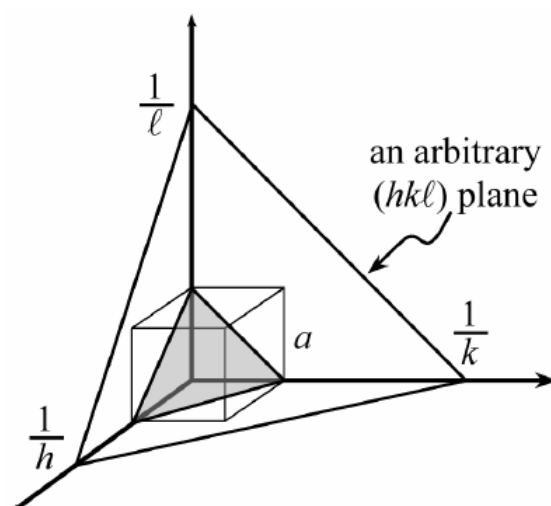


Figure 1-9. Schematics of an arbitrary plane with Miller indices (hkl) .

Many metals of technical importance, like Pt, Pd, Ag, Au, Ni and Cu, crystallize in the face centered cubic (fcc) lattice. The three low-index planes (111), (100) and (110) of fcc systems, as shown in Figure 1-10, are atomically flat with hexagonal, square and rectangular arrangement of the surface atoms, respectively [3]. The (0001) plane of hcp systems has also a hexagonal arrangement of surface atoms.

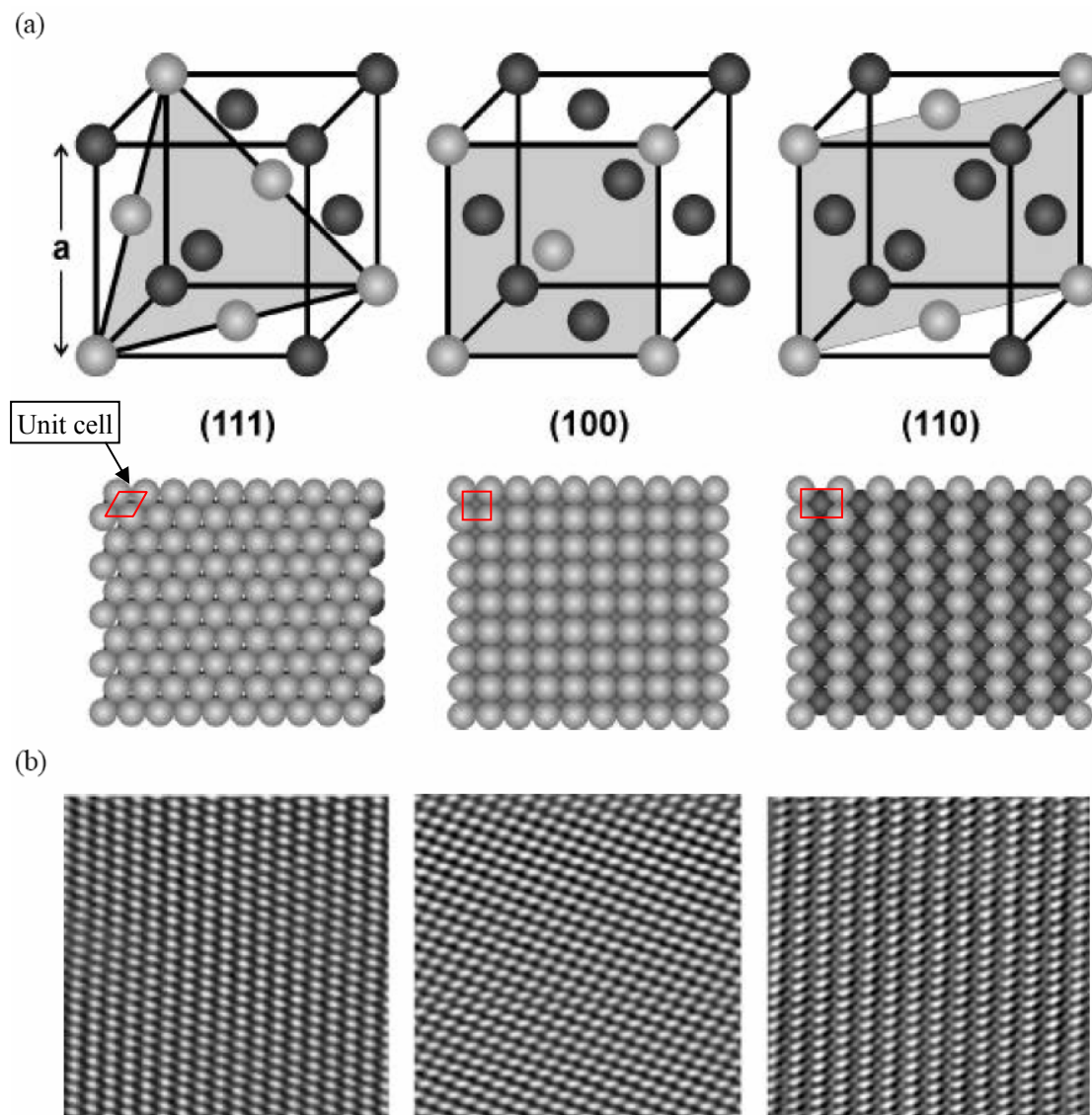


Figure 1-10. (a) Ball models of the three low-index faces of an fcc-crystal. The atoms of the respective planes are shown more brightly. (b) High-resolution STM images of Au(111), Au(100) and Au(110). 8×8 nm². Adapted from [3].

High-Miller-index planes consist of small atomically smooth terraces separated by steps and sometimes kinks, depending on the orientation. These high-index planes are of great importance in studying the role that steps or defects play in the physicochemical behavior of the surface by varying the amount of steps and kinks in a systematic way. Two stepped surfaces, Pt(665) and Pt(332), are shown in Figure 1-11. To express the geometry of the surface in terms of simple low-Miller-index vectors, *Lang notation*, also known as *step notation* [4], is normally adopted in the form of $n(hkl)_t \times (hkl)_s$, where $(hkl)_t$ and $(hkl)_s$ are the Miller indices assigned to the terrace and step, respectively, and n is the number of atoms in one terrace (including the first and last one). For example, the (665) surface has (111)-oriented terraces of 12 atomic lines separated by steps with the same orientation and thus is written as $12(111) \times (111)$. (665) can also be seen as $11(111) \times (110)$.

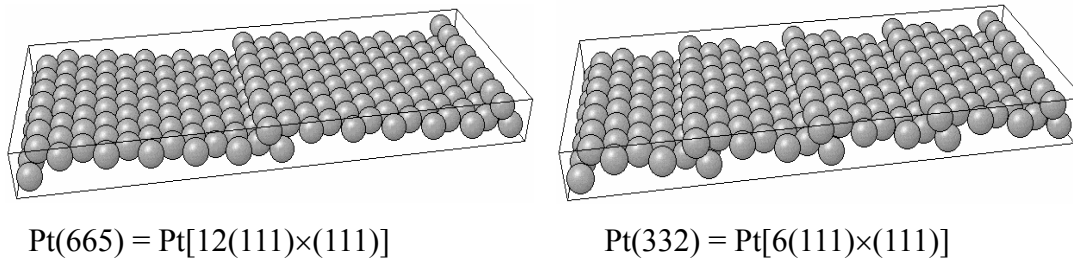


Figure 1-11. Ball models of high index single crystal Pt(665) and Pt(332).

The density of surface atoms (ρ) can be calculated from dividing the number of atoms by the area of one unit cell (s), $\rho = n/s$. The surface atomic densities for low-index planes are much easier to calculate than that of high-index one since the unit cells are simple, as displayed in Figure 1-10. And the calculation of each is shown in the following.

$$\rho_{111} = \frac{1}{d \cdot (\sqrt{3}d/2)} = \frac{1}{2\sqrt{3}r^2} \quad (1-3)$$

$$\rho_{100} = \frac{1}{d \cdot d} = \frac{1}{4r^2} \quad (1-4)$$

$$\rho_{110} = \frac{1}{d \cdot \sqrt{2}d} = \frac{1}{4\sqrt{2}r^2} \quad (1-5)$$

For high-Miller-index plane, the calculation is more complicated. For a Pt(332) surface with (111) orientation in both terrace and step, as shown in Figure 1-12, there are $(n-1)$ atoms in each unit cell. The geometrical relationship is also displayed below it in a triangle, with three sides composed of the projection of the length of the unit cell (l), the distance between two (111) terrace planes (d_{111}) and the length of the unit cell (l_{hkl}). The surface area for one unit cell and the density of surface atoms can be deduced as the following.

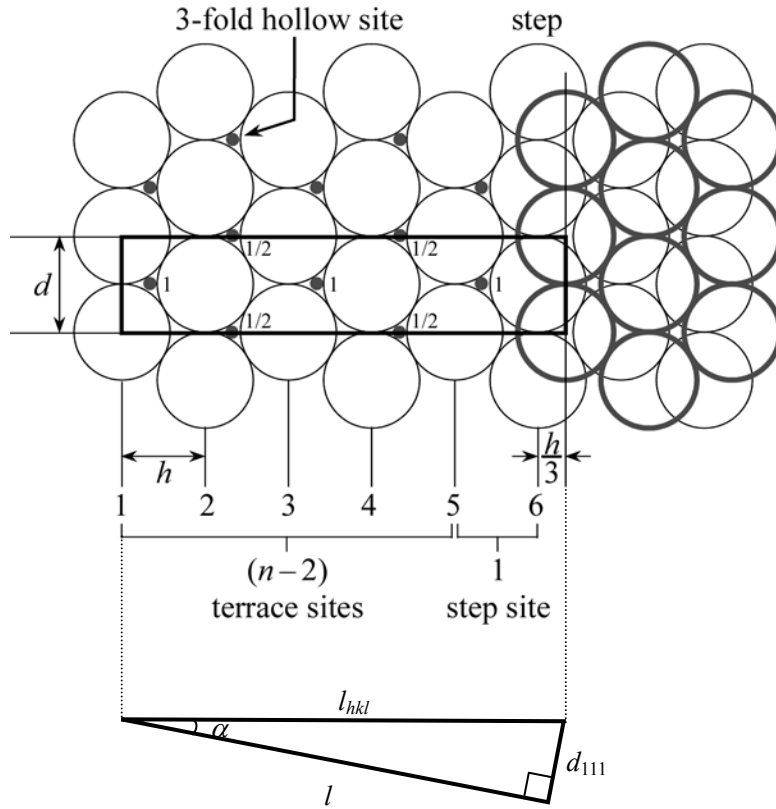


Figure 1-12. Surface unit cell for the (332) = 6(111) × (111) surface. Adapted from [5].

$$l = \left(n - \frac{2}{3}\right)h = \left(n - \frac{2}{3}\right)\sqrt{3}r \quad (1-6)$$

$$d_{111} = \frac{2\sqrt{2}}{\sqrt{3}}r \quad (1-7)$$

The angle between the surface plane and the terrace is then given by

$$\alpha = \arctan\left(\frac{d_{111}}{l}\right) = \arctan\left(\frac{2\sqrt{2}}{3n-2}\right) \quad (1-8)$$

Then l_{hkl} can be acquired as

$$l_{hkl} = \sqrt{\left(\left(n - \frac{2}{3}\right)\sqrt{3}r\right)^2 + \left(\frac{2\sqrt{2}}{\sqrt{3}}r\right)^2} = r\sqrt{3n^2 - 4n + 4} \quad (1-9)$$

The surface area of the unit cell is thus calculated to be

$$S_{hkl} = l_{hkl} \cdot d = 2r^2\sqrt{3n^2 - 4n + 4} \quad (1-10)$$

The surface atomic density is then obtained as the following.

$$\rho_{n(111)\times(111)} = \frac{n-1}{S_{hkl}} = \frac{n-1}{2r^2\sqrt{3n^2-4n+4}} \quad (1-11)$$

The properties of the crystal are much dependent on its step density, which can be calculated as the following.

$$\rho_{\text{step}(n(111)\times(111))} = \frac{1}{S_{hkl}} = \frac{1}{2r^2\sqrt{3n^2-4n+4}} \quad (1-12)$$

Single crystals can be prepared by several ways. Thin films of single crystal quality can be obtained by vacuum evaporation of noble metals on suitable substrates. Massive metal single crystals are normally grown by controlled cooling from a fluid phase, and followed by a procedure of orienting with the help of X-ray diffraction (XRD) and polishing mechanically, and thus an orientation accuracy of smaller than 0.1° can be achieved [6]. The small spherical single crystals with (111) facets in an octahedral configuration can be prepared by melting one end of a high purity wire and the crystallographic plane other than (111) can be obtained by orienting and polishing the bead crystals. [7]

The final preparation of the single crystals before investigation can be carried out in the following. Single crystal surface can be prepared in ultrahigh vacuum (UHV) by cycles of Ar-ion sputtering and high temperature annealing [8], and checked in the surface structure and chemical composition just after the preparation. Clavilier et al [7, 9] developed flame annealing and quenching method to handle the Pt bead single crystals without the use of UHV system. The flame annealing is very effective for removing organic contaminants in the presence of oxygen. This cheap and convenient method was later extended to the preparation of Au, Ag, Ir and Pd single crystal electrode with small diameter (< 2 mm) [10]. For large single crystals, annealing and cooling procedure can be used. The cooling down can be carried out in inert atmosphere (N_2 or Ar), or with the existence of reductive gas such as H_2 or CO. This simple, practical method of flaming annealing made it possible to work with single crystals for many electrochemistry groups all over the world and thus brought about a huge variety of results. For an extensive discussion on the preparation and characterization of noble metal single crystal electrodes by flame annealing method, the reader is referred to the work of Kibler [11].

1.1.5 Charge transfer coefficient and Tafel plot

Charge transfer coefficient, also called symmetry factor, is defined as the fraction of the interfacial potential at an electrode-electrolyte interface that helps in reducing the activation free energy for the electrochemical reaction. If α represents the transfer coefficient for anodic process, $0 < \alpha < 1$ with typical value of 0.5, then $(1-\alpha)$ is the coefficient for the cathodic process. As interpreted in Figure 1-13, if the potential is changed by $\Delta E = E - E^{0'}$, the anodic and cathodic activation free energies can be expressed as

$$\Delta G_a^\ddagger = \Delta G_{0a}^\ddagger - \alpha F(E - E^{0'}) \quad (1-13)$$

$$\Delta G_c^\ddagger = \Delta G_{0c}^\ddagger + (1 - \alpha)F(E - E^{0'}) \quad (1-14)$$

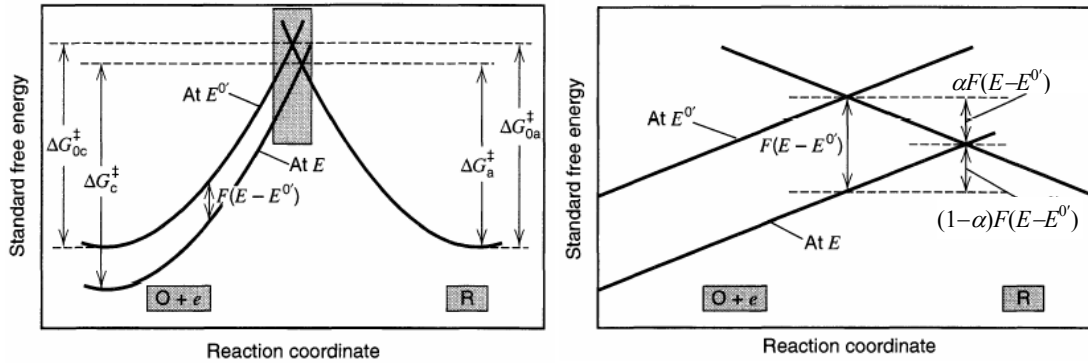


Figure 1-13. Effects of a potential change on the standard free energies of activation for oxidation and reduction. The right frame is a magnified picture of the boxed area in the left one. Adopted from [12].

For an electrochemical process, the rate constant can be expressed as the following:

$$k = B \exp(-\Delta G^\ddagger / RT)$$

Here B is a constant with the same dimensions as k . If the molar concentration of the oxidized and reduced materials outside the double layer are $[Ox]$ and $[Red]$, then the net current density at the electrode is given by,

$$j = j_a - j_c = FB_a[Red]\exp(-\Delta G_a^\ddagger / RT) - FB_c[Ox]\exp(-\Delta G_c^\ddagger / RT) \quad (1-15)$$

If we substitute the equations of (1-13) and (1-14) into (1-15) and introduce the parameters of exchange current density j_0 , which is denoted as the value of j_a or j_c when there is no net current at the electrode, and overpotential η , the deviation of potential from its equilibrium value, the Butler-Volmer equation can be obtained:

$$j = j_0 \left\{ \exp\left(\frac{\alpha n F \eta}{RT}\right) - \exp\left[-\frac{(1-\alpha)n F \eta}{RT}\right] \right\} \quad (1-16)$$

At very low overpotential, $|\eta|$ less than about 10 mV in practice, according to the Taylor series expansion, from equation (1-16) we obtain,

$$\begin{aligned} j &= j_0 \left\{ \left(1 + \frac{\alpha n F \eta}{RT}\right) + \dots - \left[1 - \frac{(1-\alpha)n F \eta}{RT} + \dots\right] \right\} \\ &= j_0 \frac{n F \eta}{RT} \end{aligned} \quad (1-17)$$

$$\text{Then } \frac{\eta}{j} = j_0 \frac{RT}{nFj_0} = R_{ct} \quad (1-18)$$

Here R_{ct} is the specific resistance for charge transfer, which can be obtained from the η - j curve at low overpotentials.

At high overpotential when the backward reaction contributes less than 1% of the current, i.g., $|\eta| > 118$ mV at 25 °C, the equation can be approximated to the following:

$$\begin{aligned} \eta &= -\frac{RT}{\alpha nF} \ln j_0 + \frac{RT}{\alpha nF} \ln j \\ &= a + b \lg j \end{aligned} \quad (1-19)$$

This equation is called Tafel equation, where b is the Tafel slope, from which the transfer coefficient parameter α can be obtained at constant temperature according to the following equation.

$$b = \frac{2.303RT}{\alpha nF} \quad (1-20)$$

At room temperature, i.e. 25 °C, if only one electron is involved in the reaction and the value of α is taken as 0.5, then the Tafel slope b can be calculated to be 118 mV·dec⁻¹. The parameter a in equation (1-19) can be obtained by extrapolating the η - $\log j$ line and take the interception at $\eta = 0$, where $i = i_0$, and thus the exchange current density can be calculated.

1.2 Introduction to fuel cells and CO oxidation

1.2.1 Introduction to fuel cells

What is a fuel cell?

A *fuel cell* is an electrochemical device which can convert chemical energy to electrical energy with continuous supply of fuel and oxidant. The first fuel cell was invented in 1838 by Grove during his investigation on the reverse reaction of electrolysis of water. He found that a constant current would flow through the two platinum electrodes when one end of each was immersed in sulfuric acid and the other two ends were sealed in containers of oxygen and hydrogen separately. But the further research and application is impeded by the development of steam engine and cheap fossil energy source. In the later nineteenth century, Ostwald provided much of the theoretical understanding of how fuel cells work and laid the groundwork for later fuel cell research. In 1939, Bacon developed an alkali electrolyte fuel cell that used nickel gauze electrodes and operated under pressure as high as 207 bars. Bacon continued in developing an alkaline fuel cell for the application in submarine and finally got his fuel cells used for the power supply in the Apollo spacecraft, which made fuel cells well known to the world afterwards. From then on, fuel cell attracted much attention from space mission, as well from other industries as a potential alternative energy

source.

A typical fuel cell model[13] is displayed in Figure 1-14. A fuel cell is composed of an anode, a cathode, electrolyte, separator and auxiliary parts such as device to feed reactants and as well as a battery to supply energy for start-up. The fuel used in the anode compartment could be hydrogen, or natural gas, or methanol, or ethanol. The oxidant for the reaction at the cathode is either oxygen, or air, or hydrogen peroxide. The electrolyte can be base, acid or salts, depending on the type of fuel cells.

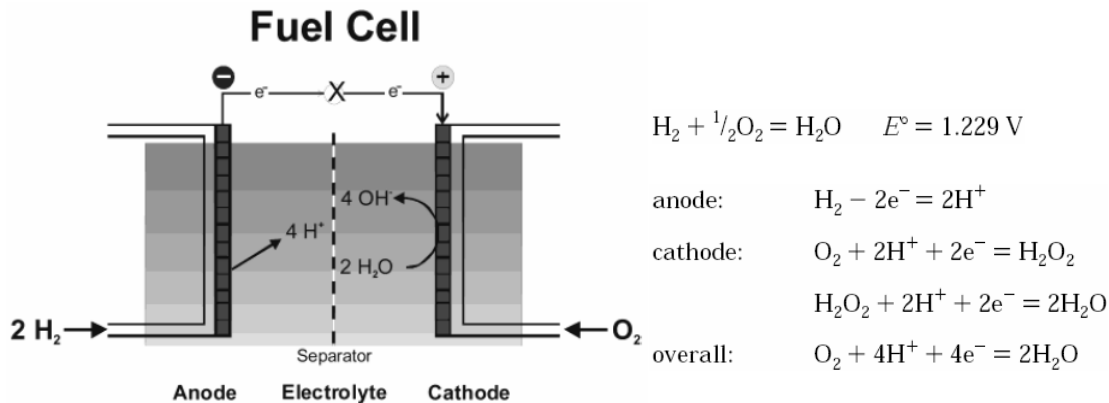


Figure 1-14. Schematics of Fuel cell and the corresponding reactions. Adopted from [13].

What for is fuel cell?

Fuel cells are attracting more and more attention because of the following three reasons.

Firstly, fuel cells are one of the most promising substitutes for the internal combustion engines which consume non-renewable fossil energy source. The fossil energy source, including petroleum, natural gas and coal, could be used out in less than 150 years according to the storage and the daily usage now. The limited storage and location of the fossil energy source made the prices increase by more than ten times in the last one hundred years. The oil price even reached its record to be 147.50 \$ a barrel in July of 2008 from about 5 \$ a barrel 36 years ago. Wars or conflicts are frequently triggered by energy source dispute. Fuel cells can also, at least in theory, improve the efficiency of energy source since the chemical energy is transferred directly into electrical energy, $W_e = \Delta G$, instead of the traditional way from chemical energy to heat and than to kinetic energy, $W = \Delta H \cdot (\Delta T/T)$, with energy loss of 70% or more due to the limitation of Carnot cycle and the friction of machine.

Secondly, fuel cells, especially those using hydrogen or methanol as anodic materials, have no or lower emission of the greenhouse gases, mostly CO_2 , compared with the engines using fossil energy source today. The greenhouse gases are believed to be responsible for the climate change recent years. And the abnormal climate change is also thought as one of the reasons for the catastrophic cases of recent flood, tsunami, hurricane, snowstorm and drought. As described by US president Obama in his inauguration, “the ways we

use energy threaten our planet”. So the reduction of emission of such greenhouse gases is one of the urgent topics to prevent the climate change and reduce the disaster from abnormal climate.

Thirdly, fuel cells are “green” energy source which don’t give out poisonous emission. The normal fossil energy sources give out emission of poisonous gases, i.g. SO₂ and NO_x, and dusts to the air, which caused direct threat to the health of human beings and responsible for the death of hundreds of thousands of people each year. The pollution of traditional energy sources adds to the urgency in investigating substitute energy sources such as fuel cells or solar cells that do no harm to the globe.

The advantages and disadvantages of fuel cells are listed in Table 1-1.

Table 1-1. Advantages vs. disadvantages of fuel cells, adopted from [13]

advantages	disadvantages
high efficiency, 90% is possible	complex to operate
modular construction	expensive
nonpolluting	impurities in gas stream shorten life
low maintenance	pulse demands shorten cell life
silent	limited availability
safe	Low durability
high energy density	Low power density per volume

Application of fuel cells.

The applications of fuel cells depend much on their powers, as listed in the following:

5-25 W: a replacement for Li-ion or Ni-MH batteries for portable electronics and the most promising one is direct methanol fuel cell.

50-75 kW: a power source for automobile and bus propulsion, which have the advantage of low emission and high efficiency.

200-300 kW: an uninterruptible power source for companies, hospitals, and buildings.

≥1MW: a stationary power source for central and dispersed power stations, e.g., electricity supply for remote countryside.

Classification of fuel cells

Mostly the fuel cells are classified according to the electrolyte used. Typically there are five types: alkaline fuel cell (AFC) [14], polymer electrolyte membrane fuel cell (PEMFC, also called Proton exchange membrane fuel cell)[15], phosphoric acid fuel cell (PAFC)[16], molten carbonate fuel cell (MCFC)[17] and solid oxide fuel cell (SOFC) [18, 19]. An exception to this classification is direct methanol fuel cell (DMFC), in which methanol is electrochemically oxidized directly in the fuel cell. The reactions and processes for various fuel cell systems are shown in Figure 1-15 and the advantages and disadvantages are listed in Table 1-2.

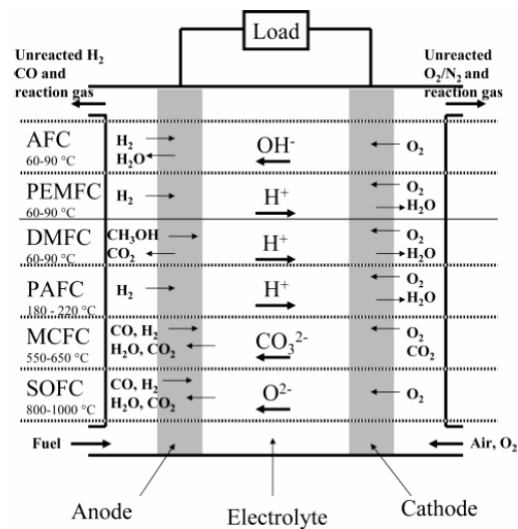


Figure 1-15. The reactions and processes that occur in various fuel cell systems. Adopted from [13].

Table 1-2. Advantages and disadvantages of various FCs. Adopted from [13]

advantages	disadvantages	comments
	Alkaline (AFC) ^a	
mechanically rechargeable low-cost KOH electrolyte	limited activated life intolerant of impurities in gas streams CO ₂ and CO pure H ₂ only suitable fuel	original development > 30 years ago Apollo fuel cell operates at room temp to 80 °C demo in vehicles in the 1970s
nonvolatile electrolyte few materials problems CO ₂ rejecting electrolyte pressure differential between anode and cathode polymer electrolyte	Polymer Electrolyte Membrane Fuel Cell (PEMFC)	
	expensive catalysts required CO a strong poison H ₂ O management essential high-cost electrolyte pure H ₂ only suitable fuel oxygen kinetics are slow intolerant of impurities limited life water management essential	operates best at 60–90 °C originally developed for space by GE hydrogen fuel (re-formed hydrocarbons, pure H ₂ , MH storage) main development efforts for automotive and stationary applications
direct fuel conversion slow electrode kinetics improved wt and vol polymer electrolyte	Direct Methanol Fuel Cell (DMFC)	
	stable reaction intermediates high catalyst loadings water management essential low overall efficiency methanol hazardous	operates best at 60 to 90 °C) same construction as PEMFC methanol fuel eliminates reformer lower current capability methanol crossover reduces efficiency needs new membrane, higher efficiency high catalyst loadings main effort for portable electronic devices
CO ₂ rejecting electrolyte high fuel efficiency	Phosphoric Acid Fuel Cell (PAFC)	
	H ₂ only suitable fuel anode CO catalyst poison O ₂ kinetics hindered low conductivity electrolyte high-cost catalysts limited life	operates best at ~200 °C stationary energy storage (nominal units, 250 kW) available commercially
fast electrode kinetics high efficiency CO/CH ₄ usable fuel direct reforming feasible high-grade heat available	Molten Carbonate Fuel Cell (MCFC)	
	materials problems and life low sulfur tolerance high ohmic electrolyte low tolerance to sulfur need to recycle CO ₂ limited life	operates best at 550 °C nickel catalysts, ceramic separator membrane hydrocarbon fuels re-formed in situ several large demonstration units significant government support
high grade heat available fast electrode kinetics in situ reforming feasible no electrolyte management high system efficiency tolerant of impurities	Solid Oxide Fuel Cell (SOFC)	
	high fabrication costs severe materials constraints high electrolyte conductivity	operates at 900 °C conducting ceramic oxide electrodes hydrocarbon fuels re-formed in situ least sensitive to sulfur, etc.

^a Metal air batteries with replaceable anodes are often considered to be a fuel cell but are not considered here.

Sometimes, fuel cells are also grouped by the operating temperature [20]. AFC, PEMFC, DMFC and PAFC are low temperature fuel cells with operating temperatures under 200 °C; high temperature fuel cells operate at 500-1000 °C, including MCFC and SOFC.

Challenges exist in the application of fuel cells.

1. High price. One main obstacle for the wide application of fuel cells is their high price compared with the systems using fossil energy sources. The catalysts employed for most of the fuel cells, including AFC, PEMFC, DMFC and PAFC, are Pt or its alloys such as PtRu, for both anodic and cathodic reaction. As a noble metal with its price higher than Au, Pt is limited in production. The high price of catalyst keeps fuel cells away from commercial application even if the first application in Apollo mission took place more than 40 years ago.

2. The production, transportation and storage of fuels. Hydrogen is one of the most investigated fuels, which can be converted from petroleum or natural gas. But the production process requires a lot of energy. The transportation and storage are the main challenges for hydrogen based fuel cells since it's in gas phase at normal pressure and temperature. Hydrogen can be stored in various ways [20]: it can be stored as a high pressured gas, or as a liquid below $-253\text{ }^{\circ}\text{C}$ with extremely good insulation, or as metal hydride with atomic hydrogen adsorbed on metals or metal alloys [21], or in gaseous form into graphite nanostructures such as nanotubes [22, 23] and nanofibres, glass microspheres [24] and Zeolites [25]. Methanol can be produced from petroleum, coal and natural gas. Ethanol is also a potential fuel since it's easy to produce from maize and other food. The storage and transportation of methanol and ethanol is not a problem since they are in liquid state.

3. The poisoning of catalyst and its durability. Since CO adsorbs strongly on Pt surfaces, the Pt catalysts are therefore poisoned in the presence of CO. The adsorption of CO has a particular negative effect on the performance of low temperature fuel cells using hydrogen and methanol/ethanol fuels. In the first case, trace amount of CO is often inevitable as an impurity in the hydrogen fuel. In the second case, CO is produced as an intermediate in the methanol/ethanol oxidation process. In both cases the existence of CO will result in increase of the overvoltage in anodic reaction. Therefore, the investigation of the electrochemical adsorption and oxidation of CO attracted extensive interests.

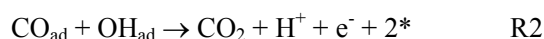
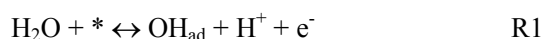
Recent progresses on the catalyst of fuel cells.

Reducing the cost of catalyst is a key step for the application of fuel cells. To reduce the cost of the catalyst, the usage of Pt should be reduced or avoided. This can be achieved by either dispersing the Pt in order to lower the load, or improving the efficiency of Pt catalyst, or developing non-Pt catalyst. Sun and coworkers produced tetrahedral platinum nanocrystals with high-index facets, which demonstrated high activity for the electro-oxidation of small organics such as HCOOH and $\text{CH}_3\text{CH}_2\text{OH}$. [26] Since the oxygen reduction reaction (ORR) at the cathode of the fuel cells plays a key role in controlling the performance of a fuel cell, the investigation of efficient ORR electrocatalysts are essential for practical applications of the fuel cells. Stamenkovic and Markovic [27] have found that $\text{Pt}_3\text{Ni}(111)$ have much larger oxygen reduction activity than $\text{Pt}_3\text{Ni}(100)$ and $\text{Pt}_3\text{Ni}(110)$: $\text{Pt}_3\text{Ni}(100) < \text{Pt}_3\text{Ni}(110) \ll \text{Pt}_3\text{Ni}(111)$. Zhang and coworkers [28] modified a Pt catalyst with Au clusters to stabilize the catalyst for ORR and showed stable activity in the course of cycling, which is in contrast to the sizable losses of pure Pt catalyst. Some others tried to use non-Pt catalysts [29, 30], e.g., transition metal chalcogenides [31], carbon nanotube-supported metal particles [32], enzymatic electrocatalytic systems [33], cobalt-polypyrrole composite catalyst [34]), conducting poly(3,4-ethylenedioxythiophene) (PEDOT)-coated membranes [35], aligned carbon nanotubes and aligned nitrogen-containing carbon nanotubes (VA-NCNTs) [36].

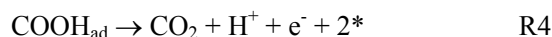
1.2.2 CO oxidation mechanism

The adsorption and oxidation of CO is one of the most investigated reactions in surface science. In electrochemical environment, CO is widely employed as a probe molecule for vibrational spectroscopy. [37-39] Since the poisoning of CO on the catalyst is one of the main obstacles for the application of fuel cells [40, 41], a detailed understanding of the mechanism for the removal of CO on noble metals, especially on Pt surface, will be helpful in optimizing the catalysts for fuel cells. There are two types of mechanisms proposed for CO oxidation: Langmuir-Hinshelwood (L-H) mechanism and Eley-Rideal (E-R) mechanism.

The L-H mechanism is firstly suggested by Gilman [42] for CO oxidation on Pt. In this mechanism, the CO adsorbed on Pt will react with an adjacent adsorbed oxide species to form CO₂. This adsorbed oxide was suggested to be hydroxyl (OH_{ad}, as widely accepted one), or discharged water (H₂O), or Platinum oxide (PtO_x). In this thesis I assume that it's OH_{ad}. The reaction steps are shown in the following.



Here the * represents the free Pt atom sites. It's also worth to mention that also some researchers believe that there's a chemical step between the two electrochemical step [43-45]. Then R2 can be replaced written as:



The Eley-Rideal mechanism describes a reaction that takes place between the adsorbed species and a non-adsorbed species. A typical reaction that follows E-R mechanism is the oxidation of CO on Ru [46]. For example, for the oxidation of gaseous CO at high pressures on oxygen precovered Ru the following reaction equation can be assumed.[47, 48]



Some researchers also believe that the adsorbed CO can reaction with water [49], as shown in the following.



In general, the L-H mechanism is favored for CO oxidation occurring at the solid-gas interface of Pt, Pd, Rh, and Ir [48]. For Ru, however, the mechanism depends also on the pressure of CO and/or O₂, e.g., an E-R type mechanism may be taken place at high CO pressure [50]. The situation at the solid-liquid interface is different from that of solid-gas interface and an E-R mechanism is also possible since the collision frequency of adsorbed species and non-adsorbed species are much higher [49].

1.2.3 The determination of the Tafel slope or apparent transfer coefficient for CO oxidation on Pt and the contradiction in literature

The Tafel slope is normally obtained by plotting the logarithm of the oxidation current versus overpotential and calculating the reciprocal of the slope. With the knowledge of Tafel slope, the (apparent) transfer coefficient can be calculated according to the equation (1-20). For the oxidation of adsorbed CO on a Pt electrode, the Tafel slope can't directly determined by the above method since the surface coverage of the adsorbed CO is changing during CO_{ad} oxidation. It is usually determined by one of the following plots:

1) $\log i_{\max}$ vs. E with i_{\max} the peak current (density). Since the current is a function of potential E and fractional coverage Θ [43], i.e.,

$$i = -q_m \frac{d\Theta}{dt} = k(E) \cdot f(\Theta) \quad (1-21)$$

At a given coverage for various potentials, the current is only a function of E , and then the Tafel slope can be determined. Here the q_m is the charge corresponding to the oxidation of a monolayer. Since in many cases the peak is symmetric, the fractional coverage at the peak is approximately half for various potentials in potential step experiment.

2) $\log t_{\max}$ vs. E with t_{\max} the time corresponding to the current maximum. If we integrate (1-21) from $t=0$ to $t=t_{\max}$, we get

$$t_{\max} = -\frac{q_m}{k(E)} = \int_{\Theta_0}^{\Theta_{\max}} \frac{d\Theta}{f(\Theta)} \quad (1-22)$$

where Θ_0 and Θ_{\max} are the initial coverage and the coverage at current maximum. Then $\log t_{\max} = \log k(E)$ and the plot of $\log t_{\max}$ vs. E will give the Tafel slope.

3) $\log v \sim E_p$ with v being the sweep rate. This is a common practice in linear sweep or cyclic voltammetry experiment since $(dE_p/d\log v)$ gives approximate value of $RT/\alpha F$, especially at high sweep rate. [51, 52]

4) $\log k'$ vs. E with k' the apparent rate constant fitted from the current transient in potential step experiment by a mean field model. The most known expression for this kind of simulation was deduced by Bergelin et al [53] based on the assumption that the adsorption of oxygen species is reversible, so that its coverage, Θ_{OH} , is always proportional to $(1-\Theta_{\text{CO}})$.

For the research of CO oxidation on Pt electrodes in acidic solution, contradictions exist so far on the value of the Tafel slopes and the rds deduced thereof. Some researchers get different Tafel slope at low and high potential. Love and Lipowski [54] reported Tafel slopes of 67 and 190 $\text{mV}\cdot\text{dec}^{-1}$ at low and high potentials on Pt(100), Pt(111) and Pt(311) in 0.1 M HClO₄. Bergelin et al [53] obtained values of 100 $\text{mV}\cdot\text{dec}^{-1}$ at potentials below 0.7 V (vs.RHE) and 280 $\text{mV}\cdot\text{dec}^{-1}$ at potential higher than 0.7 V in H₂SO₄. Koper et al [55] modeled the CO electrochemical oxidation process using Monte Carlo simulation and draw the conclusion that the Tafel slope should be 40 $\text{mV}\cdot\text{dec}^{-1}$ at low potential and 120 $\text{mV}\cdot\text{dec}^{-1}$ at high potentials and this

qualitative features are not strongly influenced by the mobility of CO. McCallum et al [56] reported $120 \text{ mV}\cdot\text{dec}^{-1}$ on a Pt wire at potential higher than 0.71 V but the Tafel slope deviated to lower values at potentials lower than 0.71 V. Some other researchers believed that there is only one Tafel slope of all the potentials. Santos et al[43] reported the slope of 57 or 67 $\text{mV}\cdot\text{dec}^{-1}$ obtained by plotting the logarithm of the peak current or the peak current time versus potential in the range of 0.66~0.72 V. Herrero et al [57] obtained Tafel slope of 70-75 $\text{mV}\cdot\text{dec}^{-1}$. Lebedeva et al[44, 45], have reported a Tafel slope of $75\pm 3 \text{ mV}\cdot\text{dec}^{-1}$ for Pt(111), $85\pm 3 \text{ mV}\cdot\text{dec}^{-1}$ for Pt(15 15 14), $78\pm 4 \text{ mV}\cdot\text{dec}^{-1}$ for Pt(554) and $97\pm 4 \text{ mV}\cdot\text{dec}^{-1}$ for Pt(553). Also some others obtained similar slopes ranging from 70 to 100 $\text{mV}\cdot\text{dec}^{-1}$. Since the Tafel slope is close to 1, Santo et al proposed a chemical step, $\text{CO}_{\text{ad}} + \text{OH}_{\text{ad}} \rightarrow \text{COOH}_{\text{ad}}$, as the rds, which is also supported by Lebedeva and other researchers who had obtained a similar single Tafel slope.

In alkaline solution, Koper et al [58] get Tafel slopes ranging from 36 to 99 $\text{mV}\cdot\text{dec}^{-1}$, which is difficult to explain with the same mechanism as Lebedeva et al[44, 45] described in acidic solution.

Table 1-3. Tafel slope reported in literature.

Electrode	Tafel slope (mv/dec)	method	Solution	Literature Author_Journal_year
Pt(111)	Main: 75 ± 3	$\log(k') \sim E$	0.5 M H_2SO_4	Lebdeva_JEC_2002 [44]
Pt(111)	Main: 70 ± 2	$\log(t_{\text{max}}) \sim E$		
Pt(111)	Plateau: 81 ± 4	$\log(i) \sim E$		
Pt(111)	67 57	$\log(t_{\text{max}}) \sim E$ $\log(i_{\text{max}}) \sim E$	0.05 M HClO_4	Santos_EA_1991 [43]
Pt(111)	70-75	(not mentioned)	0.5 M H_2SO_4	Herrero_langmuir_2000 [57]
Pt(111) Pt(100)	80 ± 5 60 ± 3	$\log(v) \sim E_p$	1 M HClO_4	Palaikis_SS_1988 [52]
Pt(100) Pt(111) Pt(311)	$E < 850\text{mV}$: 240 $E > 850\text{mV}$: 80 E_{low} : 67 E_{high} : 190 120	$\log((di/dt)^{1/2}) \sim E$ $\log(t_{\text{max}}) \sim E$ $\log(k_N/N_N) \sim E$	0.1 M HClO_4	Love & Lipkowski_ACS symp.Ser_1988 [54]
Pt(111)	$E < 700\text{mV}$: 100 $E > 700\text{mV}$: 280	$\log(t_{\text{max}}) \sim E$	0.5 and 0.05 M H_2SO_4	Bergelin_JEC_1999 [53]
	72	$\log(k') \sim E$		
Pt(111)	Main: 75 ± 3 Plateau: 81 ± 4	$\log(k') \sim E$ $\log(i) \sim E$	0.5 M H_2SO_4	Lebedeva_JPCB_2002

Pt(15 15 14)	Main: 85±3 Plateau: 82±3	$\log(k') \sim E$ $\log(i) \sim E$		
Pt(554)	Main: 78±4 Plateau: 82±3	$\log(k') \sim E$ $\log(i) \sim E$		
Pt(553)	Main: 97±4 Plateau: 111±15	$\log(k') \sim E$ $\log(i) \sim E$		
Pt(110)	Main: 81±3 Plateau: 111±15	$\log(k') \sim E$ $\log(i) \sim E$		
Pt(335)	79±4	$\log(k') \sim E$	0.5 M H ₂ SO ₄	Inkaew_PCCP_2008 [59]
	67±3	$\log(t_{\max}) \sim E$		
Pt nanoparticles	80	$\log(v) \sim E$	0.1 M H ₂ SO ₄	Maillard_JEC_2007_CO oxidation on Pt nanoparticles [60]
	70-90	$\log(t_{\max}) \sim E$		
	85	$\log(j_{\max}) \sim E$		
Pt (poly)	100±4	$\log(t_{\max}) \sim E$	0.5 M H ₂ SO ₄	Kucernak_PCCP_2008- _The role of OH on CO oxidation [61]
	82±2	$\log(t_{\min}) \sim E$		
	105±5	$\log(j_{\max}) \sim E$		
	119±7	$\log(j_{\min}) \sim E$		
Pt wire	120	$\log(i) \sim E$	1 M HClO ₄	McCallum_JEC_1976_70_P277 [56]
Pt-smooth Pt-platinized	76 70		0.5 M H ₂ SO ₄	M.W. Breiter, J. Electroanal. Chem. 101 (1979) 32 [62]
Pt(10 1 0)	70	$\log(k) \sim E$	0.5 M H ₂ SO ₄	Vidal-Iglesias, EA, 2009 [63]
	78	$\log(t_{\max}) \sim E$		
Pt(210)	120	$\log(k) \sim E$		
	122	$\log(t_{\max}) \sim E$		
Pt(510)	1st Peak: 82	$\log(k) \sim E$		
	2nd peak: 65	$\log(k) \sim E$		
	77	$\log(t_{\max}) \sim E$		
Pt(310)	100	$\log(k) \sim E$		
Pt(100) & Pt(n10) (n≥7)	75 ± 4	$\log(k) \sim E$		
Pt(111)	main: 73 plateau: 130	$\log(j) \sim E$ $\log(j) \sim E$		
Pt(1 1 1)	Pre peak: 118 main peak: 67	$\log v \sim E_p$	0.1 M NaOH	Garcia & Koper_PCCP_2008_10_p3802 [58]
Pt(15 15 14)	Step: 83	$\log(v) \sim E_p$		

	Main: 53			
Pt(5 5 4)	Step: 92 Main: 36	$\log(v) \sim E_p$		
Pt(5 5 3)	Step 75 Main: 39	$\log(v) \sim E_p$		
Pt(110)	Main: 99	$\log(v) \sim E_p$		

1.3 Volume measurement and surface volume excess

1.3.1 Basic volume measurement

Volume is an important quantity parameter of a matter. For gases, the volume is determined by the container. For liquid, the volume can be easily measured with a graduated flask. For a regular shaped solid, the volume can be determined by calculation according to its geometric shape. For irregular shaped bulk, the volume can be obtained mainly by the following two methods: (1) measuring the mass and then divide it by the density of this kind of material and (2) measuring the liquid, mostly water, it repulses when fully immersed into the liquid.

1.3.2 Partial molar volume in solution, especially H^+

Partial molar volume is the volume contribution that a component makes to the total volume in a sample. It's defined as the following:

$$v_i = \left(\frac{\partial v}{\partial n_i} \right)_{p, T, n_{j \neq i}} \quad (1-23)$$

where n_i is the molar amount of species i and $n_{j \neq i}$ means that the amount of all substances other than i in the mixture is held constant. If the mixture has two components A and B, at certain pressure and temperature, the total volume is

$$v = n_A v_A + n_B v_B \quad (1-24)$$

The partial molar volume can be measured by several methods. One of them is to measure the dependence of the molar volume (from the mass and density) on the composition and to determine the slope dv/dn at the composition of interest. A better method is "the method of intercept"[65], which will be presented in the following: For a binary system with the mean molar volume of v_m ($v_m = V/n$) and mole fraction of x_B ($x_B = n_B/n$), the following equation can be obtained:

$$v_m = v_A + \frac{dv_m}{dx_B} \cdot x_B \quad (1-25)$$

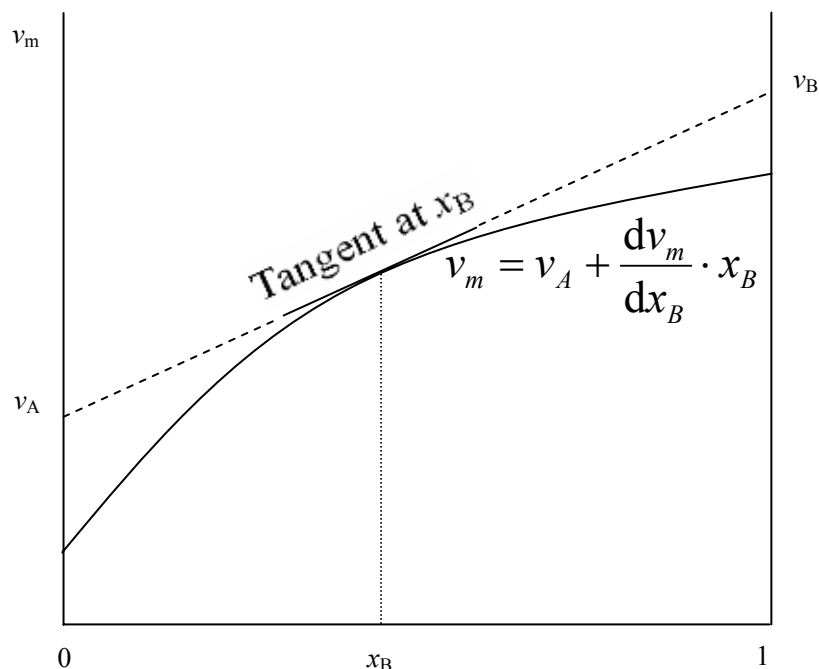


Figure 1-16. The extrapolation needed to find the partial molar volume v_A and v_B at the composition x_B .

A sketch of the method described above is shown in Figure 1-16. The tangent of v_m curve at x_B is extrapolated and the intercepts at $x_B = 0$ and $x_B = 1$ gives v_A and v_B , respectively.

The partial molar volume of an ion is more complicated and the determination is much more difficult than that of components such as methanol since cations and anions always coexist. In convention, the limiting partial molar volume of H^+ in aqueous solution is assumed to be zero at all temperatures. The relative partial molar volume of other cations and anions are calculated according to this assumption, for example, v_{Cl^-} take the value of v_{HCl} in dilute solution and v_{Na^+} is obtained by subtracting v_{NaCl} by v_{Cl^-} .

There are several methods[66] that can be used in measuring the partial molar volume of an ion:

(1) Direct methods, including the methods of ultrasonic vibration potential (UVP)[67] and sedimentation potential (SP)[68]. UVP measurement is often considered as a yardstick in judging other methods. A remarkable measurement by this method is the absolute value of H^+ , which is measured to be $-5.4 \text{ cm}^3 \cdot \text{mol}^{-1}$ and widely accepted as the value for $v_{H^+}^0$. SP measurement is also used sometimes.

(2) Reference electrolyte methods. The reference electrolyte is often specially chosen so that its cation and anion have very similar structure, low charge density and small electrostriction in order to have an equal split in partial molar volume:

$$v_{CA} = 2v_{C^+} = 2v_{A^-} \quad (1-26)$$

The salts typically employed are $\text{Ph}_4\text{AsBPh}_4$ (TATB) with ions of Ph_4As^+ and BPh_4^- or its phosphonium analogue Ph_4PBPh_4 (TPTB)[69]. This approach has been widely used for deriving a variety of single-ion partial molar volume. Compared with Ph_4As^+ , Ph_4P^+ is closer in size to BPh_4^- . Therefore, the results from TPTB are more in agreement with other methods, including UVP approach than TATB.

(3) Extrapolation methods. This method involves extrapolation of v of a series of salts with a common ion, against some suitable quantity f characterizing the counterions; with the intercept representing the volume of the common ion.[70] For example,

$$v_{X^-} = \lim_{f \rightarrow 0} v_{R_4NX} \quad (1-27)$$

Here X represents a halogen element. The f here could be either the molar mass of the anion or the number of carbon atoms.

(4) Methods involving crystallographic ionic radii. Mukerjee's method [71] assumes that univalent monatomic cations and anions of equal crystallographic size should have the equal partial molar volume. The approach by Kozlov and Novoselov [72] used the following equation:

$$v_{MX} - v_{NX} = A(r_M^3 - r_N^3) - Bz^2(r_M^{-1} - r_N^{-1}) \quad (1-28)$$

where M is a reference ion and N varies along a series of ions with the same charge.

(5) Reference ion method. This method[73] assumes that the partial molar volume of some ions equal to that of similar neutral substance in case that the electrostriction of this ion is negligible:

$$v_{\text{ion}} = v_{\text{neutral}} \quad (1-29)$$

Jolicoeur et al [74] take the assumption that $(\text{HCOCH}_2)_4\text{P}^+$ and $(\text{HCOCH}_2)_4\text{C}$ should have the same partial molar volume and obtained a reasonable value of for H^+ to be $-4.8 \text{ cm}^3 \cdot \text{mol}^{-1}$. Kay [75] [76] proposed another assumption that the coordination complex with a macrocyclic ligand has the same partial molar volume as the ligand.

In solution, it's widely agreed that the partial molar volume of an ion, v_{ion} , is made up of two major components[69]

$$v_{\text{ion}} = v_{\text{int}} + v_{\text{ele}} \quad (1-30)$$

where the v_{int} is the intrinsic partial molar volume of the ion, which can be estimated if the radius of the ion is known. v_{ele} is the electrostriction contribution to the partial molar volume.

If the solvent is water, then the ion will form a hydrated ion. And then the ionic partial molar volume v_{ion} can be written as:

$$v_{\text{ion(H}_2\text{O)}} = v_{\text{int}} + nv_{\text{ele(H}_2\text{O)}} \quad (1-31)$$

where the $v_{\text{ele(H}_2\text{O)}}$ is the electrostriction of one water molecule in the hydration shell, which is estimated to be $-2.1 \text{ cm}^3 \cdot \text{mol}^{-1}$ by Padova[77]. If v_{ion} and v_{int} is known, then the hydration number n could be calculated from the equation

$$n = \frac{v_{\text{ion}} - v_{\text{int}}}{-2.1} = \frac{v_{\text{ele}}}{-2.1} \quad (1-32)$$

Since the “traditional” partial molar volume of an ion is a value relative to v_{H^+} , the determination of the absolute value of v_{H^+} is very important in determining the absolute values of other ions. Millero[69] tabulated the values of v_{H^+} measured or estimated before the year 1971. In the table all the values are within the region of $0 \sim -8 \text{ cm}^3 \cdot \text{mol}^{-1}$, giving an average value of $-4.7 \pm 1 \text{ cm}^3 \cdot \text{mol}^{-1}$ if the two lowest values are excluded. Among these values, only the one given by Zana and Yeager[67], $v_{\text{H}^+} = -5.4 \text{ cm}^3 \cdot \text{mol}^{-1}$, was measured by experiment and therefore is widely accepted. Recently, Borsarelli[78] has employed laser-induced optoacoustic method and give a result of $-5.5 \text{ cm}^3 \cdot \text{mol}^{-1}$, which agrees well with the result reported several years earlier by Marcus[79].

1.3.3 Reaction volume

For a reaction from reactants (R) to products (P), the reaction volume is given by[80]

$$\Delta V = V_{\text{P}} - V_{\text{R}} \quad (1-33)$$

The reaction volume can be determined from (a) dilatometric or partial molar volume (density) measurements as described previously and subsequent calculation afterwards, (b) theoretical extrapolations [81] and (c) the pressure dependence of the equilibrium[82]. For the last method, in a reaction with equilibrium constant K , the following equation can be obtained:

$$d\Delta G = -RTd \ln K \quad (1-34)$$

Combining the Gibbs function equation

$$d\Delta G = -\Delta SdT + \Delta Vdp \quad (1-35)$$

then we can obtain

$$\Delta V = -RT \frac{d \ln K}{dp} \quad (1-36)$$

The measurement of the dependence of equilibrium constant on pressure will result in the reaction volume. The pressure employed could be as high as several kilobars. For detailed information about reaction volume in solution, please refer to the review articles by Asano et al[80, 82, 83].

1.3.4 Activation volume

According to the transition state theory proposed by Eyring in 1935 [84], there is a transition state between reactants and products:

Reactants (R) \leftrightarrow transition state (\ddagger) \rightarrow products (P)

The activation volume is defined as

$$\Delta V^\ddagger \equiv V^\ddagger - V_R \quad (1-37)$$

According to the assumptions of TST, the rate constant is interpreted as,

$$k = \kappa \frac{k_B T}{h} e^{-\Delta G^\ddagger / RT} = A e^{-\Delta G^\ddagger / RT} \quad (1-38)$$

This equation is called Eyring equation. Combining this equation and Gibbs function equation and if T is constant,

$$\left(\frac{\partial \ln k}{\partial p} \right)_T = \frac{-\Delta V^\ddagger}{RT} \quad (1-39)$$

Then the measurement of the dependence of $\ln k$ on p will yield ΔV^\ddagger . The activation volume is one of the very few properties of the transition state that can be accurately and easily determined (the activation enthalpy of transfer is another).

1.3.5 Surface volume excess and adsorption volume

Adsorption of hydrogen at Pt electrodes plays a key role in many electrocatalytic reactions, be it in dehydrogenative reactions, which are the first stage of alcohol oxidations [85], be it in hydrogenation of double or triple bonds, as the hydrogenation of ethene [86]. Adsorption of hydrogen is very sensitive to surface orientation and cleanliness; cyclic voltammetry in the hydrogen region therefore is an often used tool for the characterisation of single crystal electrodes.[87-90] Also the rate of hydrogen adsorption depends on the crystal orientation: it is fastest on Pt(111) both in alkaline and acidic solutions.[91-94]

From this adsorbed hydrogen, which manifests itself as a pseudocapacitive charge at potentials well above the equilibrium potential of hydrogen evolution, an adsorbed hydrogen has to be distinguished which is the intermediate during hydrogen evolution. Whereas the first type of adsorbed hydrogen cannot be observed by vibrational spectroscopies, while the second can.[95-97]

Despite of its importance, little is known on the adsorbed hydrogen, in particular on the “first” type. It is often assumed that on Pt (111) this is a hydrogen atom in threefold hollow site, which would explain its

invisibility by IR spectroscopy because of the small dynamic dipole moment.

Loewe et al have already reported on the determination of the volume of adsorption for the hydrogen adsorption reaction using a new dynamic pressure modulation technique.[98] Whereas usually for the determination of pressure dependences of chemical reactions measurements in the pressure range of up to 1000 bar (10^8 Pa) are performed, using our method activation and adsorption volumes can be determined by a pressure modulation with an amplitude of 1 bar. Changes of the volume in the adsorbed state or on the activated complex are largely determined by the charge density due to electrostriction, and therefore the volume of adsorption should give some information on the charge densities. The volume of adsorbates also could play a role in the interaction between AFM tips and the surface, because above a certain force (and thus pressure) exerted by the tip onto the surface adsorbates might be displaced. This could lead to an additional energy dissipation and thus friction.[99, 100]

The volume of adsorption is closely related to the surface volume excess, and, strictly speaking, only the latter can be directly measured.

1. Kissinger, P.T. and W.R. Heineman, *Laboratory Techniques in Electroanalytical Chemistry*. 2nd. ed. 1996: Marcel Dekker, Inc.
2. Kittel, C., *Einführung in die Festkörperphysik*. 12. ed. 1999, München: Oldenbourg Verlag.
3. Zangwill, A., *Physics at surfaces*. 1990, Cambridge: Cambridge University Press.
4. Somorjai, G., *Chemistry in Two Dimensions: Surfaces*. Baker non-resident lectureship in chemistry at Cornell University. 1981, Ithaca and London: Cornell University Press, Ltd., London.
5. Clavilier, J., K. El Achi, and A. Rodes, *xxx In situ characterization of the Pt(S)-[n(111)X(111)] electrode surfaces using electroadsorbed hydrogen for probing terrace and step sites*. Journal of Electroanalytical Chemistry, 1989. **272**: p. 253-261.
6. <http://www.mateck.de>
7. Clavilier, J., et al., *Preparation of monocrystalline Pt microelectrodes and electrochemical study of the plane surfaces cut in the direction of the {111} and {110} planes*. Journal of Electroanalytical Chemistry, 1980. **107**: p. 205-209.
8. Ross, P.N. and F.T. Wagner, *The Application of Surface Physics Techniques to the Study of Electrochemical Systems*, in *Advances in Electrochemistry and Electrochemical Engineering. XIII*, H. Gerischer and C.W. Tobias, Editors. 1984, Wiley-Interscience: N. York. p. 70-112.
9. Clavilier, J., *The role of anion on the electrochemical behaviour of a 111 platinum surface; an unusual splitting of the voltammogram in the hydrogen region*. Journal of Electroanalytical Chemistry, 1980. **107**: p. 211-216.
10. Clavilier, J., *Flame-annealing and cleaning technique*, in *Interfacial electrochemistry: theory, experiment, and applications*, A. Wieckowski, Editor. 1999, Marcel Dekker, Inc.: New York. p. 231-248.
11. Kibler, L.A., *Preparation and Characterization of Noble Metals Single Crystal Electrodes*. 2000: University of Ulm.
12. Bard, A.J. and L.R. Faulkner, *Electrochemical Methods: Fundamentals and Applications*. 2nd ed. 2001, New York, Weinheim: John Wiley & Sons Inc.
13. Winter, M. and R.J. Brodd, *What are batteries, fuel cells, and supercapacitors?* Chemical Reviews, 2004. **104**(10): p. 4245-4269.
14. McLean, G.F., et al., *An assessment of alkaline fuel cell technology*. International Journal of Hydrogen Energy, 2002. **27**(5): p. 507-526.
15. Li, Q.F., et al., *Approaches and recent development of polymer electrolyte membranes for fuel cells operating above 100 degrees C*. Chemistry of Materials, 2003. **15**(26): p. 4896-4915.

16. Watanabe, M., et al., *Activity and Stability of Ordered and Disordered Co-Pt Alloys for Phosphoric-Acid Fuel-Cells*. Journal of the Electrochemical Society, 1994. **141**(10): p. 2659-2668.
17. Acres, G.J.K., *Recent advances in fuel cell technology and its applications*. Journal of Power Sources, 2001. **100**(1-2): p. 60-66.
18. Park, S.D., J.M. Vohs, and R.J. Gorte, *Direct oxidation of hydrocarbons in a solid-oxide fuel cell*. Nature, 2000. **404**(6775): p. 265-267.
19. Minh, N.Q., *Ceramic Fuel-Cells*. Journal of the American Ceramic Society, 1993. **76**(3): p. 563-588.
20. Carrette, L., K.A. Friedrich, and U. Stimming, *Fuel cells: Principles, types, fuels and applications*. ChemPhysChem, 2000. **1**(4): p. 162-193.
21. Orimo, S.I., et al., *Complex hydrides for hydrogen storage*. Chemical Reviews, 2007. **107**(10): p. 4111-4132.
22. Baughman, R.H., A.A. Zakhidov, and W.A. de Heer, *Carbon nanotubes - the route toward applications*. Science, 2002. **297**(5582): p. 787-792.
23. Lin, J.Y., *Hydrogen storage in nanotubes*. Science, 2000. **287**(5460): p. 1929-1929.
24. *Porous glass microspheres store hydrogen, filter gases*. Advanced Materials & Processes, 2008. **166**(8): p. 18-18.
25. Chu, D. and R.Z. Jiang. *Comparative studies of polymer electrolyte membrane fuel cell stack and single cell*. 1999: Elsevier Science Sa.
26. Tian, N., et al., *Synthesis of tetrahedral platinum nanocrystals with high-index facets and high electro-oxidation activity*. Science, 2007. **316**(5825): p. 732-735.
27. Stamenkovic, V.R., et al., *Improved Oxygen Reduction Activity on Pt₃Ni(111) via Increased Surface Site Availability*. Science, 2007. **315**(5811): p. 493-497.
28. Zhang, J., et al., *Stabilization of platinum oxygen-reduction electrocatalysts using gold clusters*. Science, 2007. **315**(5809): p. 220-222.
29. Serov, A. and C. Kwak, *Review of non-platinum anode catalysts for DMFC and PEMFC application*. Applied Catalysis B-Environmental, 2009. **90**(3-4): p. 313-320.
30. Zhang, L., et al., *Progress in preparation of non-noble electrocatalysts for PEM fuel cell reactions*. Journal of Power Sources, 2006. **156**(2): p. 171-182.
31. Shukla, A.K. and R.K. Raman, *Methanol-resistant oxygen-reduction catalysts for direct methanol fuel cells*. Annual Review of Materials Research, 2003. **33**: p. 155-168.
32. Takenaka, S., et al., *Preparation of carbon nanotube-supported metal nanoparticles coated with silica layers*. Journal of Catalysis, 2008. **257**(2): p. 345-355.
33. Blanford, C.F., R.S. Heath, and F.A. Armstrong, *A stable electrode for high-potential, electrocatalytic O₂ reduction based on rational attachment of a blue copper oxidase to a graphite surface*. Chemical Communications, 2007(17): p. 1710-1712.
34. Reddy, A.L.M., N. Rajalakshmi, and S. Ramaprabhu, *Cobalt-polypyrrole-multiwalled carbon nanotube catalysts for hydrogen and alcohol fuel cells*. Carbon, 2008. **46**(1): p. 2-11.
35. Winther-Jensen, B., et al., *High rates of oxygen reduction over a vapor phase-polymerized PEDOT electrode*. Science, 2008. **321**(5889): p. 671-674.
36. Gong, K.P., et al., *Nitrogen-Doped Carbon Nanotube Arrays with High Electrocatalytic Activity for Oxygen Reduction*. Science, 2009. **323**(5915): p. 760-764.
37. Tian, Z., B. Ren, and B. Mao, *Extending surface raman spectroscopy to transition metal surfaces for practical applications. 1. Vibrational properties of thiocyanate and carbon monoxide adsorbed on electrochemically activated platinum surfaces*. Journal of Physical Chemistry B, 1997. **101**: p. 1338-1346.
38. Wang, H.C., et al., *In situ STM studies of electrochemical growth of nanostructured Ni films and their anomalous IR properties*. Journal of Physical Chemistry B, 2005. **109**(10): p. 4309-4316.
39. Savinova, E.R., F. Hahn, and N. Alonso-Vante, *Surface electrochemistry of CO as a probe molecule on carbon-supported Se-surface modified Ru nanoparticles via infrared reflection absorption spectroscopy*. Physical Chemistry Chemical Physics, 2007. **9**(42): p. 5693-5699.
40. Carrette, L., K.A. Friedrich, and U. Stimming, *Fuel Cells - Fundamentals and Applications*. Fuel Cells, 2001. **1**(1): p. 5-39.
41. Iwasita, T., *Chapter 41: Methanol and CO electrooxidation*. Handbook of Fuel Cells – Fundamentals, Technology and Applications, ed. H.A.G. Wolf Vielstich, Arnold Lamm. Vol. Volume 2: Electrocatalysis. 2003: John Wiley & Sons. 22.
42. Gilman, S., *The mechanism of Electrochemical oxidation of carbon monoxide and methanol on platinum II. The "Reactant-Pair" mechanism for electrochemical oxidation of carbon monoxide and methanol*. Journal of Physical Chemistry, 1964. **68**(1): p. 70-80.
43. Santos, E., E.P.M. Leiva, and W. Vielstich, *CO-adsorbate on Pt(111) single crystal surfaces*. Electrochimica Acta, 1991. **36**(3/4): p. 555-561.
44. Lebedeva, N.P., et al., *Mechanism and kinetics of the electrochemical CO adlayer oxidation on Pt(111)*.

- Journal of Electroanalytical Chemistry, 2002. **524**: p. 242-251.
45. Lebedeva, N.P., et al., *Role of crystalline defects in electrocatalysis: CO adsorption and oxidation on stepped platinum electrodes as studied by in situ infrared spectroscopy*. Journal of Physical Chemistry B, 2002. **106**(38): p. 9863-9872.
 46. Richarz, F., *Elektrochemisch erzeugte Pt-, Ru- und PtRu-Elektroden: Kinetik der Elektrooxidation von Kohlenmonoxid*, in *Institut für Physikalische und Theoretische Chemie*. 1995, Universität Bonn: Bonn. p. 90.
 47. Bottcher, A., et al., *CO oxidation reaction over oxygen-rich Ru(0001) surfaces*. Journal of Physical Chemistry B, 1997. **101**(51): p. 11185-11191.
 48. Stampfl, C. and M. Scheffler. *Density-functional theory study of the catalytic oxidation of CO over transition metal surfaces*. 1999: Elsevier Science Bv.
 49. Friedrich, K.A., et al., *Size dependence of the CO monolayer oxidation on nanosized Pt particles supported on gold*. Electrochimica Acta, 2000. **45**(20): p. 3283-3293.
 50. Peden, C.H.F., et al., *In situ FT-IR Study of the CO Oxidation Reaction over Ru(001) .1. Evidence for an Eley-Rideal Mechanism at High-Pressures*. Surface Science, 1991. **253**(1-3): p. 44-58.
 51. Srinivas.S and E. Gileadi, *Potential Sweep Method - a Theoretical Analysis*. Journal of the Electrochemical Society, 1965. **112**(8): p. C174-&.
 52. Palaikis, L., et al., *Surface electrochemistry of carbon monoxide adsorbed from electrolytic solutions at single crystal surfaces of Pt(111) and Pt(100)*. Surface Science, 1988. **199**: p. 183-198.
 53. Bergelin, M., et al., *Oxidation of CO adlayers on Pt(111) at low potentials: an impinging jet study in H₂SO₄ electrolyte with mathematical modeling of the current transients*. Journal of Electroanalytical Chemistry, 1999. **467**: p. 74-84.
 54. Love, B. and J. Lipkowski. *Effect of surface crystallography on electrocatalytic oxidation of Carbon monoxide on Platinum electrodes*. in *ACS Symposium Series*. 1988: Amer. Chemical Soc., 1155 16th St, NW, Washington, DC 20036.
 55. Koper, M.T.M., et al., *Monte Carlo simulations of a simple model for the electrocatalytic CO oxidation on platinum*. Journal of Chemical Physics, 1998. **109**: p. 6051-6062.
 56. McCallum, C. and D. Pletcher, *An investigation of the mechanism of the oxidation of carbon monoxide adsorbed onto a smooth Pt electrode in aqueous acid*. Journal of Electroanalytical Chemistry, 1976. **70**: p. 277-290.
 57. Herrero, E., et al., *Temperature dependence of CO chemisorption and its oxidative desorption on the Pt(111) electrode*. Langmuir, 2000. **16**(11): p. 4779-4783.
 58. Garcia, G. and M.T.M. Koper, *Stripping voltammetry of carbon monoxide oxidation on stepped platinum single-crystal electrodes in alkaline solution*. Physical Chemistry Chemical Physics, 2008. **10**(25): p. 3802-3811.
 59. Inkaew, P. and C. Korzeniewski, *Kinetic studies of adsorbed CO electrochemical oxidation on Pt(335) at full and sub-saturation coverages*. Physical Chemistry Chemical Physics, 2008. **10**(25): p. 3655-3661.
 60. Maillard, F., E.R. Savinova, and U. Stimming, *CO monolayer oxidation on Pt nanoparticles: Further insights into the particle size effects*. Journal of Electroanalytical Chemistry, 2007. **599**(2): p. 221-232.
 61. Kucernak, A.R. and G.J. Offer, *The role of adsorbed hydroxyl species in the electrocatalytic carbon monoxide oxidation reaction on platinum*. Physical Chemistry Chemical Physics, 2008. **10**(25): p. 3699-3711.
 62. Breiter, M.W., *Comparative-Study of Carbon-Monoxide Adsorption and Oxidation of the Chemisorbed Species at Smooth and Platinized Platinum-Electrodes*. Journal of Electroanalytical Chemistry, 1979. **101**(3): p. 329-340.
 63. Vidal-Iglesias, F.J., et al., *CO monolayer oxidation on stepped Pt(S) [(n - 1)(1 0 0) × (1 1 0)] surfaces*. Electrochimica Acta, 2009. **54**(19): p. 4459-4466.
 64. Spendelow, J.S., et al., *Mechanism of CO oxidation on Pt(111) in alkaline media*. Journal of Physical Chemistry B, 2006. **110**(19): p. 9545-9555.
 65. Atkins, P.W., *Physical Chemistry, 4th ed*. 1990, Oxford: Oxford University Press.
 66. Hefter, G. and Y. Marcus, *A critical review of methods for obtaining ionic volumes in solution*. Journal of Solution Chemistry, 1997. **26**(3): p. 249-266.
 67. Zana, R. and E. Yeager, *Ultrasonic Vibration Potentials and Their Use in the Determination of Ionic Partial Molal Volumes*. Journal of Physical Chemistry, 1967. **71**(No. 3): p. 521 - 536.
 68. Uosaki, K., N. Tokura, and Y. Kondo, *Apparent Molar Volumes of Tetraalkylammonium Halides in Liquid Sulfur-Dioxide*. Bulletin of the Chemical Society of Japan, 1972. **45**(3): p. 871-&.
 69. Millero, F.J., *Molal Volumes of Electrolytes*. Chemical Reviews, 1971. **71**(2): p. 147-&.
 70. Conway, B.E., Desnoyer, J.E., and R.E. Verrall, *Extrapolation Procedures for Evaluation of Individual Partial Gram Ionic Volumes*. Journal of Physical Chemistry, 1971. **75**(19): p. 3031-&.
 71. Mukerjee, P., *On Ion-Solvent Interactions .1. Partial Molal Volumes of Ions in Aqueous Solution*.

- Journal of Physical Chemistry, 1961. **65**(5): p. 740-&.
72. Kozlov, I.L. and N.P. Novoselov, *Separation of Boundary-Values of Electrolyte Partial Mole Volumes for Ionic Components*. Zhurnal Fizicheskoi Khimii, 1988. **62**(1): p. 219-221.
73. Marcus, Y., *Thermodynamic Functions of Transfer of Single Ions from Water to Nonaqueous and Mixed-Solvents .4. Selection of Extrathermodynamic Assumptions*. Pure and Applied Chemistry, 1986. **58**(12): p. 1721-1736.
74. Jolicoeur, C. and J.C. Mercier, *Ionic Scale for Partial Molal Heat-Capacities of Aqueous-Electrolytes from Chemical-Models*. Journal of Physical Chemistry, 1977. **81**(11): p. 1119-1121.
75. Kay, R.L., Faraday Discuss. Chem. Soc., 1977, 64, 252
76. Letcher, T.M., J.J. Paul, and R.L. Kay. *Apparent Molar Volumes of Crown-Ether Complexes in Several Solvents at 25-Degrees-C - an Estimation of Ionic Electrostriction*. 1991: Plenum Publ Corp.
77. Padova, J., *Ion-Solvent Interaction .2. Partial Molar Volume and Electrostriction - a Thermodynamic Approach*. Journal of Chemical Physics, 1963. **39**(6): p. 1552-&.
78. Borsarelli, C.D. and S.E. Braslavsky, *The partial molar volume of the proton in water determined by laser-induced optoacoustic studies*. Journal of Photochemistry and Photobiology B-Biology, 1998. **43**(3): p. 222-228.
79. Marcus, Y., *A Simple Empirical-Model Describing the Thermodynamics of Hydration of Ions of Widely Varying Charges, Sizes, and Shapes*. Biophysical Chemistry, 1994. **51**(2-3): p. 111-127.
80. Asano, T. and J. Lenoble, *Activation and Reaction Volumes in Solution*. Chemical Reviews, 1978. **78**(4): p. 407-489.
81. Pollmann, P., D. Rehm, and A. Weller, *Influence of Pressure on Hetero-Excimer Formation .2. Different Donor-Acceptor-Systems in N-Hexan*. Berichte Der Bunsen-Gesellschaft-Physical Chemistry Chemical Physics, 1975. **79**(8): p. 692-696.
82. Drljaca, A., et al., *Activation and Reaction Volumes in Solution*. 3. Chemical Reviews, 1998. **98**: p. 2167 - 2290.
83. van Eldik, R., T. Asano, and W.J. Le Noble, *Activation and reaktion volumes in solution*. Chemical Reviews, 1989. **89**: p. 549-688.
84. Eyring, H., *The Activated Complex in Chemical Reactions*. J. Chem. Phys., 1935. **3**(2).
85. Lanova, B., H. Wang, and H. Baltruschat, *Methanol Oxidation on Carbon Supported Pt and Ru -Modified Pt Nanoparticles: a Comparison with Single Crystal and Polycrystalline Electrodes*. Fuel Cells, 2006. **6**(3-4): p. 214-222.
86. Müller, U., et al., *Adsorption and hydrogenation of simple alkenes at Pt-group metal electrodes studied by DEMS: influence of the crystal orientation*. Surface Science, 1995. **335**: p. 333-342.
87. Clavilier, J. and D. Armand, *Electrochemical induction of changes in the distribution of hydrogen adsorption states on Pt(100) and Pt(111) surfaces in contact with sulphuric acid solutions*. J ELECTROANAL CHEM, 1986. **199**: p. 187-200.
88. Clavilier, J., et al., *Electrochemical Adsorption Behaviour of Platinum Stepped Surfaces in Sulphuric Acids Solutions*. Journal of Electroanalytical Chemistry, 1986. **205**: p. 267-277.
89. Clavilier, J., et al., *Electrochemical behaviour of the Pt(111)-As system in acidic medium: adsorbed hydrogen and hydrogen reaction*. Journal of Electroanalytical Chemistry, 1990. **294**: p. 193.
90. Furuya, N. and S. Koide, *Hydrogen adsorption on platinum single-crystal surfaces*. Surface Science, 1989. **220**: p. 18-28.
91. Oelgeklaus, R., J. Rose, and H. Baltruschat, *On the rate of hydrogen and iodine adsorption on polycrystalline Pt and Pt(111)*. Journal of Electroanalytical Chemistry, 1994. **376**: p. 127-133.
92. Morin, S., H. Dumont, and B.E. Conway, *Evaluation of the effect of two-dimensional geometry of Pt single-crystal faces on the kinetics of upd of H using impedance spectroscopy*. Journal of Electroanalytical Chemistry, 1996. **412**: p. 39-52.
93. Langkau, T. and H. Baltruschat, *The rate of anion and hydrogen adsorption on Pt(111) and Rh(111)*. Electrochimica Acta, 1998. **44**: p. 909-918.
94. Sibert, E., R. Faure, and R. Durand, *High frequency impedance measurements on Pt(111) in sulphuric and perchloric acids*. Journal of Electroanalytical Chemistry, 2001. **515**(1-2): p. 71-81.
95. Nichols, R.J. and A. Bewick, *SPECTROSCOPIC IDENTIFICATION OF THE ADSORBED INTERMEDIATE IN HYDROGEN EVOLUTION ON PLATINUM*. Journal of Electroanalytical Chemistry, 1988. **243**(2): p. 445-453.
96. Kunitatsu, K., et al., *In situ infrared spectroscopic and electrochemical study of hydrogen electro-oxidation on Pt electrode in sulfuric acid*. Journal of Electroanalytical Chemistry, 2006. **587**(2): p. 299-307.
97. Tadjeddine, A. and A. Peremans, *Vibrational spectroscopy of the electrochemical interface by visible infrared sum frequency generation*. Journal of Electroanalytical Chemistry, 1996. **409**: p. 115-121.
98. Loewe, T. and H. Baltruschat, *Pressure modulation, a new dynamic technique for the electrochemical determination of adsorption, reaction and activation volumes*. Physical Chemistry Chemical Physics,

2005. **7**(2): p. 379-384.
99. Nielinger, M. and H. Baltruschat, *Nanotribology under Electrochemical Conditions: Influence of a Copper (Sub)Monolayer Deposited on Single Crystal Electrodes on Friction Forces Studied with Atomic Force Microscopy*. Physical Chemistry Chemical Physics, 2007. **9**: p. 3965.
100. Hausen, F., et al., *Nanotribology at single crystal electrodes: Influence of ionic adsorbates on friction forces studied with AFM*. Electrochimica Acta, 2008. **53**(21): p. 6058-6063.

2. Materials, instruments and methods

2.1 Chemicals

The chemicals used are listed in Table 2-1. All the solution were prepared using water from a Millipore-Q water system with TOC less than 3 ppb and a specific resistance of 18 M Ω -cm or higher.

Table 2-1 Chemicals used in this work.

Formula / Name	Company	Purity (degree)	Usage in this work
H ₂ SO ₄	Merck	Supra pure, 95-97%	Supporting electrolyte
Li ₂ SO ₄	Merck	Supra pure, 99.99%	Cation effect experiment
Na ₂ SO ₄	Fluka	≥ 99%	Cation effect experiment
K ₂ SO ₄	Merck	p.a., ≥ 99%	Cation effect experiment
Cs ₂ SO ₄	Fluka	p.a., ≥ 99.5%	Cation effect experiment
RuCl ₃	Acros organics	35-40% Ru	Ru deposition on Pt(665)
SnCl ₂	Aldrich	99.995+%	Sn deposition on Pt(332)
HCl	KMF	37%	Supporting electrolyte for Ag/AgCl
CO	Praxair	4.7	CO oxidation experiment
Ar	Praxair	5.0	Deairing the solution and maintaining inert atmosphere
H ₂	Air Liquide	5.0	Cooling atmosphere for Pt(665) & Pt(332)
K ₃ Fe(CN) ₆	Riedel-deHaën	p.a., 99%	Test experiment for pressure modulation
Pt wire	Chempur	99.99%	Reference and working electrode
Ag	Degussa		Reference electrode
Pt(poly)	Metal crystals		Working electrode for CO oxidation experiment
Pt(111)	Ma Teck		Working electrode for CO oxidation experiment
Pt(665)	Metal crystals		Working electrode for CO oxidation experiment
Pt(332)	Metal crystals		Working electrode for CO oxidation experiment

2.2 Glassware

All the glassware was cleaned and degreased before the experiment. Degreasing was achieved by storing the glassware in 6 M KOH overnight. To remove trace amount of metal ions, the glassware was soaked overnight in chromic acid (640ml of concentrated H₂SO₄ + 360ml H₂O + 21.4 g CrO₃). From the STM experiment carried out by Michael et al in our group, it demonstrated that cleaning with Chromic acid is not

necessary if no metal ion is among the contaminants. Due to the toxicity of Cr^{6+} , cleaning in a water steam system is an alternative choice. From the experience by our group, cleaning with hot steam for 2 hours is enough to sweep the contaminants away in most cases.

A simple procedure can be adopted to check the cleanliness of the glassware as well as the solution. Using a Pt electrode as the working electrode, the potential is cycled in the supporting electrolyte until a steady CV is reached and then held in double layer region for several minutes before continuing the scan. If the hydrogen or oxygen adsorption is not suppressed, then the glass cell and solution are clean enough. Otherwise the cell should be cleaned again or maybe the solution should also be prepared again.

2.3 Electrochemical instrumentation

2.3.1 Potentiostat and Lock-in Amplifier

A potentiostat of model 273 (EG&G, Princeton applied research) is employed for the i/E measurement. The basic diagram for potentiostat is already shown in previous chapter (figure 1-5) of this thesis. A Lock-in Amplifier of type 5210 (EG&G), combined with the potentiostat, is used for the ac voltammetry measurement, the sketch of which is already shown in previous chapter as figure 1-6. With the ac voltage imposed to the Potentiostat from Lock-in Amplifier, the ac current thus generated is then separated from the dc current and recorded by the Lock-in Amplifier. Components of amplitude and phase or real and imaginary parts with respect to the phase of the input ac potential were evaluated. The data for potential, current and ac components are collected by a PC with the help of a data acquisition card and a Labview program.

2.3.2 The cells

In a normal voltammetric experiment, a three-electrode cell system is employed, as shown in Figure 2-1. The reference electrode compartment is connected to the cell body with a lugging capillary while separated in some extent with a grounded glass stopcock so that different solution from that in body cell could be used to keep the electrode from contamination of metal ions. The counter electrode compartment is separated by a fritted glass disk from the main part. On the body cell, there are several ports serving as gas inlet, gas outlet, solution inlet and so on. For the measurements of impedance or ac voltammetry, a special cell, hereafter called “Z-cell” since it’s especially for impedance (“Z”) measurement, with little differences from the cell described above was used. Here, the counter electrode, usually a Pt foil, is put inside the cell body and is placed exactly in front of the working electrode in order to increase the conductance and ensure a homogenous current distribution.

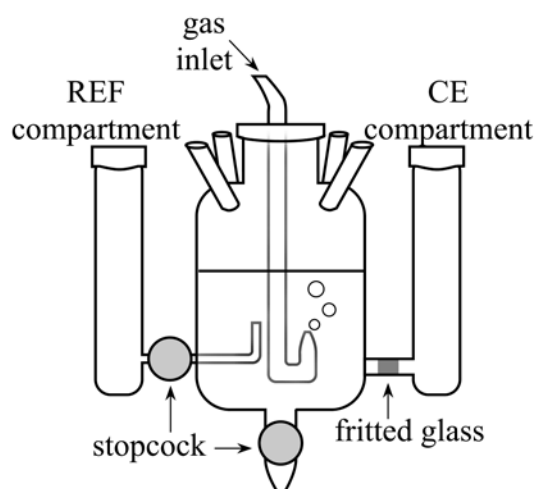


Figure 2-1. A typical cell for voltammetry measurement. Copied from [1]

2.3.3 The setup for pressure modulation

The setup for pressure modulation is shown in Figure 2-2. It is the same as that used by Loewe et al [2]. The glass cell (outer diameter: 20 mm, height: 30 mm) is made out of NB16b glass (Schott), which has special thermal expansion coefficients for sealing 3 platinum wires (0.5 mm diameter) into the glass as electrodes. For the working and counter electrodes identical Pt wire were used with an exposed length of typically 7 mm and the reference electrode was either PtO_x or freshly prepared Ag/AgCl entangled on the Pt wire. Underneath the glass cell there is a force sensor, type 9321 B (Kistler), which is mounted on a fixed base plate to measure the pressure. The pressure modulation is transmitted from the piezo-transducer, type PA41 (Physik Instrumente) and controlled by a self made piezo driver and a lock-in amplifier, via the head made out of PVDF (Polypenco), sealed with an O-ring made out of perbunan (2 mm diameter). It is attached to a height adjustable plate. Both plates are connected by three columns made out of steel. The bevel of the glass cell has an angle of 60° whereas at the head, the angle of the bevel is 55° . Thus the O-ring is self-tightening upon pressing perpendicularly onto the glass cell. The whole setup is inside of a chamber which can be vacuumized by a membrane pump, in order to remove from the solution the air, which would lead to bubbles with pressure change. The diagram for the connection of pressure modulation experiment is shown in Figure 2-3.

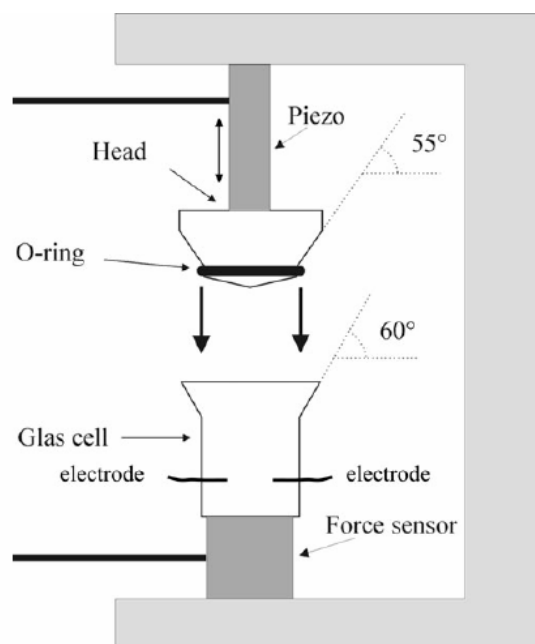


Figure 2-2. Setup of the pressure modulation cell (only two of the three electrodes are shown). Copied from [2].

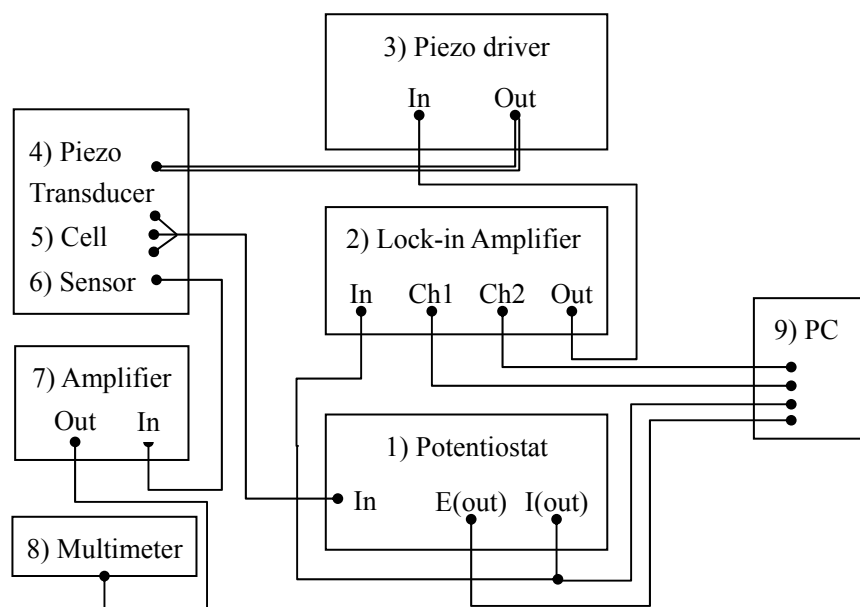


Figure 2-3. Diagram of the pressure modulation connection.

2.4 Experimental procedures

2.4.1 Preparation of the single crystal electrodes

Pt(111) is prepared according to the flame annealing method [3, 4]. After cleaning by cycling into the oxygen adsorption region for several times and rinsing carefully with water, the crystal is annealed in a

butane flame. After keeping it at red colour for 1 minute, the crystal is cooled down under strong Ar flow for 4 minutes before the experiment. The quality of the crystal can be checked by CV and judged according to the height of the typical spike at about 0.45 V. The stepped crystals Pt(665) and Pt(332) were flame-annealed in the same way as Pt(111) but cooled down under the mixture of Ar and H₂ (4:1) above water in another cell. The hydrogen is added to remove trace amount of oxygen which leads to expansion of the terrace width [5]. The crystal was transferred to the working cell after cooling down with the protection of a water droplet on the surface.

2.4.2 Preparation of reference electrodes: RHE and Ag/AgCl

A reversible hydrogen electrode (RHE) was usually used as reference electrode in the cell for voltammetry or impedance. The inside containing the Pt wire is well vacuumized with a water pump. After refilling with electrolyte, H₂ is generated by electrolysis to partially fill the bulb, as shown in Figure 2-4. This process should be repeated at least three times to ensure the purity of the hydrogen inside. Finally the bulb is half-filled with H₂ so that the Pt wire has contact with both H₂ gas and the electrolyte. Freshly prepared RHE is employed for the work of each day.

An Ag/AgCl reference electrode was used for the pressure modulation experiments. A thin layer of AgCl was formed by exposing half of the Ag wire in a 0.1 M HCl solution for half an hour. Then the Ag/AgCl wire was entangled to one of the Pt wire in the pressure modulation cell and served as reference electrode. The Ag/AgCl reference electrode should also be newly made every day to have a stable potential.

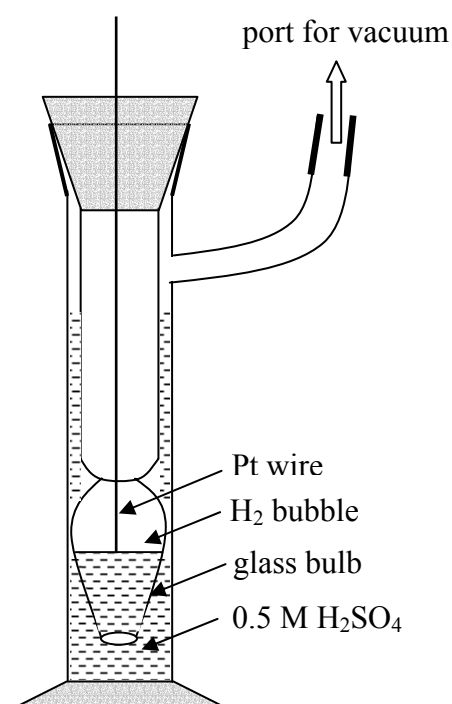


Figure 2-4. Construction of the reversible hydrogen electrode.

2.4.3 CO oxidation experiment.

Before each measurement, the solution was degassed for at least 10 minutes to get rid of oxygen. Polycrystalline platinum, denoted as Pt(poly), was cleaned by cycling in the potential range of 0.05~1.5 V for more than half an hour until the CV was stable and displayed the typical features. After the quality of the surface was guaranteed, 2 ml of CO saturated H₂SO₄, of the same concentration as the supporting electrolyte in cell, was injected into the cell from above with the potential held at 0.07 V for CO adsorption. After 5 minutes of adsorption, CO was saturated on the surface and then the solution was exchanged with fresh and degassed electrolyte while remaining the potential and keeping the contact between the solution and crystal surface. Afterwards the electrode surface was kept in meniscus with the solution and waiting for 2-3 minutes to make sure the wall of the crystal is dried. The CV or current transient and ac voltammetry was record with small ac voltage imposed. After the adsorbed CO oxidation completely, a CV was record to check the absence of CO in solution and also the quality of crystal.

2.4.4 Pressure modulation experiment

First of all the pressure modulation cell is filled with electrolyte and placed on the force sensor. The base plate where the piezo-transducer fastened is adjusted coarsely (ca. 5 mm above the glass cell). After that the surrounding chamber is closed and evacuated for about 2 hours until no bubbles evolved from the electrolyte anymore. The vacuumizing process is important since any bubble in solution will result in failure when imposed with pressure. Then the glass cell is tightened with the head by an O-ring with the force moment of 1.5 N·m. This tightening process leads to a certain “prepressure”. For each measurement, a control experiment was performed with the ac voltage applied to the piezo-transducer, but only with loose mechanical contact between the piezo-transducer head and the cell. Thus, a mere electrical cross talk between the piezo-transducer and the electrochemical cell could be excluded. Before each experiment, the electrode is cleaned by cycling the potential until a steady CV is obtained. During each experiment, the potential, dc current, pressure and ac current (with real and imaginary parts, or amplitude and phase angle) were recorded simultaneously.

2.4.5 Calibration of the force sensor

The force sensor is connected with an amplifier and is calibrated as follows: put a weight with mass of 0.5695 kg ($G=mg$) on the force sensor and suddenly take off it, and measure the voltage out of the amplifier (\tilde{V}_{out}) in the mean time. This process is repeated several times for averaging and thus reducing the deviation. The negative voltage transients induced by taking off the weight is displayed in Figure 2-5 and giving the same peak voltage. The expansion of the framed part in (a) is displayed in Figure 2-5(b), from which it's clear that the voltage is not going to infinite at the time of unloading the weight. The ratio (k) of force to voltage is thus calculated by dividing the weight with the peak voltage.

$$k = \frac{G}{\tilde{V}_{\text{out}}} = \frac{0.5695 \text{ kg} \times 9.811 \text{ m} \cdot \text{s}^{-2}}{0.208 \text{ V}} = 26.86 \text{ N} \cdot \text{V}^{-1}$$

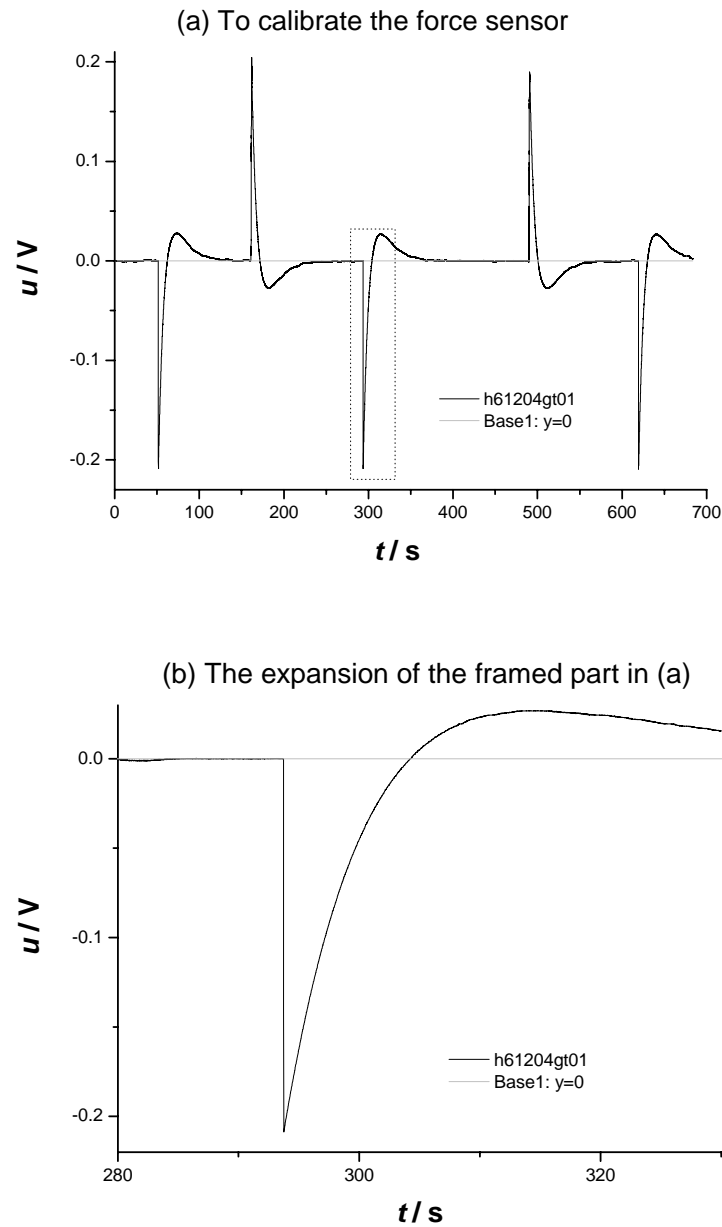


Figure 2-5. The $u \sim t$ curve for calibration of the force sensor.

The ratio of pressure to voltage of the force sensor K is calculated as the following.

$$K = \frac{k}{A} = \frac{26.86 \text{ N} \cdot \text{V}^{-1}}{\pi \times (1.15 \times 10^{-2} \text{ m})^2} = 6.46 \times 10^4 \text{ pa} \cdot \text{V}^{-1} = 0.638 \text{ bar} \cdot \text{V}^{-1}$$

Here A is the projected area of the contact surface of head and solution. The pressure and the voltage should be accordance with each other, i.e., both are effective values or amplitudes. And the pressure enforced from the O-ring directly to the glass instead of the solution could be ignored since the compressibility of water is much smaller than the O-ring.

1. F.Hernandez, Characterization of Electrodeposited Pd Adlayers on Stepped Gold Single Crystals, PhD dissertation, University of Bonn, 2006
2. Loewe, T. and H. Baltruschat, *Pressure modulation, a new dynamic technique for the electrochemical determination of adsorption, reaction and activation volumes*. Physical Chemistry Chemical Physics, 2005. **7**(2): p. 379-384.
3. Clavilier, J., et al., *Preparation of monocrystalline Pt microelectrodes and electrochemical study of the plane surfaces cut in the direction of the $\{111\}$ and $\{110\}$ planes*. Journal of Electroanalytical Chemistry, 1980. **107**: p. 205-209.
4. Clavilier, J., K.E. Achi, and A. Rodes, *In situ characterisation of the Pt(S)-[$n(111) \times (111)$] electrode surfaces using electrosorbed hydrogen for probing terrace and step sites*. Journal of Electroanalytical Chemistry, 1989. **272**: p. 253-161.
5. Samjeské, G., X.-Y. Xiao, and H. Baltruschat, *Ru decoration of stepped Pt single crystals and the role of the terrace width on the electrocatalytic CO oxidation*. Langmuir, 2002. **18**(12): p. 4659-4666.

3 Determination of the apparent charge transfer coefficient for CO oxidation on various Pt surfaces

3.1 Principles and calculations

3.1.1 Principles

For an electrochemical reaction, the current i can be described as a function of potential E and of adsorbate coverage θ , as shown in the following.

$$i = nFk_{\text{app}}(E)f(\theta) \quad (3-1)$$

Here n is the number of electrons transferred; F is Faraday constant, with a value of $96485 \text{ C}\cdot\text{mol}^{-1}$; $f(\theta)$ is a function of coverage and here θ is the fractional coverage ($\theta = \Gamma/\Gamma_{\text{max}}$); $k_{\text{app}}(E)$ is the apparent rate constant depending on E . Imposing log function on both sides of equation (3-1), and then taking the differential with respect to E , we get

$$\frac{1}{i} \cdot \frac{\partial i}{\partial E} = \frac{\partial \ln i}{\partial E} = \frac{\partial \ln k_{\text{app}}(E)}{\partial E} + \frac{\partial \ln f(\theta)}{\partial E} \quad (3-2)$$

According to Eyring equation, the rate constant for a reaction can be written as,

$$k = \frac{k_{\text{B}}T}{h} e^{-\Delta G^{\ddagger}/RT} \quad (3-3)$$

where ΔG^{\ddagger} is the Gibbs energy of activation, k_{B} is Boltzmann's constant, and h is Planck's constant, R is gas constant and T is absolute temperature. For an electrochemical process with potential involved, the reaction can be modified as

$$k(E) = k^0 e^{\alpha nFE/RT} \quad (3-4)$$

Here k^0 is the rate constant at a reference potential E_0 . α is the charge transfer coefficient, also called symmetry factor ($0 < \alpha < 1$, typically 0.5). Then the first item in equation (3-2) can be written as,

$$\frac{\partial \ln k_{\text{app}}(E)}{\partial E} = \frac{\alpha' nF}{RT} \quad (3-5)$$

where α' is the apparent charge transfer coefficient. For the second item, we can get,

$$\frac{\partial \ln f(\theta)}{\partial E} = \frac{\partial \ln f(\theta)}{\partial \theta} \frac{\partial \theta}{\partial E} \quad (3-6)$$

If a small ac voltage $u_{\text{ac}} = u_{\text{A}} \cdot \sin(\omega t)$ is superimposed during the electrochemical reaction, then

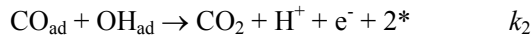
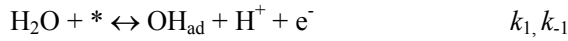
$$\left(\frac{\partial i}{\partial E}\right) \approx \frac{i_{ac}}{u_{ac}} \quad (3-7)$$

If the imposed ac voltage is small in amplitude and high enough in frequency, then the coverage of the adsorbed species can be considered as independent of the ac potential. Thereafter, the second item in the right side of equation (3-2) can be neglected and then the following equation can be obtained:

$$\alpha' = \frac{RT}{nF} \cdot \frac{i_{ac-re}}{i_{dc} u_{ac}} \quad (3-8)$$

Thus, from equation (3-8), α' can be determined by imposing an ac voltage. It is worth to note that α' can be determined at a given potential and coverage. The Tafel slope ($RT/\alpha'nF$) for the reaction can also be easily calculated. This method is much better than the traditional method that can only determine a value of α' or Tafel slope from current values measured over a wide range of potentials and fixed coverage.

This method can be easily applied to the measurement of α' or Tafel slope for CO oxidation. According to the Langmuir-Hinshelwood mechanism described in the first chapter, there are two steps in the oxidation of adsorbed CO,



$$i = nFv = nFk_2\theta_{\text{CO}}\theta_{\text{OH}} \cdot e^{\alpha_2 FE/RT} \quad (3-9)$$

Since OH_{ad} is an intermediate present at low concentration, steady state conditions can be assumed. Then

$$\frac{d\theta_{\text{OH}}}{dt} = k_1(1 - \theta_{\text{CO}} - \theta_{\text{OH}}) \cdot e^{\alpha_1 FE/RT} - k_{-1}\theta_{\text{OH}} \cdot e^{-(1-\alpha_1)FE/RT} - k_2\theta_{\text{CO}}\theta_{\text{OH}} \cdot e^{\alpha_2 FE/RT} = 0 \quad (3-10)$$

Rearrangement yields:

$$\theta_{\text{OH}} = \frac{k_1(1 - \theta_{\text{CO}})}{k_1 + k_{-1} \cdot e^{-FE/RT} + k_2\theta_{\text{CO}} \cdot e^{(\alpha_2 - \alpha_1)FE/RT}} \quad (3-11)$$

At low potential, $k_{-1} \cdot e^{-FE/RT} \gg k_1 + k_2\theta_{\text{CO}} \cdot e^{(\alpha_2 - \alpha_1)FE/RT}$; then the current can be written as

$$\begin{aligned} i &= nFk_2\theta_{\text{CO}} \frac{k_1(1 - \theta_{\text{CO}})}{k_{-1} \cdot e^{-FE/RT}} \cdot e^{\alpha_2 FE/RT} \\ &= nFKk_2\theta_{\text{CO}}(1 - \theta_{\text{CO}}) \cdot e^{(1+\alpha_2)FE/RT} \end{aligned} \quad (3-12)$$

Where $K (=k_1/k_{-1})$ is the equilibrium constant for OH adsorption.

At high potential, if $k_1 \gg k_{-1} \cdot e^{-FE/RT} + k_2\theta_{\text{CO}} \cdot e^{(\alpha_2 - \alpha_1)FE/RT}$,

$$i = nFk_2\theta_{\text{CO}}(1 - \theta_{\text{CO}}) \cdot e^{\alpha_2 FE/RT} \quad (3-13)$$

In the case of high potential and if $k_2\theta_{\text{CO}} \cdot e^{(\alpha_2-\alpha_1)FE/RT} \gg k_{-1} \cdot e^{-FE/RT} + k_1$,

$$\begin{aligned} i &= nFk_2\theta_{\text{CO}} \frac{k_1(1-\theta_{\text{CO}})}{k_2\theta_{\text{CO}} \cdot e^{(\alpha_2-\alpha_1)FE/RT}} \cdot e^{\alpha_2FE/RT} \\ &= nFk_1(1-\theta_{\text{CO}}) \cdot e^{\alpha_1FE/RT} \end{aligned} \quad (3-14)$$

According to previous equations (3-1) to (3-5), equations (3-12) to (3-14) can be generalized as the following,

$$\begin{aligned} i &= nFk_{\text{app}}(E)f(\theta_{\text{CO}}) \\ &= nFk'f(\theta_{\text{CO}}) \cdot e^{\alpha'FE/RT} \end{aligned} \quad (3-15)$$

Where k' is the apparent rate constant at a reference potential. Then the apparent charge transfer coefficient can be expressed as,

$$\alpha' = \begin{cases} 1 + \alpha_2 & \text{At low potential} \\ \alpha_1 \text{ or } \alpha_2 & \text{At high potential} \end{cases}$$

Since α_i is typically 0.5, then from low to high potential, α' will give values from about 1.5 to 0.5, and the Tafel slope will increase from $40 \text{ mV} \cdot \text{dec}^{-1}$ to $120 \text{ mV} \cdot \text{dec}^{-1}$, which agree with the simulation by Koper et al.[1]

3.1.2 Correction for slow ion adsorption

In practice, the effect of ion adsorption, including ions of OH^- and $\text{HSO}_4^-/\text{SO}_4^{2-}$, should be taken into account. The equivalent circuit during CO oxidation process can be interpreted as in Figure 3-1.

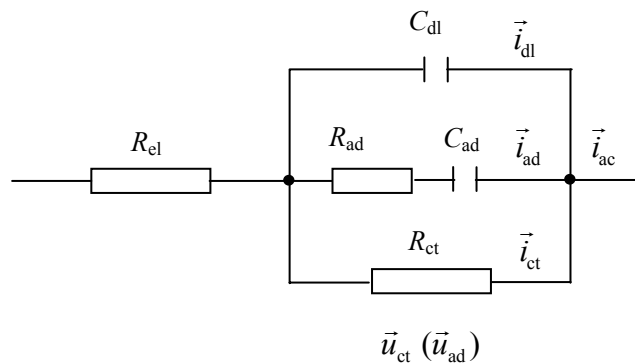


Figure 3-1. Equivalent circuit during CO oxidation process.

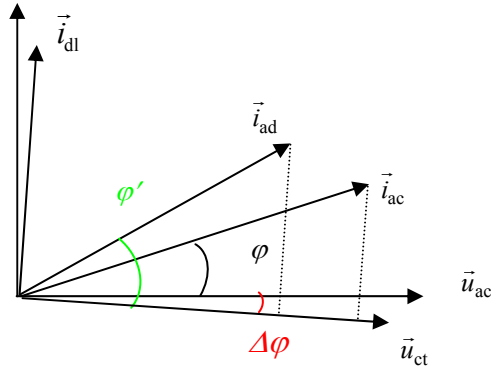


Figure 3-2 A diagram of the phasors and related phase angles during CO oxidation.

Here R_{el} is the electrolyte resistance, C_{dl} the double layer capacitance, R_{ct} the charge transfer resistance for CO oxidation, R_{ad} and C_{ad} the adsorption resistance and capacitance, respectively. A diagram of the phasors and related phase angles during CO oxidation is displayed in Figure 3-2. The ac voltage across the charge transfer resistance, u_{ct} , can be calculated from the measurement using the following equation.

$$\vec{u}_{ct} = \vec{u}_{ac} - \vec{i}_{ac} \cdot R_{el} = |u_{ct}| \cdot (\cos(-\Delta\varphi) + j\sin(-\Delta\varphi)) \quad (3-16)$$

Here, $-\Delta\varphi$ is the phase shift of ac voltage over the charge transfer resistance for CO oxidation with reference to the imposed ac potential. From equation (3-16), $|u_{ct}|$ and $\Delta\varphi$ can be calculated. In practice, R_{el} is smaller than $2 \text{ Ohm}\cdot\text{cm}^2$, and thus the difference of the absolute values of between u_{ct} and u_{ac} is less than 3 per cent so for $|u_{ct}|$ the value of $|u|$ can be taken in the calculation. Normally the phase shift $\Delta\varphi$ is less than 2° . If the ac current has a phase shift of φ versus the ac voltage imposed, then the ac current in phase with \vec{u}_{ct} is $i_{ac} \cdot \cos(\varphi + \Delta\varphi)$, which includes the contribution of charge transfer process of CO oxidation and ad/desorption process of ions and can be written as the following equation:

$$i_{ac} \cdot \cos(\varphi + \Delta\varphi) = i_{ct} + i_{ad} \cdot \cos(\varphi') \quad (3-17)$$

Here φ' is the phase shift of \vec{i}_{ad} versus \vec{u}_{ct} . The second term in equation (3-17) can be interpreted according to the impedance of the adsorption process as the following.

$$i_{ad} \cdot \cos(\varphi') = u_{ct} \cdot \frac{R_{ad}}{|Z_{ad}|} = u_{ct} \cdot \frac{R_{ad}}{R_{ad}^2 + \frac{1}{(\omega C_{ad})^2}} \quad (3-18)$$

Since both $1/R_{ad}$ and C_{ad} are proportional to the surface area of CO free site, $(1-\theta_{CO})$, the contribution from ion ad/desorption, equation (3-18), is also proportional to $(1-\theta_{CO})$ if the small change of potential over the adsorption impedance is ignored. This contribution is expressed as follows:

$$i_{ad} \cdot \cos(\varphi') = i_{ad(\text{CO-free})} \cdot \cos(\varphi') \cdot (1-\theta_{CO}) \quad (3-19)$$

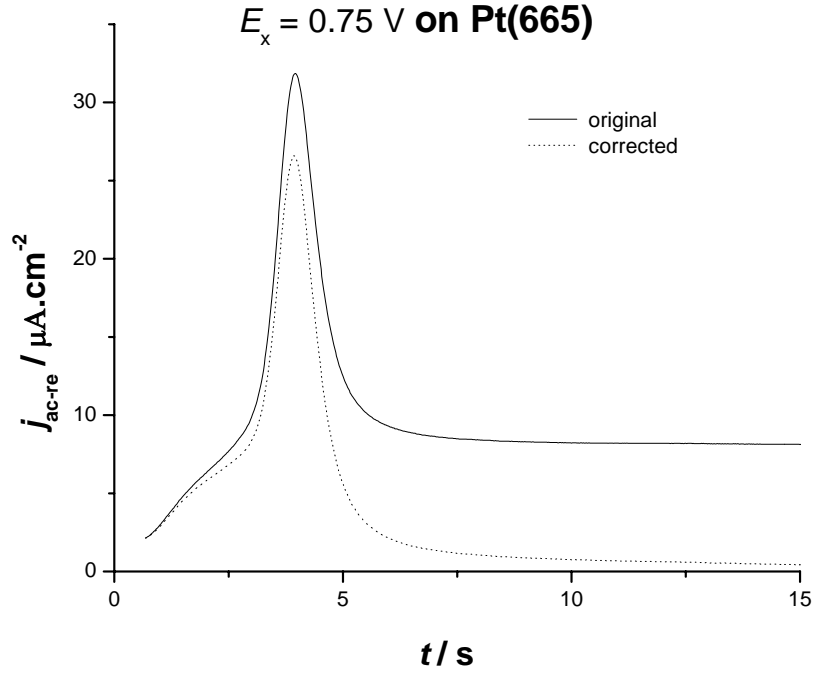


Figure 3-3 Correction of the real part of ac current due to ion ad/desorption process to. Black line: original; black dotted: corrected; red line: absolute correction; green dashed: relative correction. $E_{ac} = 3$ mV.

The ratio of CO free surface can be determined by integration of the dc current, as shown in the following:

$$1 - \theta_{CO} = \frac{Q_{CO-OX}}{Q_{CO-OX(max)}} = \frac{\int_{t_0}^t i_{dc} dt}{\int_{t_0}^{\infty} i_{dc} dt} \quad (3-20)$$

Since the contribution of $i \cdot R$ can be ignored, the real part of the ac current on the CO free surface originates from slow ion adsorption, as proved from the impedance measurements presented later. Then from equation (3-17) to (3-19) we can obtain the following equation:

$$i_{ct} = i_{ac} \cdot \cos(\varphi + \Delta\varphi) - i_{ac(CO-free)} \cdot \cos(\varphi') \cdot (1 - \theta_{CO}) \quad (3-21)$$

Equation (3-21) can be used for the accurate calculation. But the calculation process is complicated. The calculation can be simplified according to the following: since $\Delta\varphi$ is very small compared with φ and $(90^\circ - \varphi)$, so $\cos(\varphi + \Delta\varphi) \approx \cos(\varphi)$; Thus equation (3-21) can be approximated as:

$$i_{ct} \approx i_{ac-re} - i_{ac-re(CO-free)} \cdot (1 - \theta_{CO}) \quad (3-22)$$

One example of the correction for CO oxidation on Pt(665) at 0.75 V according to equation (3-22) is

shown in Figure 3-3, with the original and corrected real part of ac current, the absolute and relative correction demonstrated. Replace i_{ac-re} in equation (3-8) with i_{ct} in equation (3-22), then the apparent transfer coefficient can be determined from the following equation:

$$\alpha' = \frac{RT}{nF} \frac{1}{i_{dc}} \cdot \frac{i_{ac-re} - i_{ac-re(CO-free)} \cdot (1 - \theta_{CO})}{u_{ac}} \quad (3-23)$$

In many cases at high potential, $i_{ac-re(CO-free)} \ll i_{ac-re(CO-OX)}$, e.g., the correction due to ion ad/desorption is less than 5%, then the value of i_{ac-re} can be taken for that of i_{ct} in the calculation.

3.2 Polycrystalline platinum

3.2.1 Cyclic voltammetry (CV) and electrochemical impedance spectroscopy (EIS)

A disk polycrystalline Pt electrode, denoted as Pt(poly), with geometric area 0.785 cm^2 (diameter of 1 cm) was employed. A typical CV is displayed in Figure 3-4, from which two pairs of peaks are observed at 0.12 V and 0.26 V, corresponding to hydrogen ad/desorption on (110) and (100) facets. The small shoulder between the two H-desorption peaks is widely recognized as the sign of the cleanness of Pt(poly). The hydrogen ad/desorption charge is integrated to be $229.6 \mu\text{C}$ in the potential region of 0.07~0.45 V. The real surface area is calculated to be 1.093 cm^2 taking the specific charge of $210 \mu\text{C}\cdot\text{cm}^{-2}$ for H adsorption on Pt. The current plateau starting at 0.8V corresponds to the adsorption of oxygen species, first OH and then O, and the reduction of them takes place at 0.76 V, giving rise to a large negative peak.

The EIS was recorded for bared Pt(poly) in 0.5 M H_2SO_4 in order to have a rough idea of the circuits and the related parameters. Two models of equivalent circuits were employed to fit the recorded values. A model with a resistor (R_1) in series with the parallel combination of a capacitor (C_1) and series-wound another resistor (R_2) and capacitor (C_2), as shown in Figure 3-6(a) denoted as $R_1-(C_1||R_2-C_2)$, is employed and the fitting data is shown in Table 3-1. R_2 and C_2 represent the resistance and capacitance of adsorption process. Since the surface is far from homogenous as the perfect low-index single crystals, another model with C_2 replaced by a constant phase element (CPE), as shown in Figure 3-6(b), leaves to a better fit to the experimental data; the fitting values are tabulated in Table 3-2. From the EIS we can see that the phase angle is also shifted to remarkably lower than 90° , e.g., the phase angle of impedance at both 0.85 V and 0.9 V are shifted to 76° , which proved the existence of low speed adsorption. This is the reason for using the complicated scheme of Figure 3-1 for the correction.

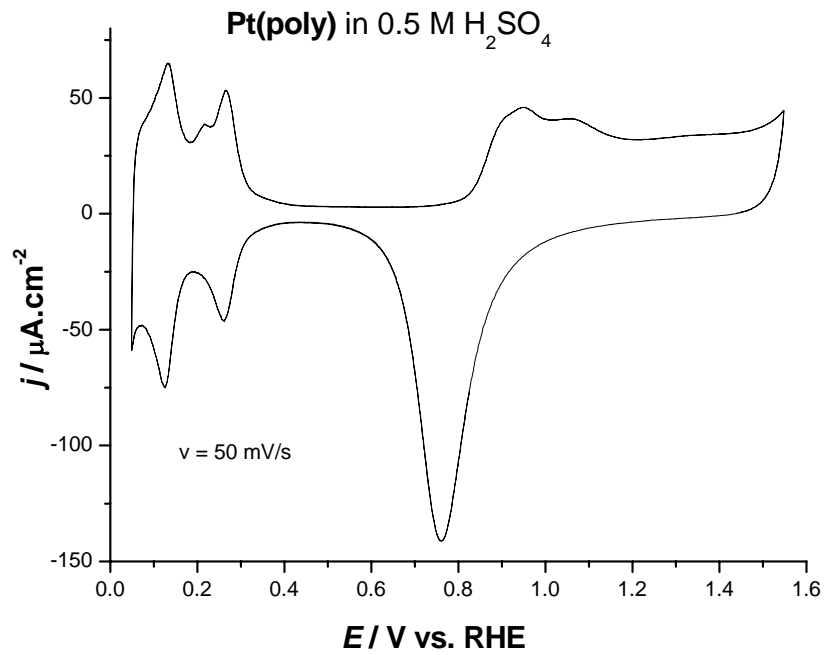


Figure 3-4. CV of polycrystalline platinum in 0.5 M H₂SO₄. $v = 50 \text{ mV}\cdot\text{s}^{-1}$.

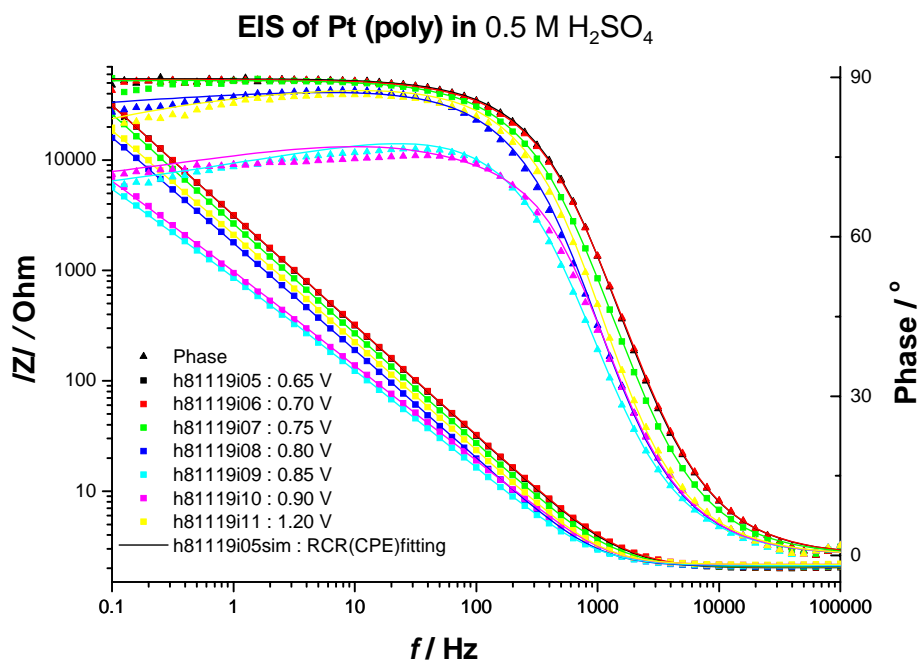


Figure 3-5. The EIS of Pt(poly) in 0.5 M H₂SO₄ at various potentials.

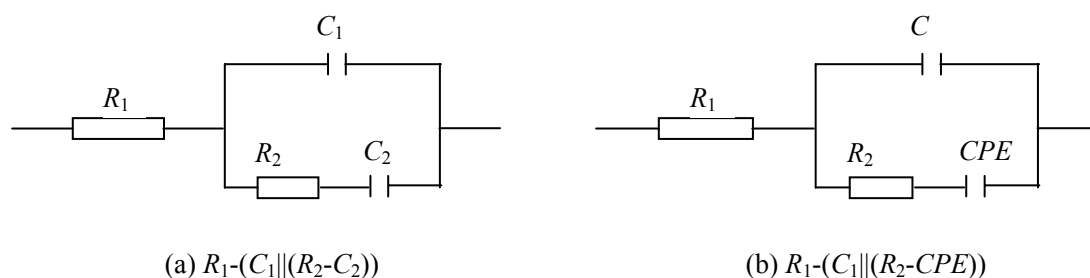


Figure 3-6 Equivalent circuits used for the fitting of the EIS results.

 Table 3-1 The fitting data for the EIS on Pt(poly) using $R_1-(C_1||R_2-C_2)$ model.

E / V	filename	R_1 / Ω	C_1 / F	R_2 / Ω	C_2 / F
0.65	h81119i05	2.021	4.457E-5	19.23	5.6645E-6
0.7	h81119i06	2.048	4.4151E-5	27.46	5.7517E-6
0.75	h81119i07	2.062	5.2976E-5	35.62	6.5345E-6
0.8	h81119i08	2.121	8.21E-5	19443	1.7853E-5
0.85	h81119i09	2.157	1.0474E-4	782	1.3171E-4
0.9	h81119i10	2.186	8.7351E-5	510.7	1.0576E-4
1.2	h81119i11	2.176	6.9934E-5	35506	2.01E-5

 Table 3-2 The fitting data for the EIS on Pt(poly) using $R_1-(C_1||R_2-CPE)$ model.

E / V	filename	R_1 / Ω	C_1 / F	R_2 / Ω	CPE_1	$CPE_1(+)\alpha$
0.65	h81119i05	2.02	4.39E-05	13.73	6.82E-06	0.98137
0.7	h81119i06	2.044	4.31E-05	16.09	7.60E-06	0.96985
0.75	h81119i07	2.06	5.16E-05	18.24	9.16E-06	0.95762
0.8	h81119i08	2.103	7.42E-05	24.97	2.36E-05	0.79949
0.85	h81119i09	2.121	6.94E-05	2.1255E-6	2.00E-04	0.71934
0.9	h81119i10	2.168	7.11E-05	32.97	1.59E-04	0.72885
1.2	h81119i11	2.172	6.65E-05	132.2	1.89E-05	0.98137

3.2.2 Potential sweep measurement

After adsorbing CO on the electrode surface at 0.07 V to saturation (5 minutes is enough), the CO-containing solution in cell is replaced with CO-free solution while holding the potential and maintaining the contact of the electrode and the solution. The current for oxidation of adsorbed CO during a potential sweep on polycrystalline Pt versus the sweeping potential is displayed in Figure 3-7. With the potential sweep rate of $10 \text{ mV}\cdot\text{s}^{-1}$, a peak current of $57.5 \mu\text{A}\cdot\text{cm}^{-2}$ is recorded located at 0.69V. A typical

prepeak can also be observed at around 0.54 V, similar to those observed by other researchers [2, 3]. The real part of the ac current, which is mainly arising from the Faraday current of CO oxidation with ac voltage imposed, is expanded by a factor of 20 for better comparison and shows similar features as the dc current. The j_{ac-re} is nearly zero at a potential lower than 0.45 V since no reaction takes place on the CO blocked surface, indicating that the main contribution of j_{ac-re} comes from the Faraday current. After CO oxidation is completed, instead of falling to zero, the j_{ac-re} still gives a remarkable value, which is due to anion adsorption on the CO-free solution. The slow anion adsorption had been demonstrated by the electrochemical impedance spectroscopy (EIS) shown previously, in which the phase at low frequency deviated gradually from 90° to 75° with the potential increase from 0.7 to 0.85 V, indicating an increasing slow adsorption process in addition to double layer charging.. The apparent charge transfer coefficient, which is calculated according to equation (3-23), is also plotted versus the scanning potential (blue line), as shown in Figure 3-8(b). The values around the potential of the main peak and prepeak are 1.47 and 0.53, corresponding to Tafel slopes of $40 \text{ mV}\cdot\text{dec}^{-1}$ and $111 \text{ mV}\cdot\text{dec}^{-1}$, respectively. It is worth mentioning that the coefficient measured around the main peak, i.e., for a CO coverage between 1/3 and 2/3, is most reliable since the corresponding signal of both ac and dc current are higher than that at higher or lower coverage, giving a high ratio of signal to noise, and also less affected by anion adsorption.

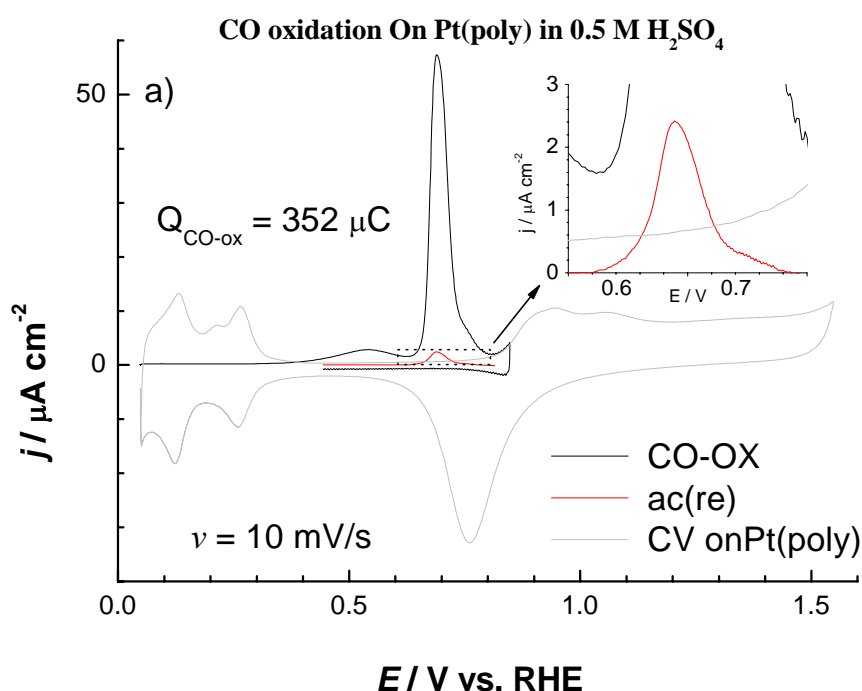


Figure 3-7 Oxidation of adsorbed CO on Pt(poly) with potential sweep in 0.5 M H₂SO₄. $u_{ac} = 1 \text{ mV}$. Black: dc current in CO oxidation; red: ac current in real part; grey: CV with CO free.

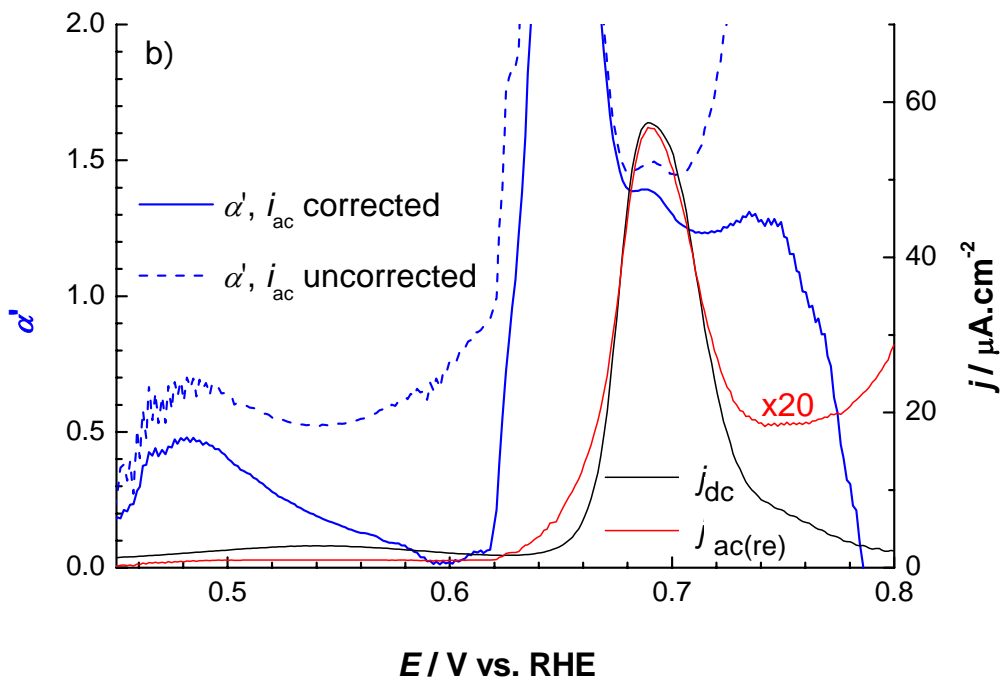


Figure 3-8 Apparent transfer coefficient for CO oxidation on Pt(poly). Blue line: α' with $j_{ac(re)}$ uncorrected; Blue dashed: α' with $j_{ac(re)}$ corrected; black: dc current; red dotted: real part of ac current (corrected, $\times 20$).

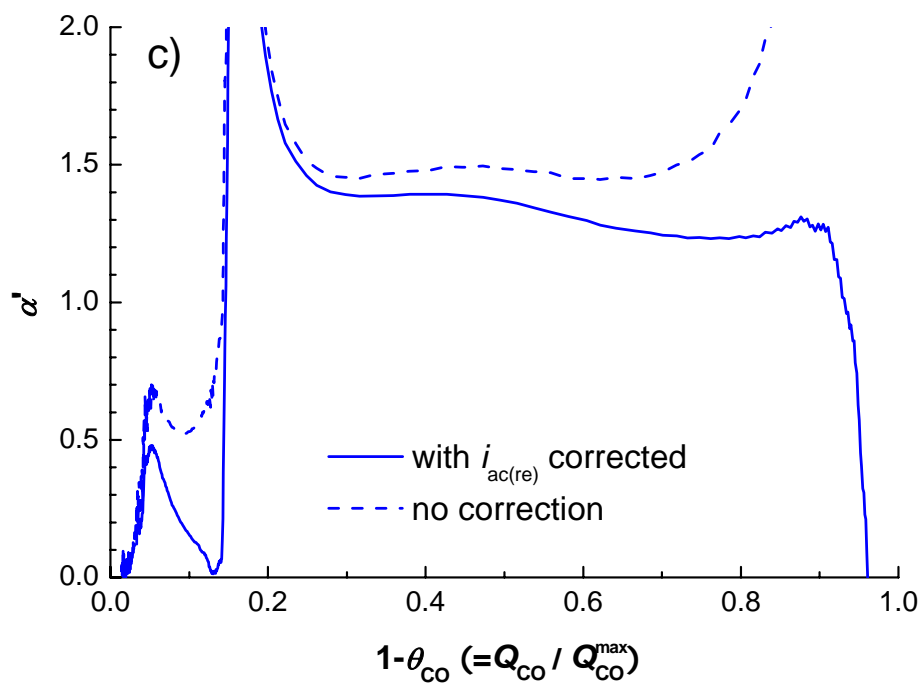


Figure 3-9 Apparent transfer coefficient (blue) versus $(1 - \theta_{CO})$. Blue line: α' with correction; Blue dashed: α' without correction.

3.2.3 Potential step experiments

The current transients for CO oxidation at various potentials are displayed in (a) and (b) of Figure 3-10. The peak current (j_{\max}) and the time of the current maximum (t_{\max}) are listed in Table 3-3. A general trend is observed that, j_{\max} increased and t_{\max} decreased with the increase of E . However, not all the values of j_{\max} and t_{\max} are in accordance with this trend, e.g., the current at 0.75 V is smaller than that at 0.73V and the same phenomenon is observed for the real part of the ac current, as shown in Figure 3-11, which is due to small disturbance of the surface by potential cycling to oxygen adsorption region each time after CO oxidation completed. This disorder is due to the difference of surface conditions, which play a large role in determination of the onset potential for CO oxidation and the maximum current.

Table 3-3 t_{\max} and j_{\max} for CO oxidation on Pt(poly) at various potentials.

E / V	filename	t_{\max} / s	$-\log(t_{\max})$	$j_{\max} / \mu\text{A}$	$\log(j_{\max})$
0.65	h81118xy04	13.8	-1.13988	12.35	1.09167
0.67	h81118xy09	14.5	-1.16137	16.24	1.21059
0.69	h81118xy11	14.2	-1.15229	17.81	1.25066
0.71	h81118xy13	11.2	-1.04922	27.31	1.43632
0.73	h81118xy15	3.62	-0.55871	83.63	1.92236
0.75	h81118xy17	4.07	-0.60959	74.47	1.87198
0.77	h81118xy19	2.06	-0.31387	161	2.20683
0.79	h81118xy21	3.01	-0.47857	111.1	2.04571
0.81	h81118xy23	1.91	-0.28103	187.2	2.27231
0.83	h81118xy25	1.58	-0.19866	205.4	2.3126
0.85	h81118xy27	1.21	-0.08279	236.4	2.37365

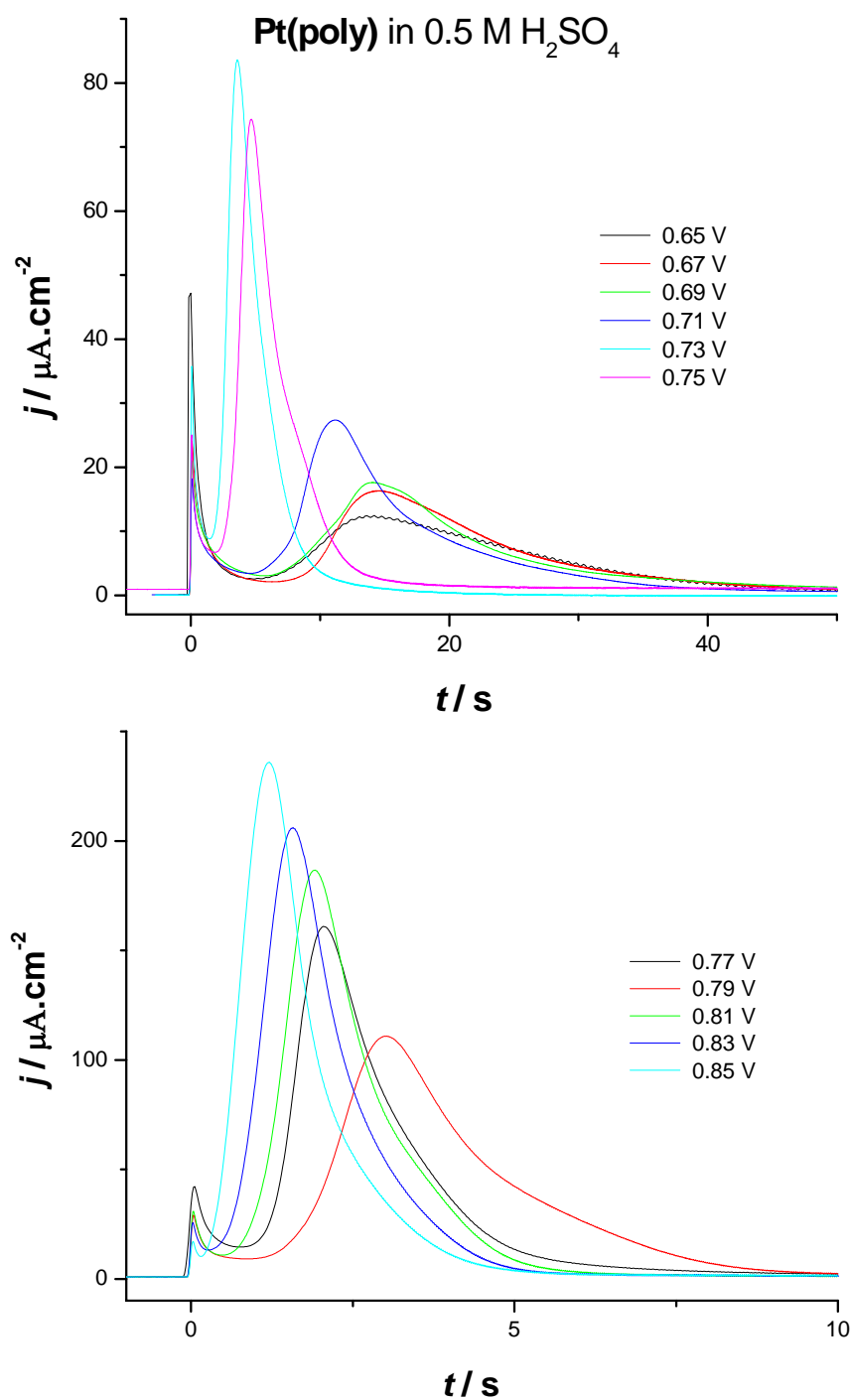


Figure 3-10. The current transients for CO oxidation on Pt(poly) at various stepped potentials. Solution: 0.5 M H₂SO₄.

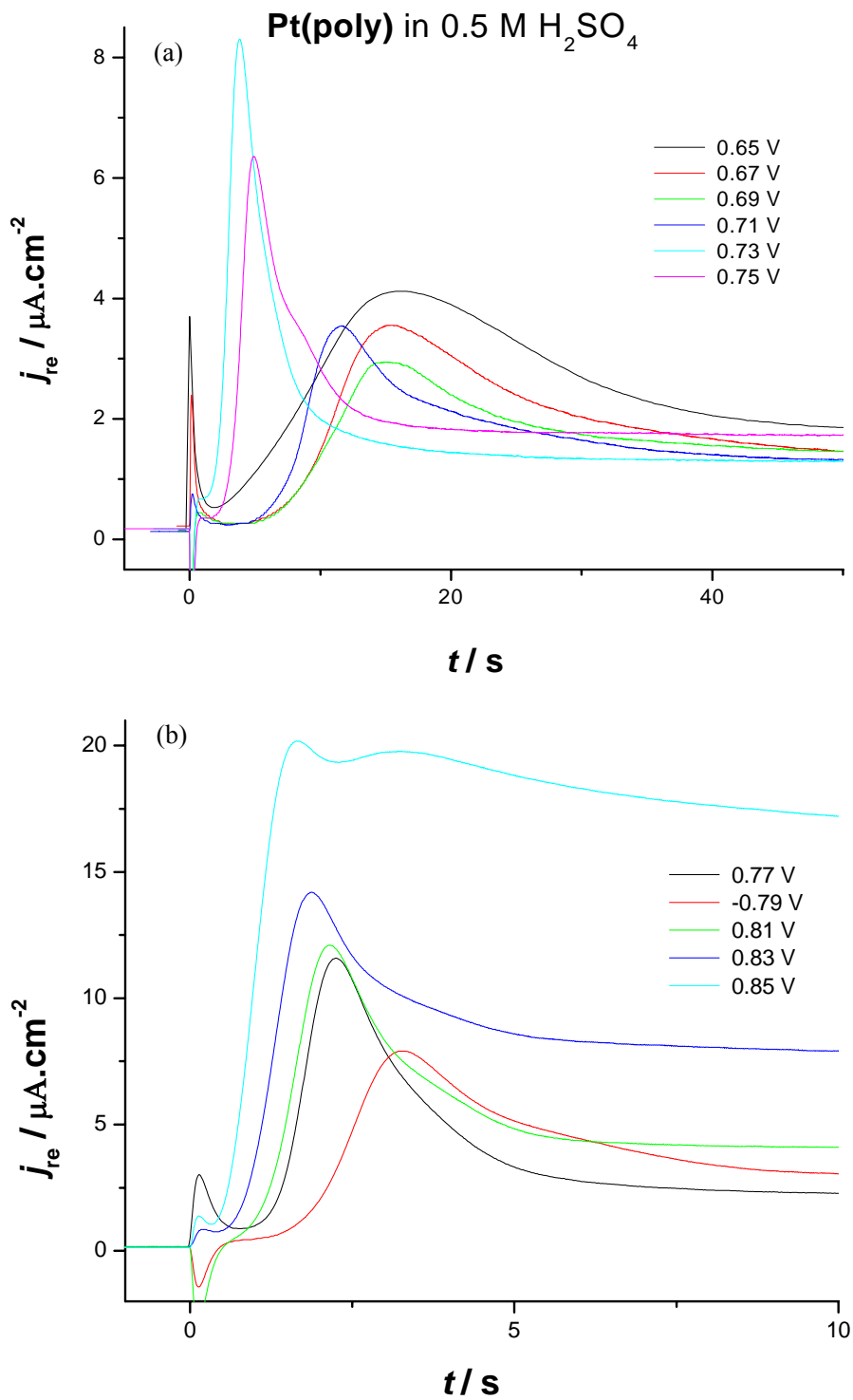


Figure 3-11. The ac currents in real part for CO oxidation on Pt(poly) at various stepped potentials. Solution: 0.5 M H₂SO₄. $u_{ac} = 3$ mV.

The imaginary parts of the ac current for CO oxidation at potential 0.69 V and 0.83 V are also displayed in Figure 3-12 together with their corresponding real parts for the sake of comparison. It's obvious that the

imaginary part, which is arising from the capacitance of double layer charging and anion adsorption, increases steeply during the CO oxidation process and finally reaches a constant value. The imaginary part is much larger than the real part, which indicates that a small phase shift will result in much deviation of the calculated result or much more complex in calculation.

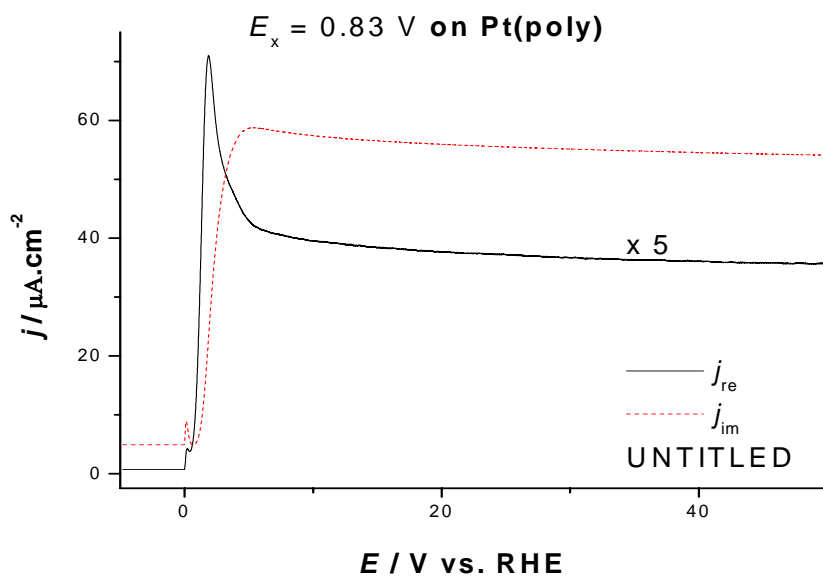
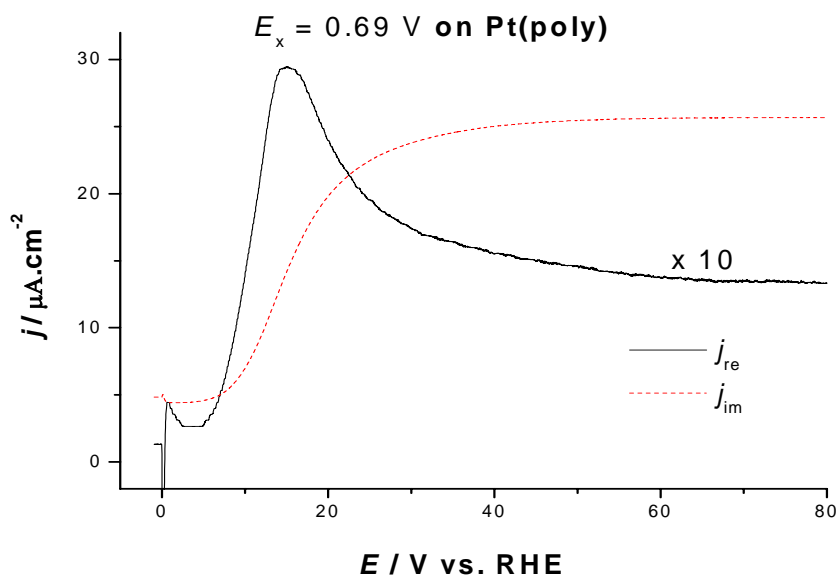


Figure 3-12. The real (black, magnified) and imaginary part (red dotted) of the ac current. $u_{ac} = 3 \text{ mV}$.

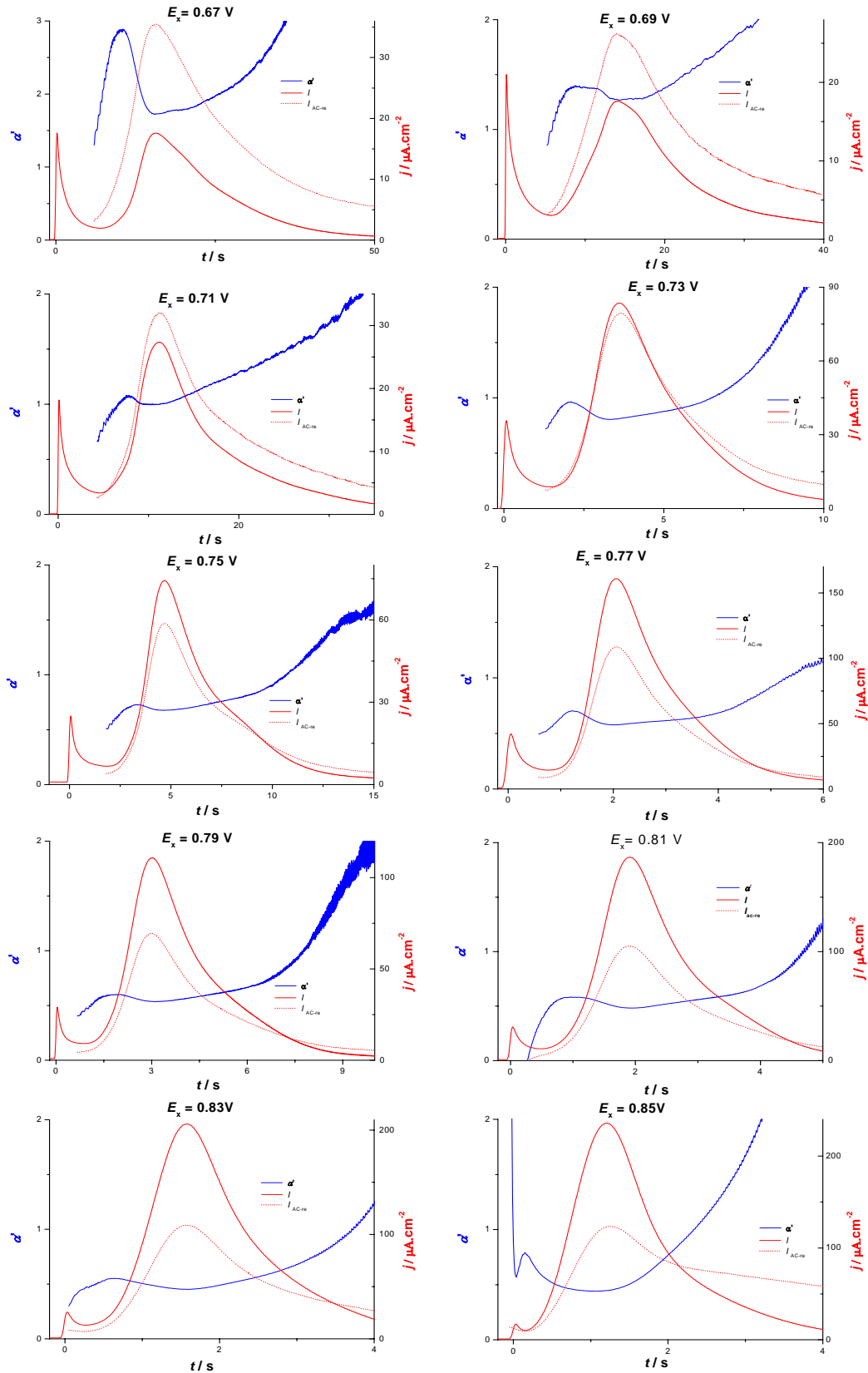


Figure 3-13. The apparent transfer coefficient (blue) for CO oxidation on Pt(poly) at various potentials. The dc current (red) and real part of ac current ($\times 10$, corrected, real dotted) are also displayed.

The charge transfer coefficients for CO oxidation at various potentials are plotted separately in Figure 3-13. The dc current and the modified real part of ac current are also shown. In the plots, the coefficients at a CO coverage between 1/4 to 3/4 are nearly constant for almost all the potentials applied, indicating that the mechanism doesn't change with the CO coverage and also demonstrating the reliability of this method in measuring the α' for CO oxidation. It's understandable that with less than 1/4 of the surface covered by CO, the calculation of the coefficient is largely affected by the signal of ad/desorption process of anions, as shown in the imaginary part of Figure 3-12, and result in non-reliable values. The part of current plateau just prior to the current peak gives a coefficient of around 0.5 for all the stepped potentials measured, similar to that of prepeak for CO oxidation with potential scanning shown previously. The plateau current, especially those at low stepped potentials, are widely believed to have the same origin as the prepeak in potential scanning experiment.[2, 4-7] The change of CO coverage (black) with time during CO oxidation was plotted as an example, see Figure 3-14, from which we can clearly see that α' is almost constant with the coverage change in most of the coverage range.

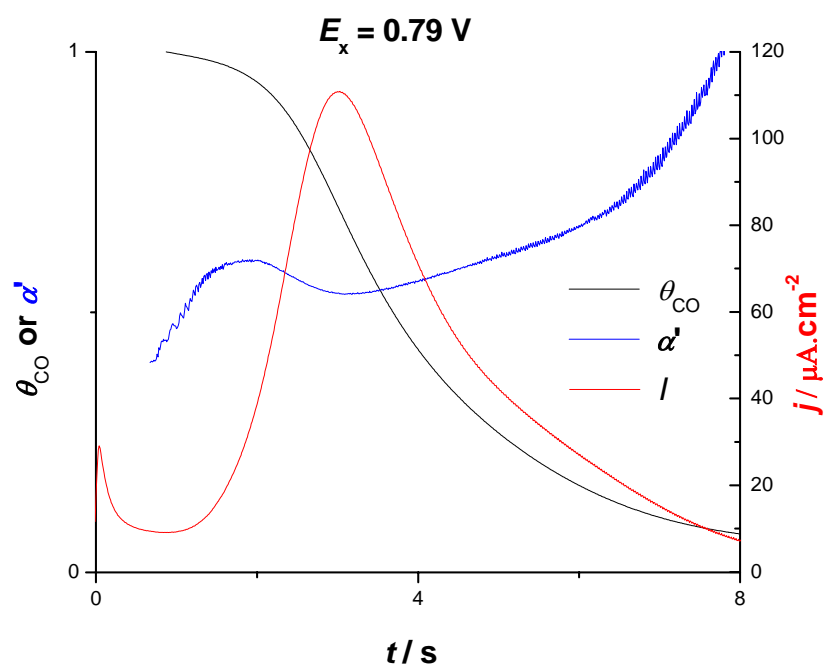


Figure 3-14. The change of CO coverage (black) with time during CO oxidation at 0.79 V. The apparent charge transfer coefficient (blue) and current transient (red) are added for comparison.

The charge transfer coefficient at the current peak is plotted versus the corresponding step potential, see Figure 3-15. It's obvious that, with potential increasing, the apparent transfer coefficient decreases from values between 1 and 2 to an almost constant value of about 0.45, which signifies a considerable change of the potential dependence of the apparent rate constant. The Tafel slope is calculated to be 35

$\text{mV}\cdot\text{dec}^{-1}$ at 0.67V, and increases to $133 \text{ mV}\cdot\text{dec}^{-1}$ at 0.83 V and 0.85 V. The apparent transfer coefficient at the plateau part is measured to be ca. 0.5 for all the potentials, and gives a Tafel slope of about $120 \text{ mV}\cdot\text{dec}^{-1}$. From the literature, McCallum [8] reported a value of $120 \text{ mV}\cdot\text{dec}^{-1}$ for the main peak on Pt wire by plotting $\log(i) \sim E$ and Kucernak [9] reported 105 and $100 \text{ mV}\cdot\text{dec}^{-1}$ for the main peak by plotting $\log(j_{\text{max}}) \sim E$ and $\log(t_{\text{max}}) \sim E$, which are between the slopes I obtained at low and high potentials. Kucernak also reported 119 and $82 \text{ mV}\cdot\text{dec}^{-1}$ for the current plateau part by plotting $\log(j_{\text{min}}) \sim E$ and $\log(t_{\text{min}}) \sim E$, in which the first value is in good agreement with the one reported in this work..

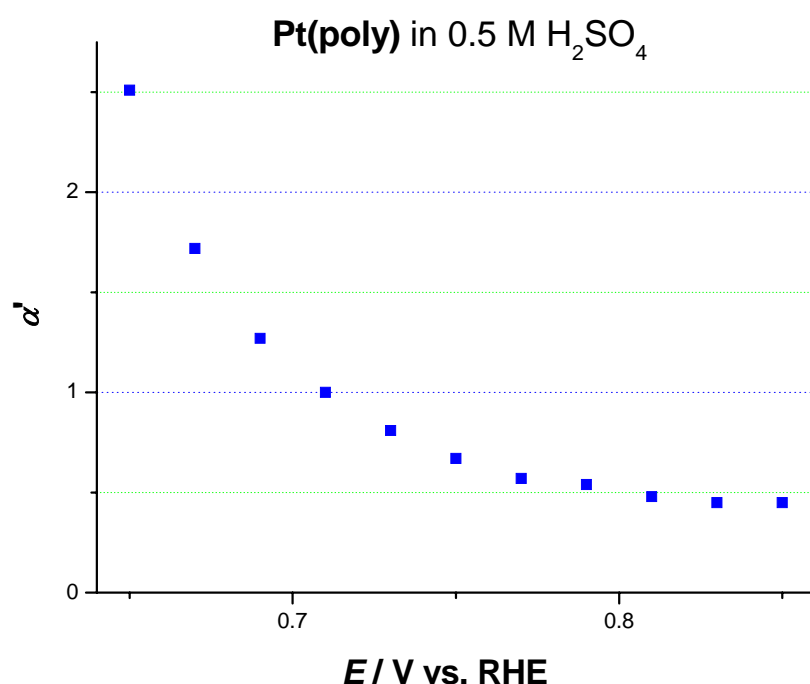


Figure 3-15. Plot of the apparent charge transfer coefficient versus various stepped potentials.

As for comparison, the traditional ways for obtaining Tafel slope reported in literature are also displayed. $\log(j_{\text{max}})$ and $-\log(t_{\text{max}})$ are plotted versus step potentials, as shown in Figure 3-16 and Figure 3-17, and the slope will give Tafel slopes as suggested by Santos et al [10]. From the plots of $\log(j_{\text{max}}) \sim E$ and $-\log(t_{\text{max}}) \sim E$, $143 \text{ mV}\cdot\text{dec}^{-1}$ and $167 \text{ mV}\cdot\text{dec}^{-1}$ are obtained for all the potential range, respectively, slightly higher than reported from literature [8, 9] and my previous result at high potentials from ac voltage measurement. At high potentials, both plots give values of about $240 \text{ mV}\cdot\text{dec}^{-1}$, which agreed well with that by Love et al [11]. At low potentials, the value is not so reasonable since the surface conditions varied too much. As pointed out by Bergelin et al [12], the Tafel slope obtained by plotting $\log(j_{\text{max}}) \sim E$ and $-\log(t_{\text{max}}) \sim E$ are flexible since t_{max} and j_{max} depend much on the conditions of the surface and it's normal that different researchers got different t_{max} and j_{max} on the same type of well prepared crystal.

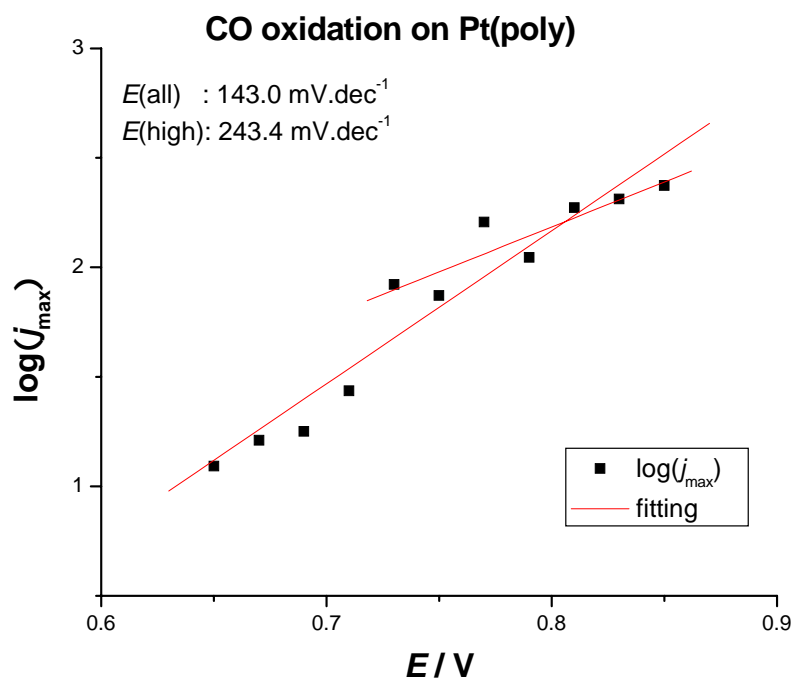


Figure 3-16 Tafel slope for CO oxidation on Pt(poly) measured by plotting $\log(j_{\text{max}}) \sim E$.

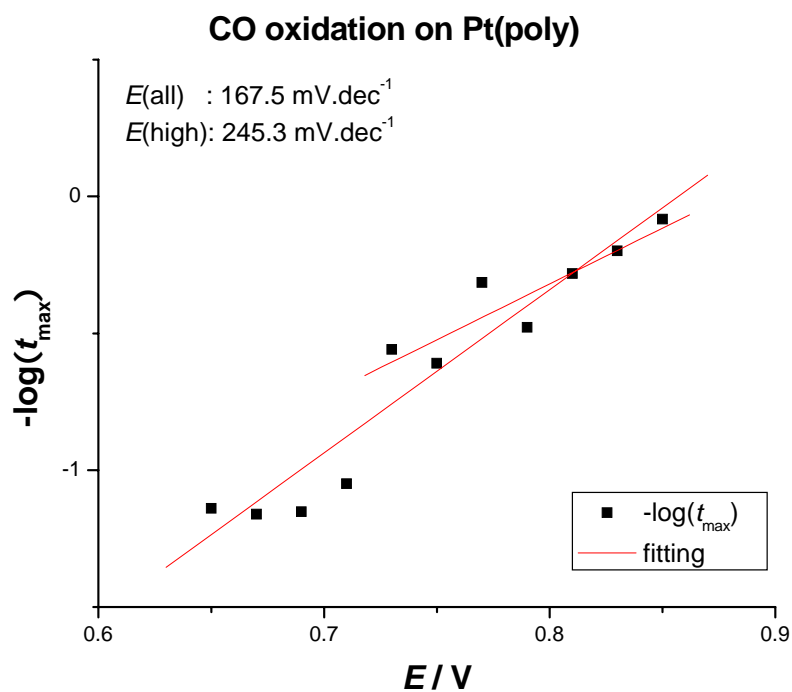


Figure 3-17 Tafel slope for CO oxidation on Pt(poly) measured by plotting $-\log(t_{\text{max}}) \sim E$.

3.3 Pt(111)

3.3.1 CV and EIS

A Pt(111) disk with diameter of 0.95 cm was employed with an area calculated to be 0.7 cm². A typical CV of Pt(111) is displayed in

Figure 3-18. The current between 0.09 V and 0.32 V corresponds to the adsorption and desorption of hydrogen. Some defects lead to the peaks corresponding to (110) and (100) orientation. The hump after 0.32 V is mainly attributed to the adsorption and desorption of HSO₄⁻, maybe together with small amount of SO₄²⁻. [13] One pair of spikes located at 0.44 V corresponds to the disorder/order phase transition of (bi)sulphate and is considered as the fingerprint feature of Pt(111) with the height being the yardstick for its quality. The small peaks at about 0.7 V are thought to be the adsorption and desorption of oxygen species, mostly OH, at Pt(111) surface [14].

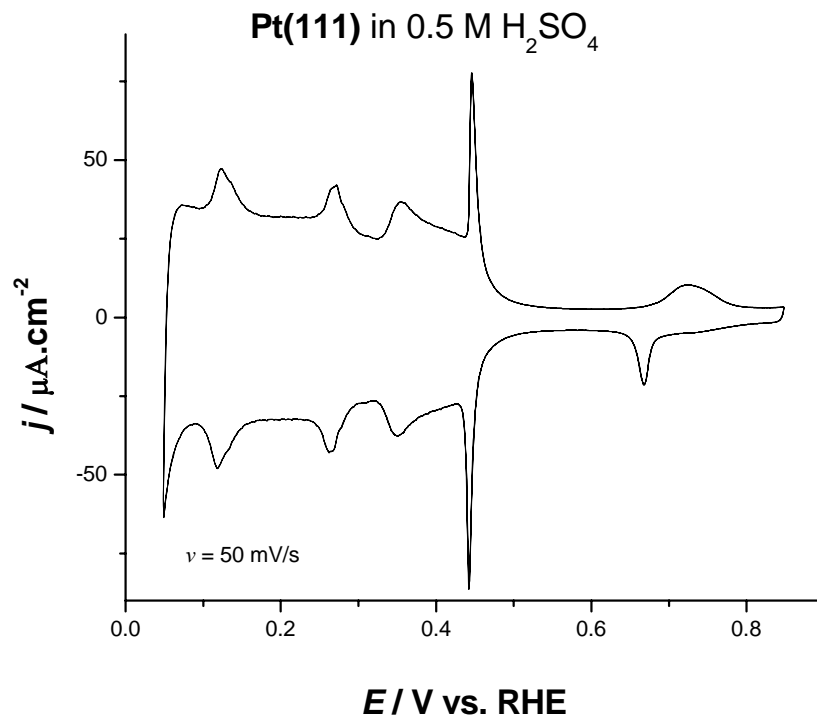


Figure 3-18. CV of Pt(111) in 0.5 M H₂SO₄.

The EIS was also recorded for Pt(111) free of CO in 0.5 M H₂SO₄. A $R_1-(C_1//R_2-C_2)$ model is employed to simulate the circuit and the values for the related parameters are listed in Table 3-4. Since the surface is not free of defects, an equivalent circuit of $R_1-(C_1//R_2-CPE)$ is also applied in order to have a better fitting and the values for corresponding parameters are tabulated in Table 3-5.

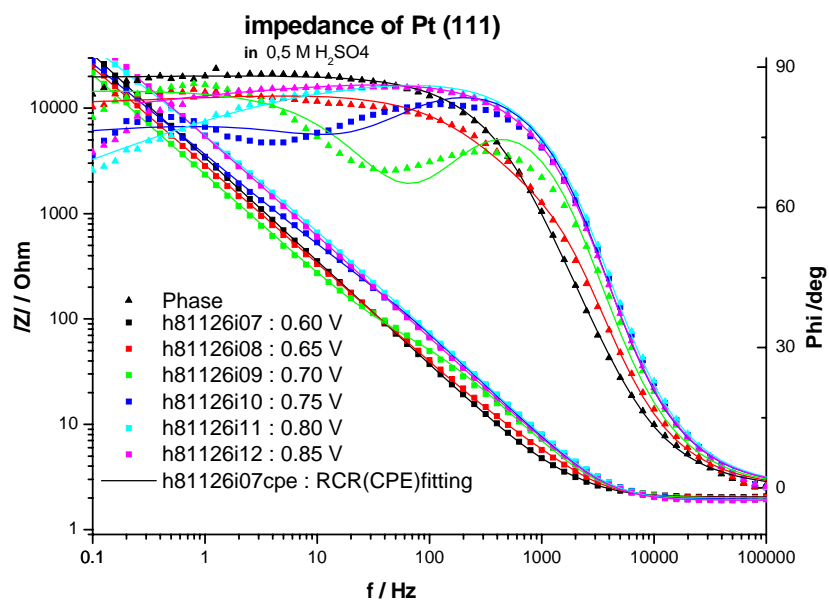

 Figure 3-19 EIS of Pt(111) in 0.5 M H₂SO₄ at various potentials.

 Table 3-4 The fitting data for the EIS on Pt(111) using $R_1-(C_1/(R_2-C_2))$ model.

E / V	filename	R_1 / Ω	C_1 / F	R_2 / Ω	C_2 / F
0.6	h81126i07	2.079	3.67E-05	52.07	8.99E-06
0.65	h81126i08	2.083	3.37E-05	248.3	2.11E-05
0.7	h81126i09	2.01	2.50E-05	143.3	4.20E-05
0.75	h81126i10	1.944	2.29E-05	1766	2.72E-05
0.8	h81126i11	1.919	2.25E-05	23414	2.11E-05
0.85	h81126i12	1.914	2.47E-05	48632	1.46E-05

 Table 3-5 The fitting data for the EIS on Pt(111) using $R_1-(C_1/(R_2-CPE))$ model.

E / V	filename	R_1 / Ω	C_1 / F	R_2 / Ω	CPE_1	$CPE_1(+) \alpha$
0.6	h81126i07	2.05	3.27E-05	10.6	1.61E-05	0.9323
0.65	h81126i08	2.02	2.75E-05	20.48	3.60E-05	0.8597
0.7	h81126i09	2.006	2.41E-05	104.3	5.08E-05	0.91924
0.75	h81126i10	1.951	2.16E-05	554.8	3.60E-05	0.77661
0.8	h81126i11	1.919	2.04E-05	83.39	2.03E-05	0.6004
0.85	h81126i12	1.908	2.23E-05	116.5	1.34E-05	0.68258

3.3.2 Potential sweep measurement

The dc current (in red), the real part of ac current (red dotted) and the apparent transfer coefficient of CO oxidation on Pt(111) with potential sweeping are displayed in Figure 3-20. The charge of CO oxidation is integrated to be $385 \mu\text{C}\cdot\text{mol}^{-1}$. At the main peak for CO oxidation, the apparent coefficient is calculated to be 1.63 at the peak potential, corresponding to a Tafel slope of $37 \text{ mV}\cdot\text{dec}^{-1}$. At the prepeak part, the coefficient is measured to be 0.48, i.e., the Tafel slope is $125 \text{ mV}\cdot\text{dec}^{-1}$. The very high values of α' below 0.5 V is an experimental artifact due to the faradaic current being close to zero. A broad shoulder around 0.7 V, which is due to specific adsorption as described previously, is responsible for the high value for α' since the faradaic current at that potential range is very small.

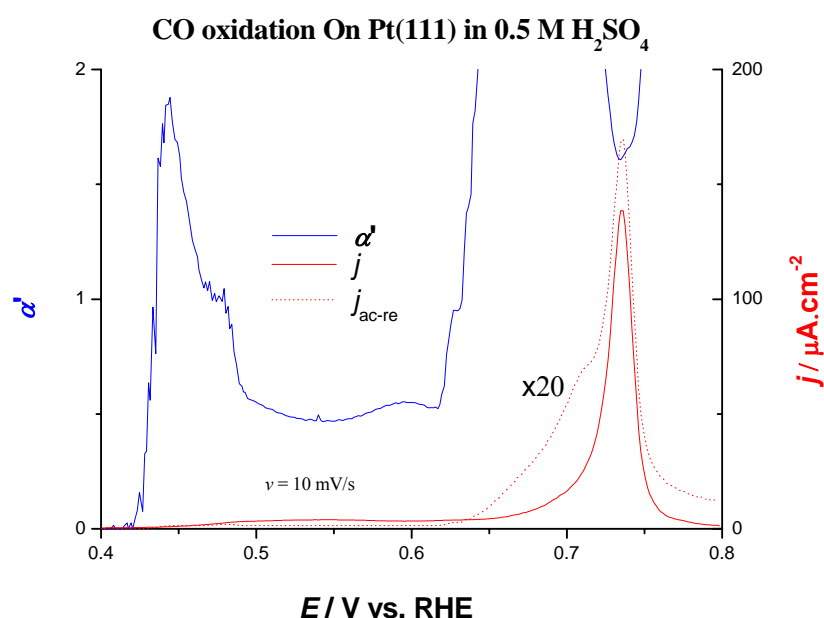


Figure 3-20. The dc current (in red), the real part of ac current (red dotted) and the apparent transfer coefficient of CO oxidation on Pt(111) with potential sweep. The ac voltage is 1 mV.

3.3.3 Potential step measurement

The current transients for CO oxidation on Pt(111) are displayed in Figure 3-21(a). With the increase of step potential, the current increases accordingly. The real part of the ac current at the corresponding potentials is also displayed in Figure 3-21 (b). At low potentials, from 0.71 V to 0.77 V, an extra peak prior to the peak for CO oxidation in the real part of the ac current is observed with relatively high value compared with the dc current transient at the same potential, the same problem as in Figure 3-20 at around 0.7 V attributing to specific adsorption. The real part of ac current remains high and constant after CO oxidation completed, which are due to the adsorption of anions on the CO-free surface as described

previously.

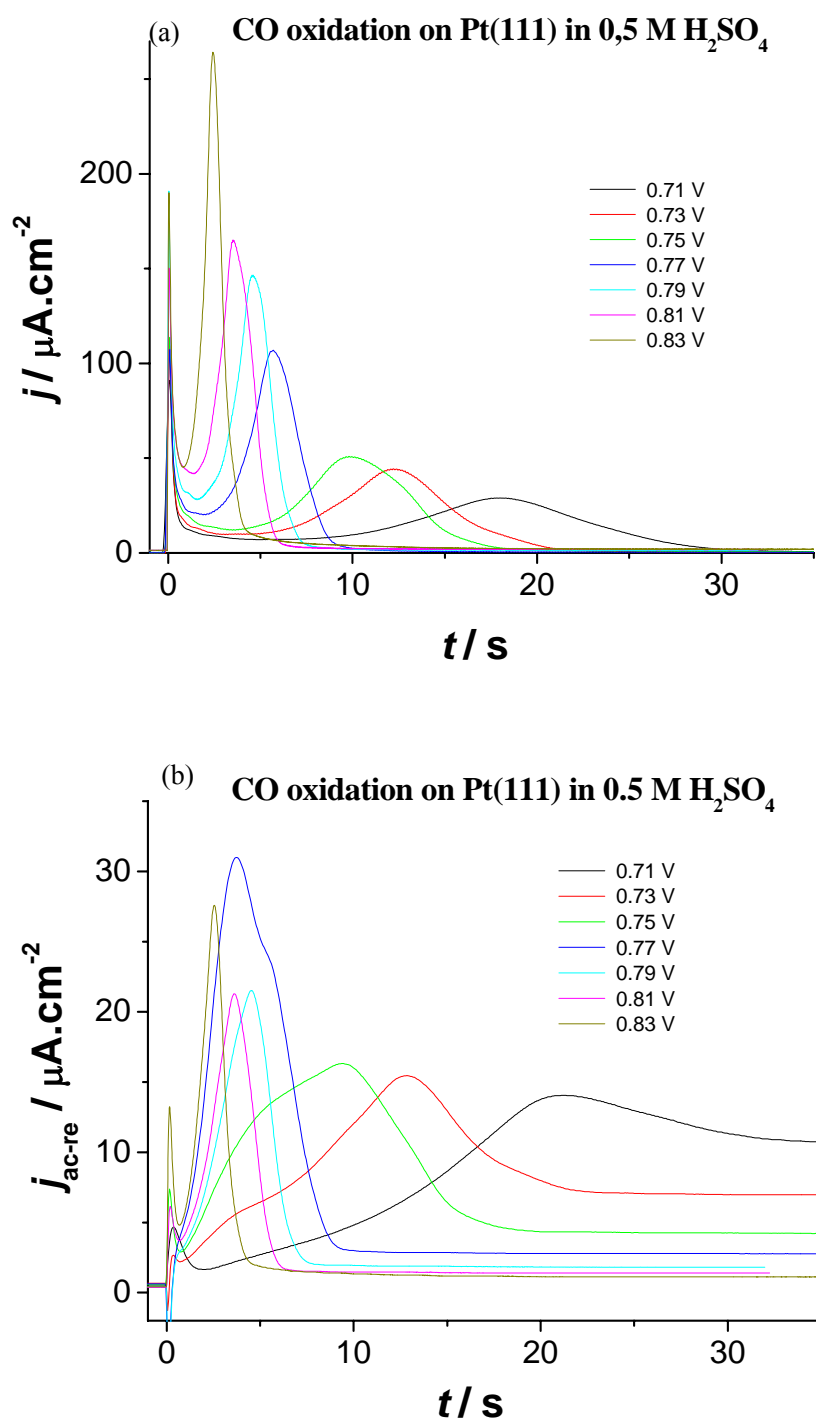


Figure 3-21. The current transient (a) and real part of ac current (b) for CO oxidation on Pt(111). The ac voltage is 3 mV.

The apparent transfer coefficients are plotted in Figure 3-22. At low potentials, from 0.71 to 0.77V, the coefficients are around 1.6 (Tafel slope: 37 mV·dec⁻¹); with the potential increases, the coefficient decreases and gives values about 0.85 (Tafel slope: 71 mV·dec⁻¹) at 0.83 V and 0.85V, which showed the similar trend as that of on polycrystalline platinum. On the same type of crystal, many researchers obtained Tafel slope around 70 mV·dec⁻¹ in H₂SO₄ or HClO₄: Palaikis [15] reported a value of 80±5 mV·dec⁻¹ by plotting $\log(v) \sim E_p$; Santos [10] obtained 67 and 57 mV·dec⁻¹ by plotting $\log(t_{\max}) \sim E$ and $\log(i_{\max}) \sim E$; Bergelin [12] obtained 72 mV·dec⁻¹ by plotting $\log(k') \sim E$, where the value of k' is obtained by simulation; Herrero [16] reported 70-75 mV·dec⁻¹; Lebedeva [17] reported 75±3 and 70±2 mV·dec⁻¹ by plotting $\log(k') \sim E$ and by $\log(t_{\max}) \sim E$, respectively. Those values are close to the value obtained in this work at high potential. However, some researchers observed the transition of the Tafel slope with the potential increase: Love [11] obtained 80 and 240 mV·dec⁻¹ at low and high potentials, respectively, by plotting $\log(t_{\max}) \sim E$; Bergelin [12] reported 100 and 280 mV·dec⁻¹. As mentioned by Lebedeva, no transition of Tafel slope observed from their work maybe due to the limited potential range investigated. What's more, their measurement is also limited by their methods since a wide range of potentials is necessary to get one Tafel slope.

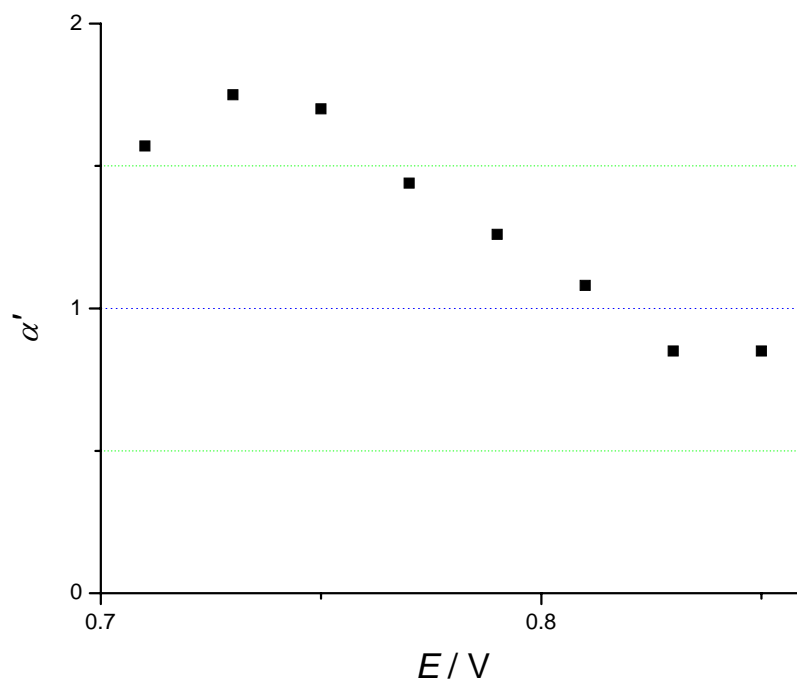


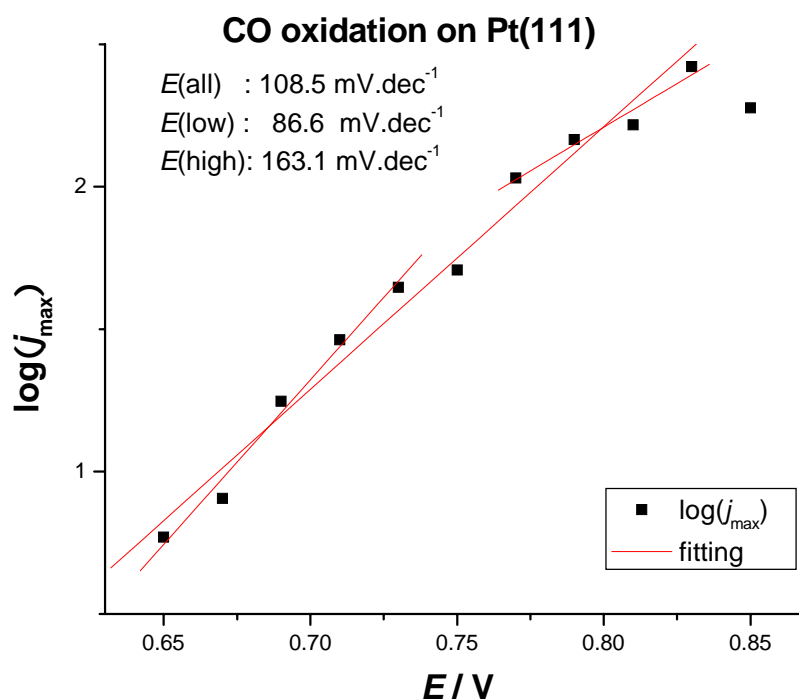
Figure 3-22. Apparent transfer coefficient for CO oxidation on Pt(111)

The values of j_{\max} and t_{\max} are tabulated in Table 3-6 and the plots of $\log(j_{\max}) \sim E$ and $-\log(t_{\max}) \sim E$ are displayed in Figure 3-23 and Figure 3-24. From the plots, slopes of 109 and 124 mV·dec⁻¹ are obtained for

all the potential range, respectively. A slope change is observed for each plot at different potential range. Slopes of 87 and 102 $\text{mV}\cdot\text{dec}^{-1}$ are obtained at low potentials and 163 $\text{mV}\cdot\text{dec}^{-1}$ is obtained in both cases, which are twice as large as those observed by the ac voltage method.

 Table 3-6 t_{\max} and j_{\max} for CO oxidation on Pt(111) at various potentials.

E / V	filename	t_{\max} / s	$-\log(t_{\max})$	$j_{\max} / \mu\text{A}$	$\log(j_{\max})$
0.65	h81124xy14	73.4	-1.8657	5.88	0.76938
0.67	h81124xy 16	46.3	-1.66558	8.05	0.9058
0.69	h81124xy 18	28.3	-1.45179	17.63	1.24625
0.71	h81124xy20	18	-1.25527	29	1.4624
0.73	h81124xy 22	12.3	-1.08991	44.3	1.6464
0.75	h81124xy 24	9.8	-0.99123	51	1.70757
0.77	h81124xy 26	5.7	-0.75587	107.2	2.03019
0.79	h81124xy 32	4.57	-0.65992	146.4	2.16554
0.81	h81124xy 34	3.54	-0.549	165	2.21748
0.83	h81124xy 36	2.43	-0.38561	264	2.4216
0.85	h81124xy 38	2.38	-0.37658	188.8	2.276


 Figure 3-23 Tafel slope for CO oxidation on Pt(111) measured by plotting $\log(j_{\max}) \sim E$.

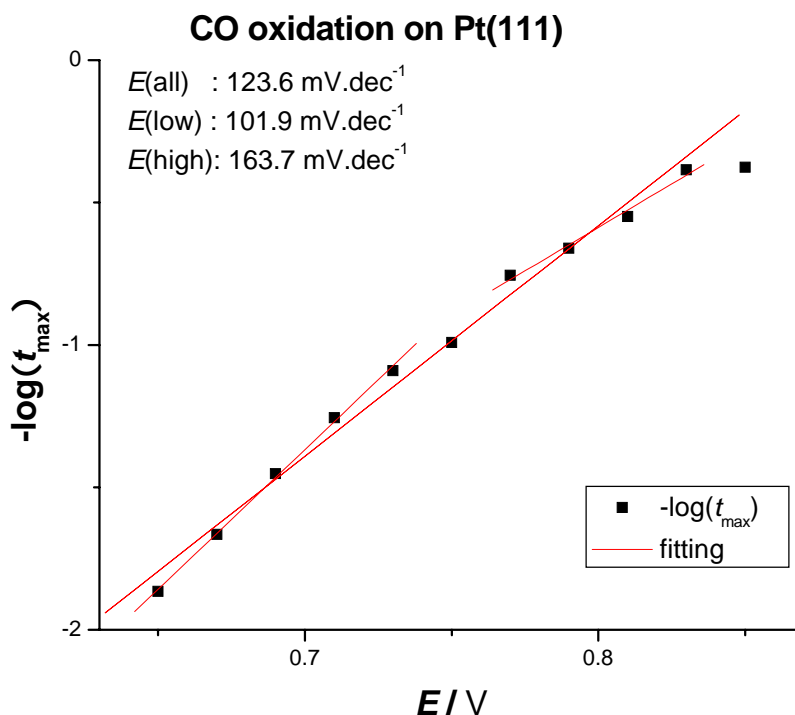


Figure 3-24 Tafel slope for CO oxidation on Pt(111) measured by plotting $-\log(t_{\text{max}}) \sim E$.

3.4 Pt(665)

3.4.1 CV and EIS

A typical CV of Pt(665) is shown in Figure 3-25. The hydrogen ad/desorption charge is integrated to be $162.9 \mu\text{C}\cdot\text{cm}^{-2}$ in the range of 0.09-0.36 V without subtracting the double layer charge. A pair of sharp peaks at 0.12 V is corresponding to H ad/desorption at step sites with (110) orientation and is integrated to have a charge of $22.6 \mu\text{C}\cdot\text{cm}^{-2}$.

The EIS for Pt(665) was also checked at various potentials, as shown in Figure 3-26. Equivalent circuits of $R_1-(C_1//R_2-C_2)$ and $R_1-(C_1//R_2-CPE)$ are used to fit the measured data and the best fitting values for those parameters at each potential are listed in

Table 3-7 and Table 3-8.

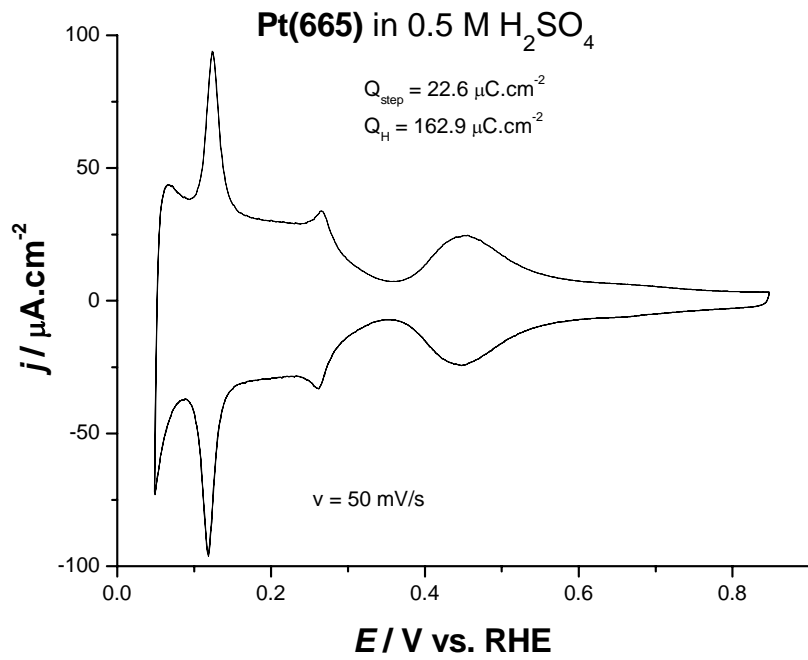


Figure 3-25. CV of Pt(665) in 0.5 M H₂SO₄.

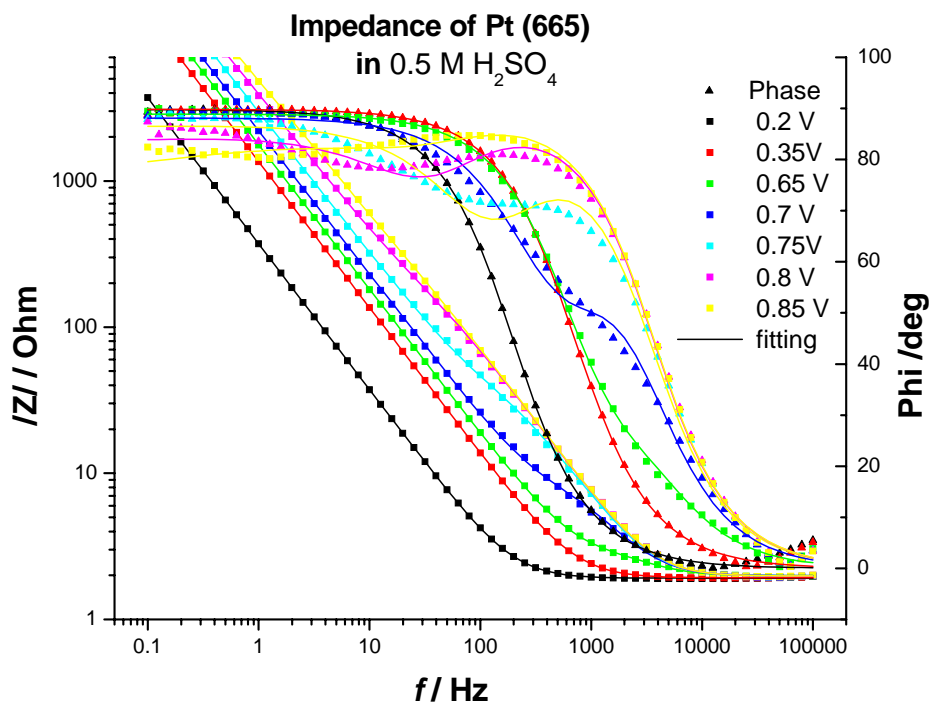


Figure 3-26 EIS of Pt(665) in 0.5 M H₂SO₄ at various potentials.

Table 3-7 The fitting data for the EIS on Pt(665) using $R_1-(C_1//R_2-C_2)$ model.

E / V	filename	R_1 / Ω	C_1 / F	R_2 / Ω	C_2 / F
0.2	i40	1.915	4.24E-04	2660	5.28E-06
0.35	i41	1.93	1.13E-04	84.77	3.87E-06
0.65	i42	2.001	4.65E-05	3.584	4.16E-05
0.7	i43	2.008	2.91E-05	13.74	4.14E-05
0.75	i44	1.992	2.43E-05	102.3	2.86E-05
0.8	i45	1.978	2.29E-05	854.5	1.88E-05
0.85	i46	1.981	2.31E-05	5137	1.42E-05

 Table 3-8 The fitting data for the EIS on Pt(665) using $R_1-(C_1//R_2-CPE)$ model.

E / V	filename	R_1 / Ω	C_1 / F	R_2 / Ω	CPE_1	$CPE_1(+) \alpha$
0.2	h80926i40	1,914	0,00010957	8,3906E-8	0,00032127	0,997
0.35	h80926i41	1,93	0,00011276	55,57	5,0766E-6	0,95655
0.65	h80926i42	1,989	4,1923E-5	2,562	5,0147E-5	0,97745
0.7	h80926i43	1,994	2,7592E-5	11,24	4,7542E-5	0,96722
0.75	h80926i44	1,985	2,339E-5	73,93	3,4176E-5	0,93699
0.8	h80926i45	1,977	2,2106E-5	422,3	2,3668E-5	0,87666
0.85	h80926i46	1,982	2,1875E-5	765,5	1,8186E-5	0,76499

3.4.2 Potential sweep measurement

The current for CO oxidation on Pt(665) are displayed in Figure 3-27. A prepeak and a main peak are observed at 0.55 and 0.70 V, respectively. The real part of the ac current showed the similar features. According to the dc current and the real part of ac current, the apparent charge transfer coefficient at the main current peak is calculated to be 1.53, i.e., the Tafel slope is $39 \text{ mV} \cdot \text{dec}^{-1}$, and at the prepeak to be 0.53, corresponding to a Tafel slope of $113 \text{ mV} \cdot \text{dec}^{-1}$.

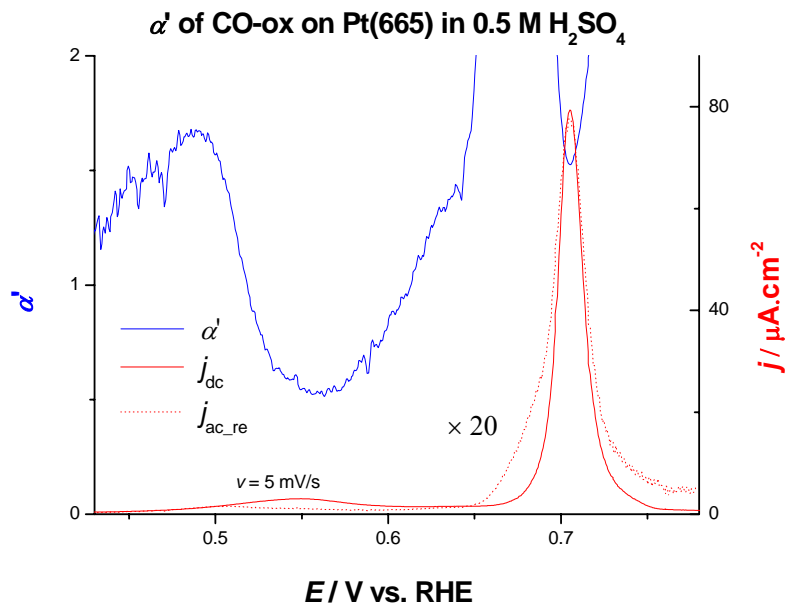


Figure 3-27. Apparent transfer coefficient for CO oxidation on Pt(665) with potential sweep. $u_{ac} = 1$ mV.

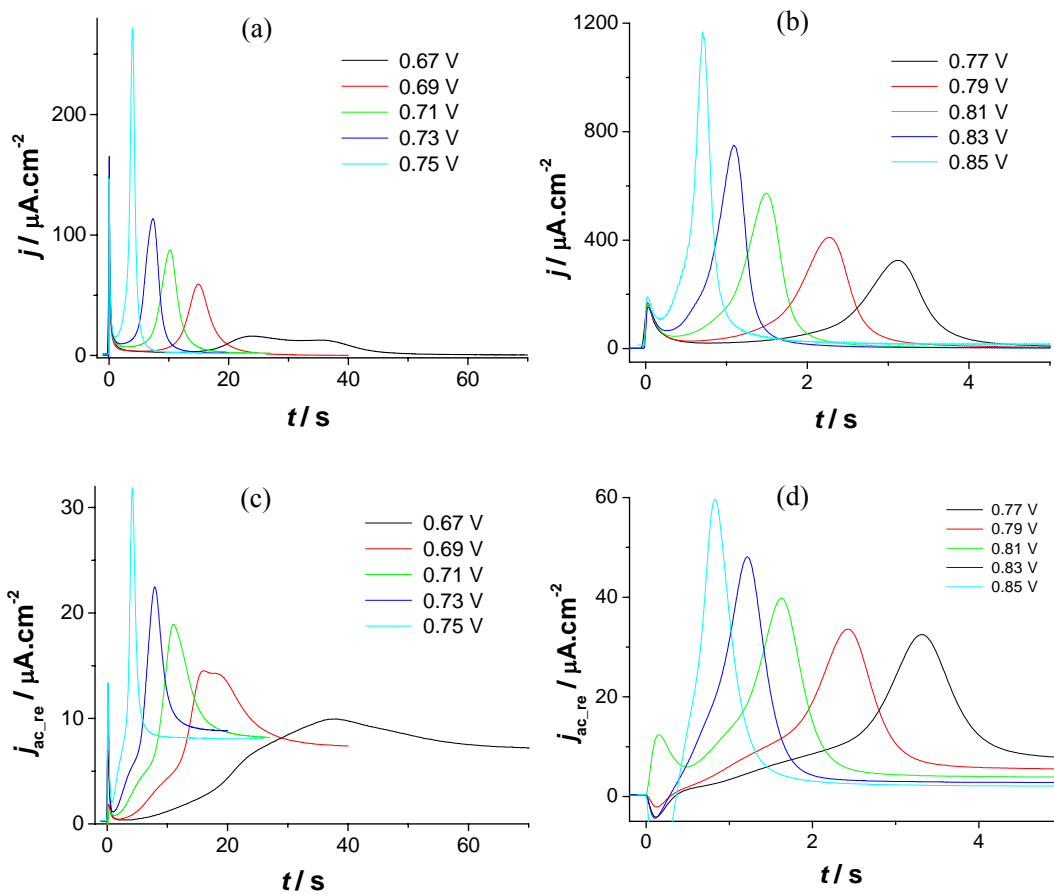


Figure 3-28. Current transient, (a) and (b), and real part of ac currents, (c) and (d), of CO oxidation on Pt(665) at various potentials. $u_{ac} = 3$ mV.

The current transient and the real part of ac current for CO oxidation at each potential are displayed in Figure 3-28. With the increase of potential, the current gradually decreases and the time at peak current decreases. Similar features are also observed for the real part of the current.

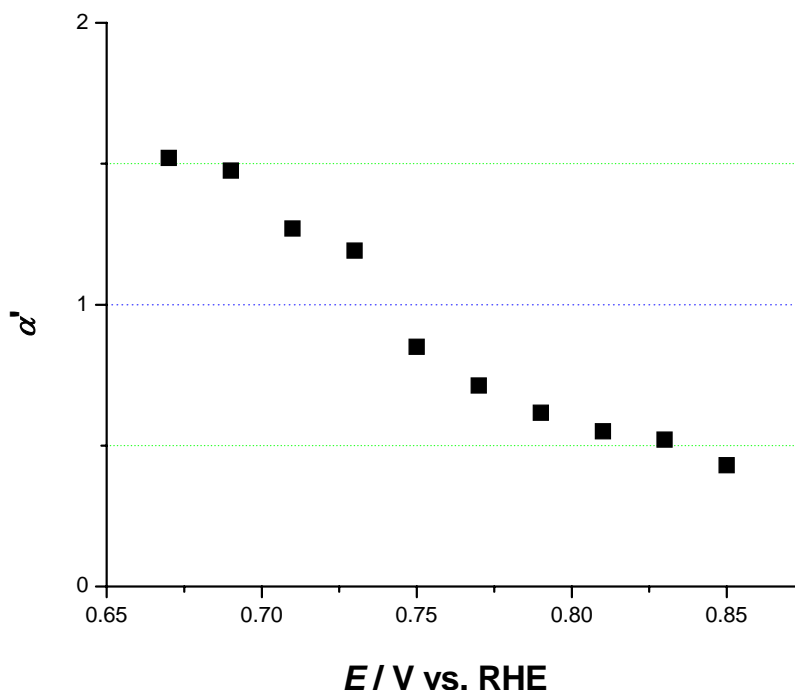


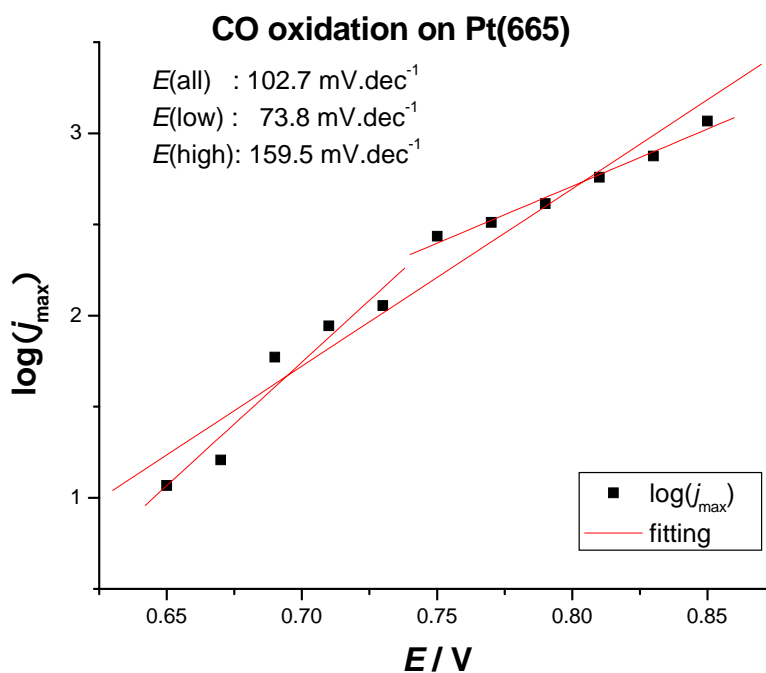
Figure 3-29. Apparent charge transfer coefficient for CO oxidation on Pt(665).

The apparent charge transfer coefficient is calculated and the values at peak current are plotted in Figure 3-29, from which we can see that with the potential increase the coefficient changes gradually from about 1.5 to 0.5, corresponding to the Tafel slope change from $40 \text{ mV}\cdot\text{dec}^{-1}$ to $120 \text{ mV}\cdot\text{dec}^{-1}$.

The values of j_{\max} and t_{\max} are tabulated in Table 3-9 and the plots of $\log(j_{\max})\sim E$ and $-\log(t_{\max})\sim E$ are displayed in Figure 3-30 and Figure 3-31. From the plots, slopes of 103 and $114 \text{ mV}\cdot\text{dec}^{-1}$ are obtained for total range of potentials, respectively. A transition of slope is observed in both cases with potential increase. Slopes of 74 and $100 \text{ mV}\cdot\text{dec}^{-1}$ are obtained at low potentials and 160 and $133 \text{ mV}\cdot\text{dec}^{-1}$ are obtained in high potential range, higher than observed by ac voltage method.

Table 3-9 t_{\max} and j_{\max} for CO oxidation on Pt(665) at various potentials.

E / V	filename	t_{\max} / s	$-\log(t_{\max})$	$j_{\max} / \mu A$	$\log(j_{\max})$
0.65	h81126xy18	48.2	-1.68305	11.7	1.06819
0.67	h81126xy20	24.1	-1.38202	16.1	1.20683
0.69	h81126xy22	14.95	-1.17464	59.2	1.77232
0.71	h81126xy24	10.21	-1.00903	87.7	1.943
0.73	h81126xy26	7.34	-0.8657	113.5	2.055
0.75	h81126xy28	3.92	-0.59329	272.5	2.43537
0.77	h81126xy30	3.12	-0.49415	324.9	2.51175
0.79	h81126xy32	2.27	-0.35603	411	2.61384
0.81	h81126xy34	1.49	-0.17319	573	2.75815
0.83	h81126xy36	1.09	-0.03743	749	2.87448
0.85	h81126xy40	0.705	0.15181	1166	3.0667


 Figure 3-30 Tafel slope for CO oxidation on Pt(665) measured by plotting $\log(j_{\max}) \sim E$.

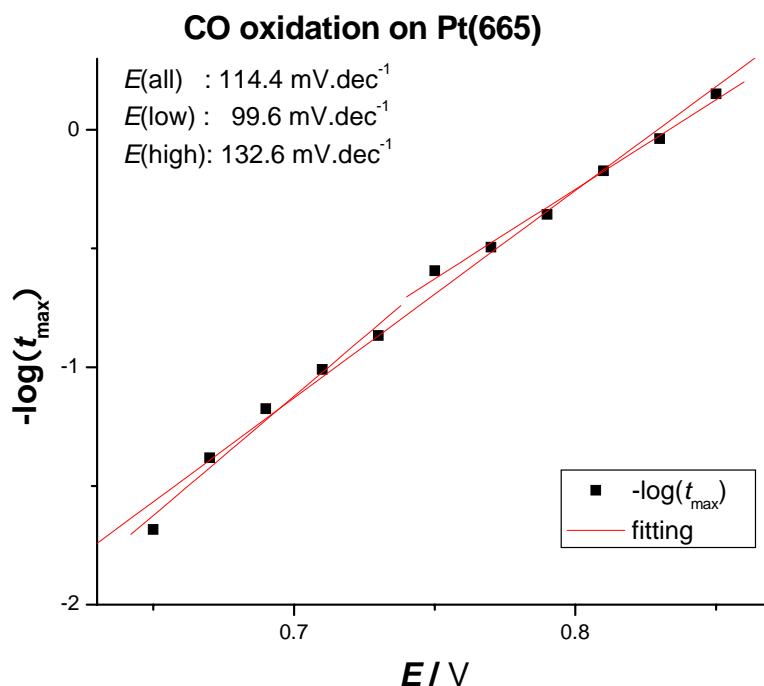


Figure 3-31 Tafel slope for CO oxidation on Pt(665) measured by plotting $-\log(t_{\text{max}}) \sim E$.

3.5 Pt(332)

3.5.1 CV

A typical CV for Pt(332) in 0.5 M H_2SO_4 is displayed in Figure 3-32. The charge for hydrogen ad/desorption is integrated to be $174.1 \mu\text{C}\cdot\text{cm}^{-2}$ in the region of 0.07~0.35 V. The current peak at 0.12 V is integrated to be $52.3 \mu\text{C}\cdot\text{cm}^{-2}$ and corresponds to H ad/desorption at step sites in (110) orientation.

3.5.2 Potential sweep experiment

The oxidation of adsorbed CO on well prepared Pt(332) was carried out with potential sweeping. The dc current, the real part of the ac current were recorded and the apparent transfer coefficient was calculated, as displayed in Figure 3-33. Both the dc current and the real part of ac current reached a maximum at 0.66 V, corresponding to CO oxidation on Pt(332). This peak potential is much lower than that on Pt(111) (0.73 V) and also lower than that on Pt(poly) (0.69 V) and Pt(665) (0.70 V), suggesting that the step density plays a large role on the rate of CO oxidation. The α' is measured to be 1.52 at peak current potential, corresponding to a Tafel slope of $40 \text{ mV}\cdot\text{dec}^{-1}$ and indicating the step of the second electron transfer as the rds.

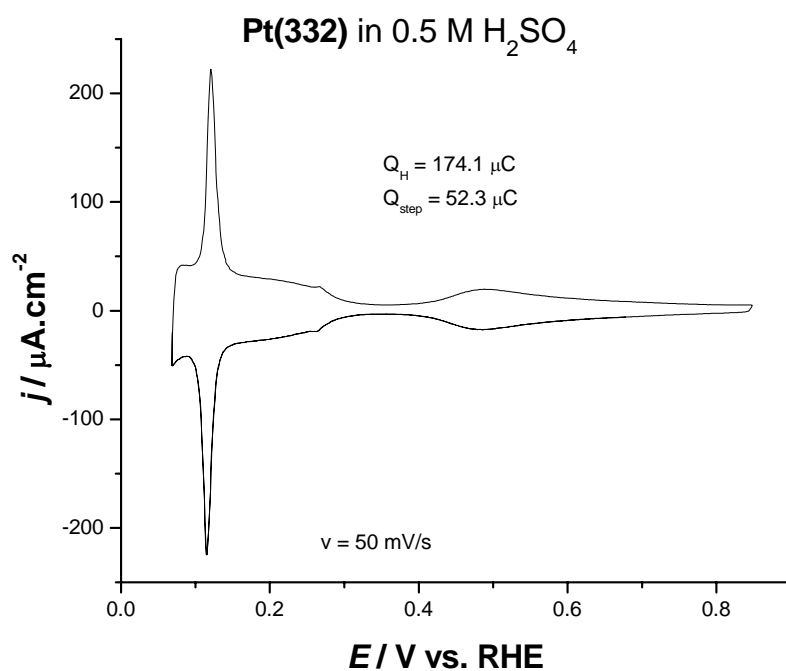


Figure 3-32. CV of Pt(332) in 0.5 M H₂SO₄.

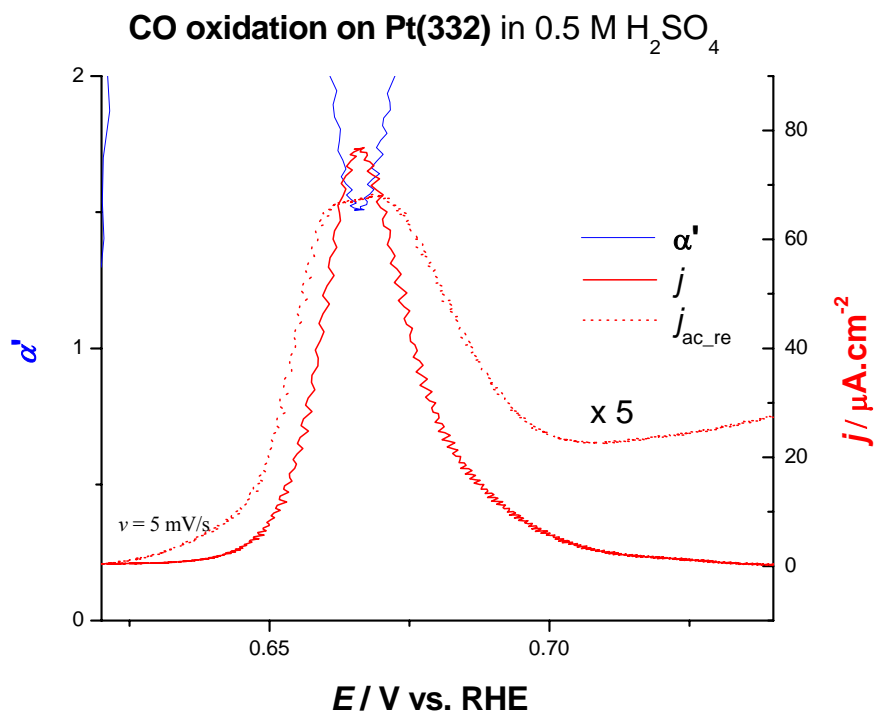


Figure 3-33. The current, the real part of ac current and the apparent charge transfer coefficient for CO oxidation on Pt(332). Solution: 0.5 M H₂SO₄. $u_{\text{ac}} = 3 \text{ mV}$.

3.5.3 Potential step measurements

The current transient at various step potentials and the corresponding real part of ac current are displayed in Figure 3-34. With the increase of stepped potential, increasing trends of both ac and dc current are observed with a decreasing time of the current maximum.

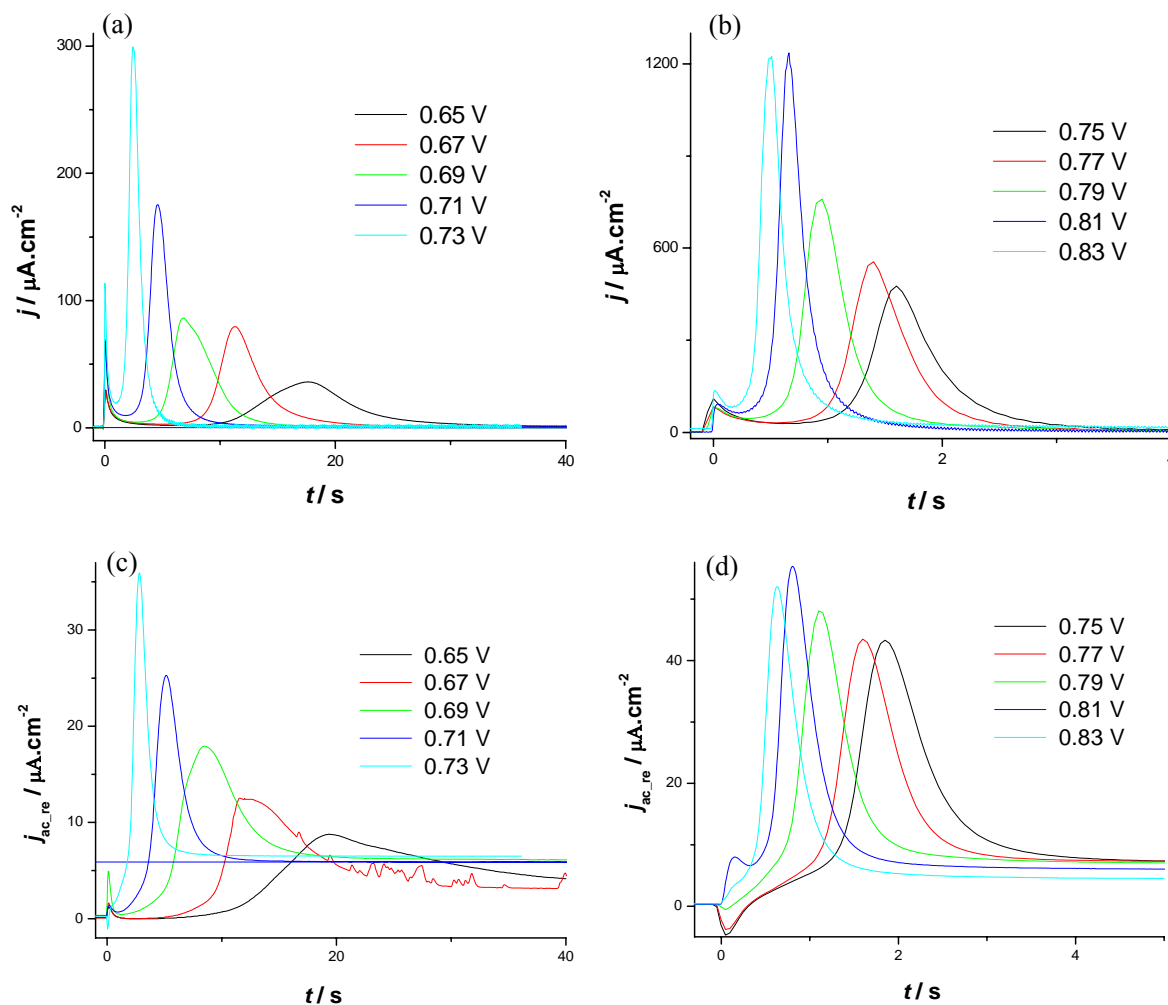


Figure 3-34. Current transient (a and b), real part of ac current transient (c and d) for CO oxidation on Pt(332). Solution: 0.5 M H₂SO₄. $u_{ac} = 3$ mV.

The apparent transfer coefficient is thus calculated and plotted in Figure 3-35. The change of α' from around 1.5 at low potentials ($E < 0.7$ V) to about 0.5 at high potentials ($E > 0.8$ V), are observed, corresponding to a slope increase from ca. 40 to 120 mV·dec⁻¹. These values are similar to those observed on Pt(665), which has the similar surface structure as Pt(332) except for different step density.

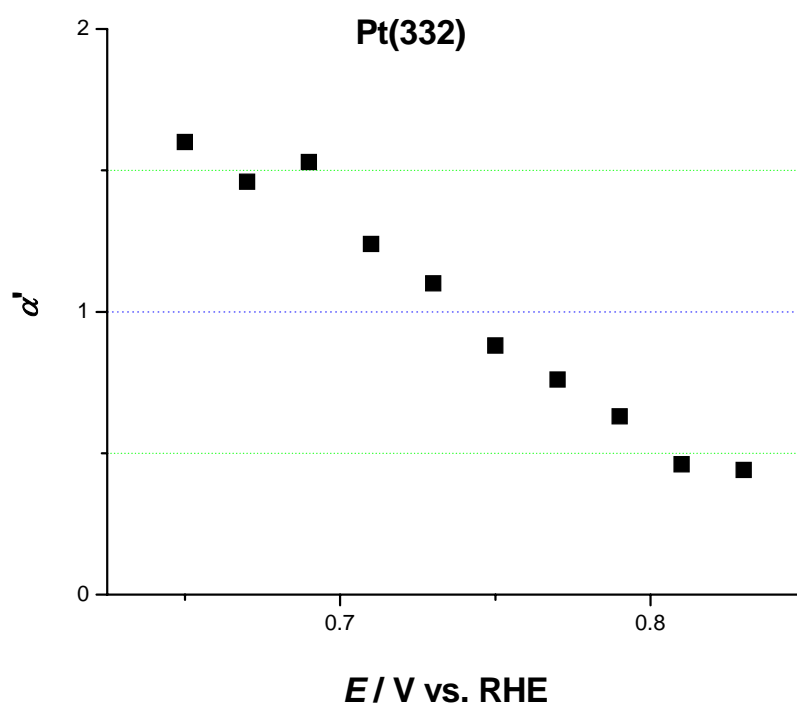


Figure 3-35. Apparent charge transfer coefficient for CO oxidation on Pt(332).

 Table 3-10 t_{\max} and j_{\max} for CO oxidation on Pt(332) at various potentials.

E / V	filename	t_{\max} / s	$-\log(t_{\max})$	$j_{\max} / \mu\text{A}$	$\log(j_{\max})$
0.65	h90303xy09	17.6	-1.24551	36.1	1.55751
0.67	h90303xy11	11.3	-1.05308	79.6	1.90091
0.69	h90303xy13	6.79	-0.83187	86.5	1.93702
0.71	h90303xy15	4.6	-0.66276	175.5	2.24428
0.73	h90303xy17	2.45	-0.38917	299.2	2.47596
0.75	h90303xy19	1.6	-0.20412	475.7	2.67733
0.77	h90303xy21	1.39	-0.14301	555.3	2.74453
0.79	h90303xy23	0.94	0.02687	765.6	2.884
0.81	h90303xy25	0.66	0.18046	1236.6	3.09223
0.83	h90303xy27	0.49	0.3098	1223.5	3.0876

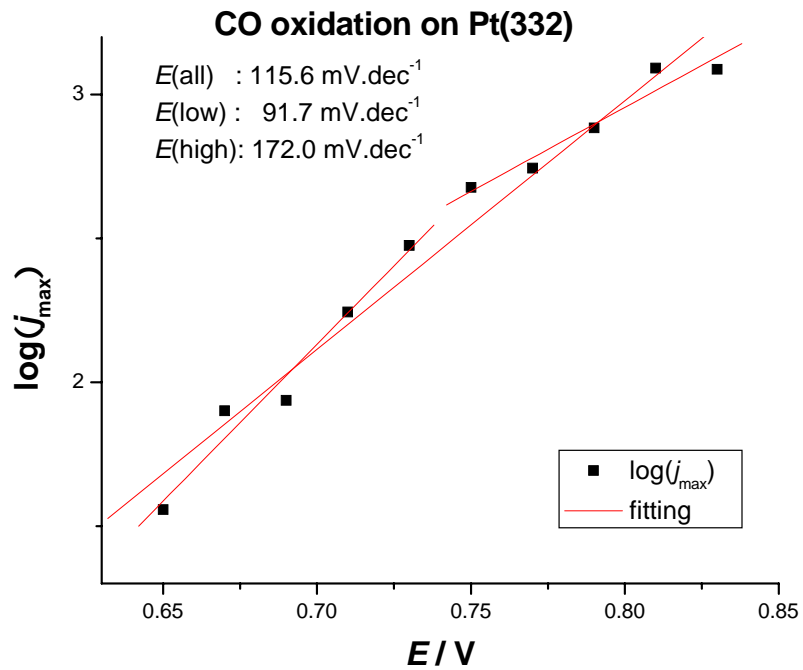


Figure 3-36 Tafel slope for CO oxidation on Pt(332) measured by plotting $\log(j_{\max}) \sim E$.

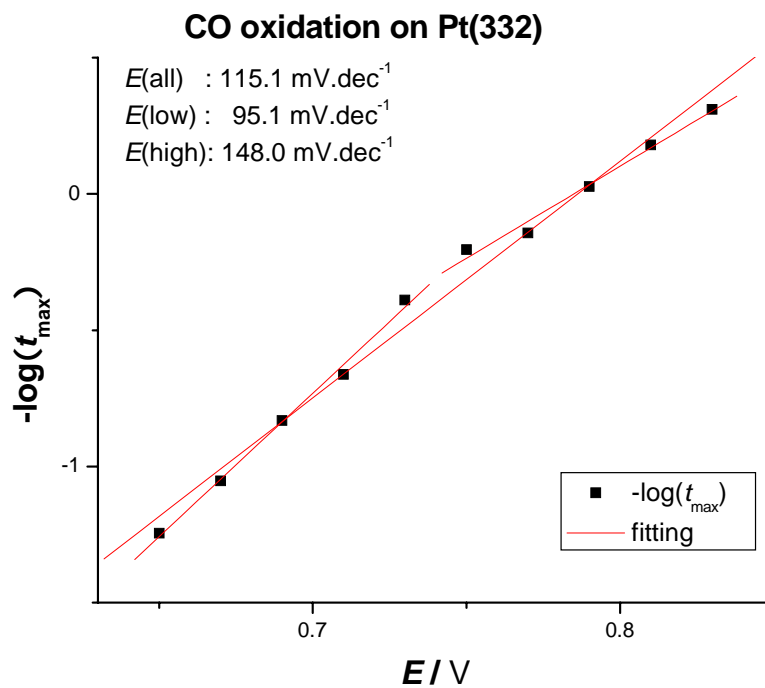


Figure 3-37 Tafel slope for CO oxidation on Pt(332) measured by plotting $-\log(t_{\max}) \sim E$.

The values of j_{\max} and t_{\max} are listed in Table 3-10 and $\log(j_{\max})\sim E$ and $-\log(t_{\max})\sim E$ are plotted in Figure 3-36 and Figure 3-37. From each plot, the same slope of $115 \text{ mV}\cdot\text{dec}^{-1}$ is obtained for the total range of potentials. A change of slope is observed at potential near to 0.75 V in both cases. Slopes of 92 and $95 \text{ mV}\cdot\text{dec}^{-1}$ are obtained at low potentials and 172 and $148 \text{ mV}\cdot\text{dec}^{-1}$ are obtained in high potential range, higher than observed by ac voltage method and similar to those observed on Pt(665).

3.6 General discussion for the mechanism of CO oxidation on Pt

3.6.1 General review of our results

The apparent transfer coefficients for CO oxidation at all the four Pt surfaces are listed in Table 3-11 and plotted together in Figure 3-38. It's clearly observed that α' for all the crystals studied decrease with the potential increase. For Pt(poly) and the two stepped crystals Pt(665) and Pt(332), the α' changes from 1.5 at low potentials, e.g., 0.67 V , gradually to about 0.5 at high potentials, $E > 0.8 \text{ V}$, demonstrating a clear Tafel slope change from around ca. $40 \text{ mV}\cdot\text{dec}^{-1}$ to ca. $120 \text{ mV}\cdot\text{dec}^{-1}$. For that of Pt(111), the trends of this change can also be observed while the potential for the change is shifted in positive direction by dozens minivolts, e.g., ca. 70 mV delayed compared with that of Pt(665) and Pt(332). The α' at the highest potential (0.85 V), is not close to 0.5 , which is due to this potential applied is not high enough. For the assignment of the rate determining step, it's clear that at low potential the rate is controlled by the second step, the formation of CO_2 from CO_{ad} and OH_{ad} . However it's complicated for the determining of rds at high potentials. The rds can be decided by the rate constant of the two steps. If $k_2 \gg k_1$, then the rds is the first step and the current transient would be linearly proportional to $(1-\theta_{\text{CO}})$, which is observed in many cases especially on Pt(111). If $k_2 \ll k_1$, then the reaction step for 2^{nd} electron transfer is the rds, which is believed by many researchers since they believed that OH adsorption should be very fast and also the peak shape of most current transient are nearly symmetric. As pointed out by Kucernak et al [9], adsorption of OH or its diffusion could also be slow, especially at polycrystalline surface. And also, OH is not fully covered on the surface after CO oxidation completed, which suggests that there could be some OH active sites that OH fully covered and OH non-active sites that no OH adsorbed during the oxidation process. Anyway, these investigations could contribute much to the determination of the Tafel slope for CO oxidation on Pt and provide important information for the understanding of the mechanism.

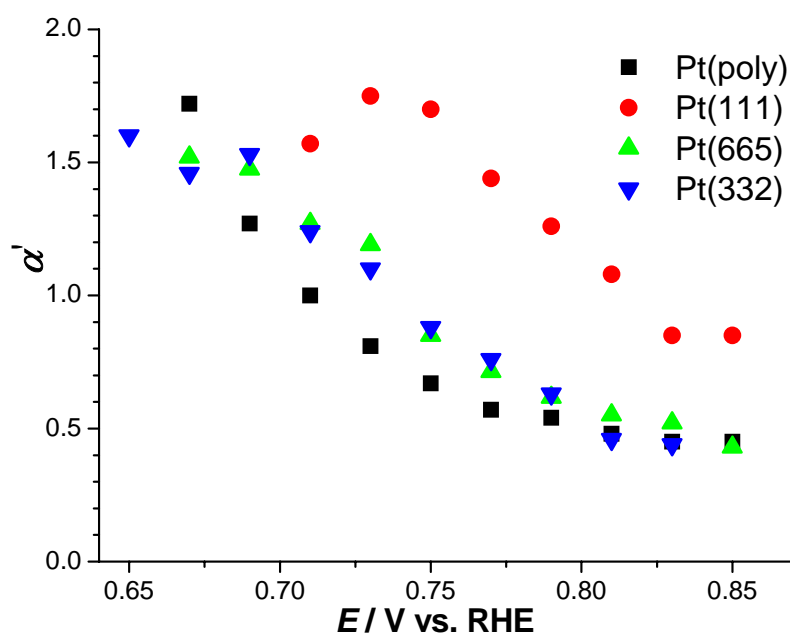


Figure 3-38. Apparent transfer coefficient for the oxidation of pre-adsorbed CO on Pt(poly), Pt(111), Pt(665) and Pt(332) at various potentials determined in the maximum of the current transients of potential step experiments.

Table 3-11 α measured for CO oxidation at Pt(poly), Pt(111), Pt(665) and Pt(332).

E / V	α			
	Pt(poly)	Pt(111)	Pt(665)	Pt(332)
0.65	2.51		2.74	1.6
0.67	1.72		1.52	1.46
0.69	1.27		1.48	1.53
0.71	1.00	1.57	1.27	1.24
0.73	0.81	1.75	1.19	1.1
0.75	0.67	1.7	0.85	0.88
0.77	0.57	1.44	0.71	0.76
0.79	0.54	1.26	0.62	0.63
0.81	0.48	1.08	0.55	0.46
0.83	0.45	0.85	0.52	0.44
0.85	0.45	0.85	0.43	

For the plateau in minimum of the current transients, Lebedeva et al. [6, 7] obtained a Tafel slope of 81 mV dec⁻¹ for Pt(111) (i.e. $\alpha' \approx 0.73$) and 111 mV dec⁻¹ for Pt(553) and Pt(110) (i.e., $\alpha' \approx 0.53$) from $\log i_{min}$ vs potential plots and Kucernak et al. [9] report values of about 82 mV dec⁻¹ and 120 mV dec⁻¹ for polycrystalline Pt (i.e. $\alpha' \approx 0.72$ and 0.5), depending on how the slopes were determined. ($\log i_{min}$ vs potential or $\log t_{min}$ vs potential). From the same data evaluation as used by Lebedeva et al. [6, 7] ($\log i_{min}$ vs. potential plots) we get for the current minimum in the transients α' values of 0.47, 0.51, and 0.55 for Pt(111)(0.71 – 0.83 V), Pt(665) (0.69 – 0.85 V), and Pt(332) (0.65 – 0.83 V), respectively, in good agreement with our results for the pre-peak from the ac measurements in potential sweep experiments, but different from the findings of Lebedeva et al. for Pt(111).

3.6.2 About the contradiction in Tafel slope in literature

From the investigation of CO oxidation on Pt(poly), Pt(111), Pt(665) and Pt(332) in sulfuric acid, with the ac voltage method it is concluded that with increasing potential, the apparent charge transfer coefficient changes from about 1.5 to 0.5, corresponding to Tafel slope change from 40 to 120 mV·dec⁻¹. This result is different from that by Lebedeva and some other researchers [6, 7, 10, 16, 18]. A series of Tafel slopes in the literature has already been listed in the first chapter of this thesis and also discussed in some extent. Here I will concentrate on the Tafel slopes of CO oxidation on Pt in acidic electrolyte and leave those in the alkaline solution to later part. By modeling the apparent rate constant using the mean-field approximation, Lebedeva[7] gave a single slope for each electrode ranging from 75 to 97 mV·dec⁻¹, instead of a slope change from 40 to 120 mV·dec⁻¹ as predicted by Koper [1]. Actually it's understandable that Lebedeva got those values since she drew only one Tafel slope for one crystal at a series potentials, e.g., 0.725~0.90 V for Pt(554), which include the potential region where Tafel slope changes from around 40 to 120 mV·dec⁻¹. In this case the fitting with one straight line could cover the difference of slopes between high and low potentials. In one article Lebedeva [6] explained this one slope instead of two on the research of Pt(111) as the result of narrow range of potential investigated. As mentioned before, our method with ac voltammetry can successfully avoid the problem of using a wide potential range since a single potential is enough to measure the potential dependence of the current, which can largely increase the accuracy of the measurement of transfer coefficient or Tafel slope.

Another important point for the dispute of rds and Tafel slope is the possibility of the nucleation of oxygen species, most probably OH, as the rds. Santos [10] and Lebedeva [6, 7] believed that the OH adsorption should be very fast so that this process could not be the rate control step. However, the following facts imply that it's possible that the rate of the whole reaction is determined by OH adsorption:

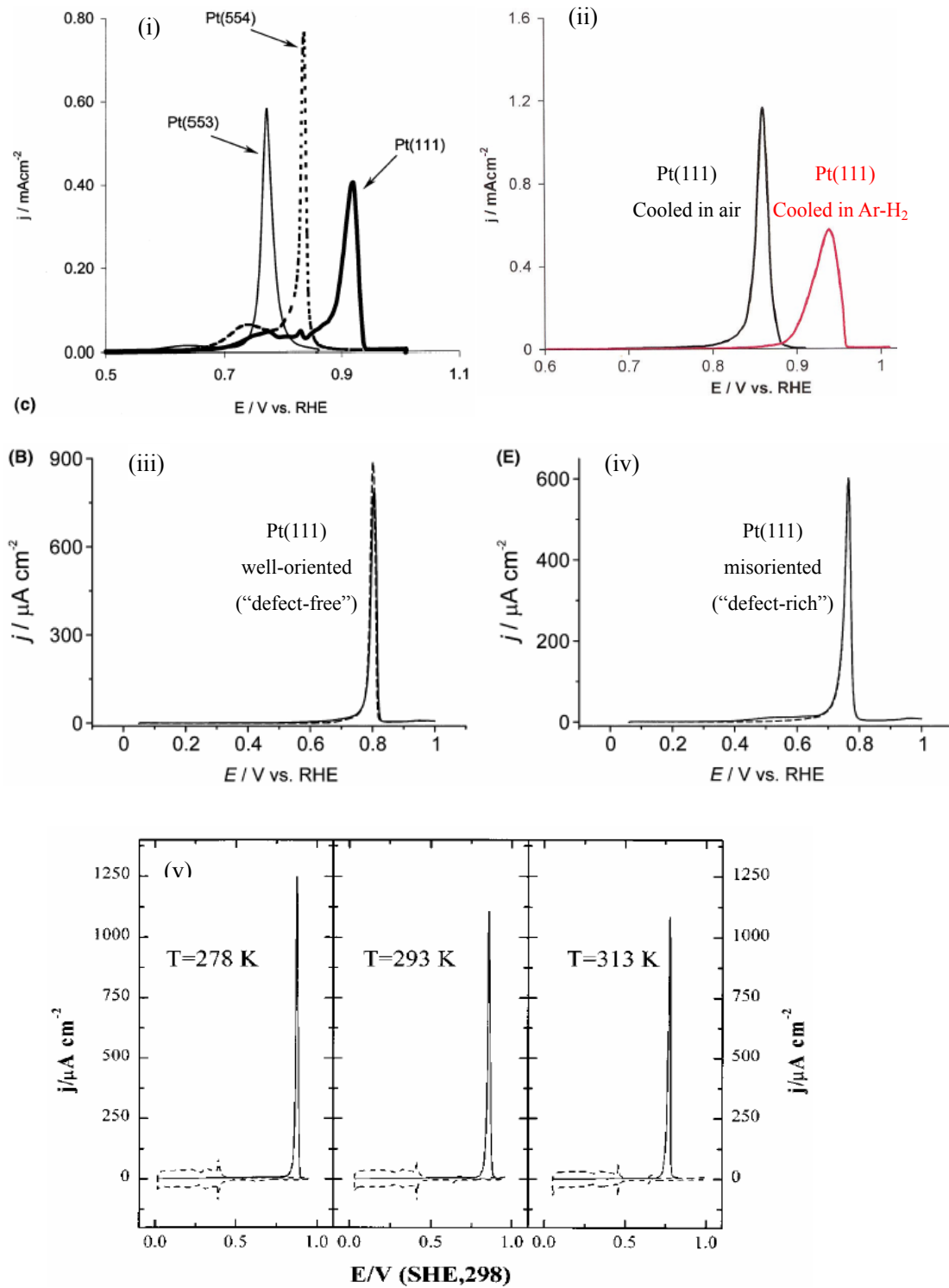


Figure 3-39. CO oxidation on Pt(111) taken from various articles. (i) is adopted from fig.5 of [19]; (ii) adopted from fig.2 of [20]; (iii) and (iv) are adopted from fig.3 of [4]; (v) is adopted from fig.1 of [16].

1) If the 2nd step is the rds, the shape of current peak should be symmetric since the CO oxidation rate is proportional to $\theta_{\text{CO}}(1-\theta_{\text{CO}})$. However, many researchers [4, 19, 20] [16, 18] reported asymmetric peak with a linear increase on the left side and a sudden slump on the right side, as displayed in Figure 3-39, is in favor of equation (3-14) that the reaction rate is proportional to $(1-\theta_{\text{CO}})$ and suggests that the OH

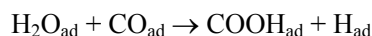
adsorption step is the rds. This type of shape is especially observed on Pt(111) since the wide terrace of Pt(111) made it more difficult for OH adsorption compared with those step surfaces. For the step surface, this shape of CO oxidation peak is not so obvious since the OH nucleation rate is different at different type of sites.

2) Kucernak et al [9] have reported the role of adsorbed hydroxyl species in the CO oxidation on Pt(poly) and drawn a conclusion that it may be the formation and diffusion of OH_{ad} across the surface that limits the rate of CO_{ad} oxidation, instead of the widely believed assumption that the formation of OH is fast enough and the mobility of CO is high enough. The supporting fact is that a clear power law decay can be observed in the current transients both in the presence and absence of an adlayer of CO. The presence of strongly adsorbed anions will also delay the adsorption process of OH. Cuesta [2, 4, 5] believed that the main peak is due to CO oxidation at terrace sites, which indicated that either CO mobility is not so fast or OH formation and diffusion is not so fast enough.

3) High Tafel slope near to $120 \text{ mV}\cdot\text{dec}^{-1}$ are obtained in literature. MaCallum reported Tafel slope of $120 \text{ mV}\cdot\text{dec}^{-1}$ for CO oxidation on Pt wire in 1M HClO_4 . Lebedeva et al [7] got a Tafel slope of $97 \text{ mV}\cdot\text{dec}^{-1}$ (corresponding to $\alpha'=0.61$) on Pt(553). Kucernak et al [9] got Tafel slope of $100 \text{ mV}\cdot\text{dec}^{-1}$ ($\alpha'=0.59$) and $105 \text{ mV}\cdot\text{dec}^{-1}$ ($\alpha'=0.56$) on Pt(poly) by plotting $\log(t_{\text{max}})\sim E$ and $\log(j_{\text{max}})\sim E$, respectively. Vidal-Iglesias et al[21] obtained $120 \text{ mV}\cdot\text{dec}^{-1}$ on Pt(210) electrode and $100 \text{ mV}\cdot\text{dec}^{-1}$ on Pt(310) surface. High Tafel slopes indicate that OH adsorption is not in equilibrium and there is the possibility that OH adsorption is the rds.

3.6.3 About the chemical step as the rds and the detection of COOH_{ad} in literature

Santos et al [10] suggested a chemical step, $\text{CO}_{\text{ad}} + \text{OH}_{\text{ad}} \rightarrow \text{COOH}_{\text{ad}}$, between the two electrochemical steps, as the rds to explain the Tafel slope of “close” to $60 \text{ mV}\cdot\text{dec}^{-1}$. This assumption is agreed by Herrero et al[16], Lebedava et al[6, 7], and so on. As a proof for the existence of this intermediate, Lebedeva cited the detection of COOH_{ad} by Zhu et al [22] using infrared spectroscopy. Surprisingly, Zhu only detected COOH_{ad} at potential region prior to the prepeak instead of that of the main current peak and observed the decrease of the COOH_{ad} signal with the increase of prepeak and finally no signal after prepeak. In this case, Zhu ascribed the prepeak to the oxidation of detected COOH_{ad} species and explained it's formation as the following process:



Where H_{ad} is repulsed by further adsorbed CO and given out as H_2 .

Actually no researcher showed solid proof for the existence of this intermediate COOH_{ad} . And also from our results it is unnecessary to assume such an intermediate and such a chemical step as the rds as suggested by Santos et al.[10]

3.6.4 About the origin of the prepeak

There are several explanations about the origin of the prepeak for CO oxidation on Pt:

1) The prepeak for CO oxidation on Pt is widely observed. Herrero [16] believed that the prepeak for CO oxidation on Pt(111) is due to partial oxidation of adsorbed CO from the more compact layer, $(2 \times 2)\text{-}3\text{CO}$ structure with $\theta_{\text{CO}}=0.75$, to less compact layer, $(\sqrt{19} \times \sqrt{19})R23.4^\circ\text{-}13\text{CO}$ structure with $\theta_{\text{CO}}=0.68$, as shown in Figure 3-40. This kind of structure change was observed by Villegas et al [23] and Oda et al [24] with *in situ* STM.

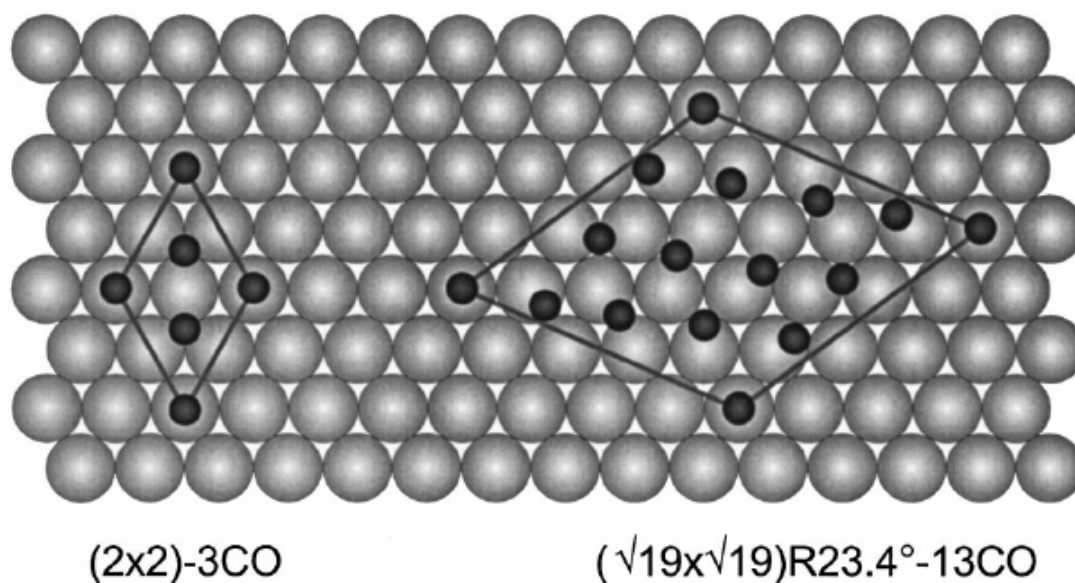


Figure 3-40. Two types of CO adsorption model: $(2 \times 2)\text{-}3\text{CO}$ and $(\sqrt{19} \times \sqrt{19})R23.4^\circ\text{-}13\text{CO}$, which were suggested by Villegas et al [23]. Adopted from [25].

2) Cuesta et al [2, 4, 5] have a systematical investigation on the origin of prepeak for CO oxidation on Pt(111), Pt(100) and Pt(poly) by studying the potential dependence of the saturation coverage of CO on Pt electrodes. They concluded that the prepeak in the voltammogram is due to the oxidation of adsorbed CO on step or defect sites and of a small amount of adsorbed CO diffused from the terraces to these sites, and the main peak corresponds to CO oxidation on terraces where oxygenated species, most probably OH, start to nucleate at higher potentials. This interpretation implies a slow migration of adsorbed CO molecules from terraces to steps or defects, at least for saturated CO adlayers. Prior to the investigation by Cuesta et al, Akemann et al [25] have also assigned the prepeak to the oxidation of CO adjacent to the defects and steps.

3) Markovic *et al.* [3] proposed the existence of two adsorbed CO species on Pt(111), a weakly bonded ($\text{CO}_{\text{ad,w}}$) and a strongly bonded ($\text{CO}_{\text{ad,s}}$). The oxidation of $\text{CO}_{\text{ad,w}}$ at low potential corresponds to the prepeak and in the mean time relaxed the adlayer to low coverage but still fully blocked the surface. The

main peak are due to the oxidation of the rest strong bonded CO.

4) Zhu et al [22] believed that the prepeak is due to the oxidation of COOH_{ad} species, which is formed from adsorbed CO and water at low potentials, since they observed bands of IR absorbance at the wavenumber of COOH species and this signal disappeared after the prepeak.

It is worth to note that many researchers believed that the plateau part of the current transient in potential step experiments shares the same origin as the prepeak.

Actually the explanations about the prepeak from 1) to 3) are not contradictory but result in a consistent picture: different structures of adsorbed CO are formed at different coverage; in the prepeak, CO at high coverage is weakly bonded and firstly oxidized at the defect or step sites; this will relax the CO to a low coverage with a stronger bond.

According to my results, the prepeak part gives an apparent transfer coefficient of around 0.5, which proved that the prepeak follows different mechanism from the main peak. This result is not contradictory to the above assumptions while giving more information on the oxidation mechanism at the prepeak.

3.6.5 About the potential dependence of Tafel slope for CO oxidation in alkaline solution

To elucidate the complexity of CO oxidation, the research progress on the determination of Tafel slope for CO oxidation in alkaline solution is also reviewed and compared with those in acidic solution.

Spendelow et al [26] investigated CO oxidation on Pt(111) in 0.1 M NaOH and got a Tafel slope of $73 \text{ mV}\cdot\text{dec}^{-1}$ on the main peak, similar to that in acidic solution, and concluded that the same mechanism as in acidic electrolyte works for that of alkaline solution, i.e., the Langmuir-Hinshelwood reaction between adsorbed CO and OH to form COOH_{ad} is the rds. García and Koper get a similar slope, $67 \text{ mV}\cdot\text{dec}^{-1}$, for that of Pt(111) and believed in the assumption by Spendelow. For the stepped surfaces, García[27] reported different Tafel slopes at two current peaks corresponding to steps and terraces sites, respectively, and obtained different Tafel slopes. For CO oxidation on step sites, slopes of 83, 92 and $75 \text{ mV}\cdot\text{dec}^{-1}$ were reported on Pt(15,15,14), Pt(554) and Pt(553), respectively. Surprisingly, values of 53, 36 and 39 were reported for α' on terrace sites of these step surfaces. A slope of around $40 \text{ mV}\cdot\text{dec}^{-1}$ corresponds to an apparent transfer coefficient of 1.5, which can be explained by the mechanism that the OH adsorption with one electron transfer is in quasi-equilibrium and the 2nd electron transfer step is the rds. But from the Tafel slopes it seems that the rds at step sites is different from that of terrace sites and also varies on different crystals. In this case, as stated by Gercía, “at the present time, with the available data, it is not really possible to decide which explanation would be the most plausible.” Actually, even for CO oxidation on Pt(111), it's also interesting to observe the shape change with the increase of the sweep rate, as shown in Figure 3-41 cited from the fig.4 of [27]. It is clear that the drop line in the left side of the peak getting steeper and steeper. The Tafel slope at prepeak of CO oxidation current was reported to be $130 \text{ mV}\cdot\text{dec}^{-1}$ by Spendelow and was interpreted as reflecting repulsive lateral interaction in the CO/OH adlayer, while García and Koper believe that it's due to the formation of OH in the CO adlayer as the rds.

The remarkable difference of Tafel slope on different Pt electrode in alkaline solution suggested that the mechanism for CO oxidation is complicated. This also suggests that a rough value of Tafel slope for all the oxidation potentials by Santos and Lebedeva [6, 7, 10] in acidic solution can't give much information on the mechanism. And our method using potential modulation method could offer much more information since a Tafel slope or apparent transfer coefficient is obtained in each potential and independent on the CO coverage.

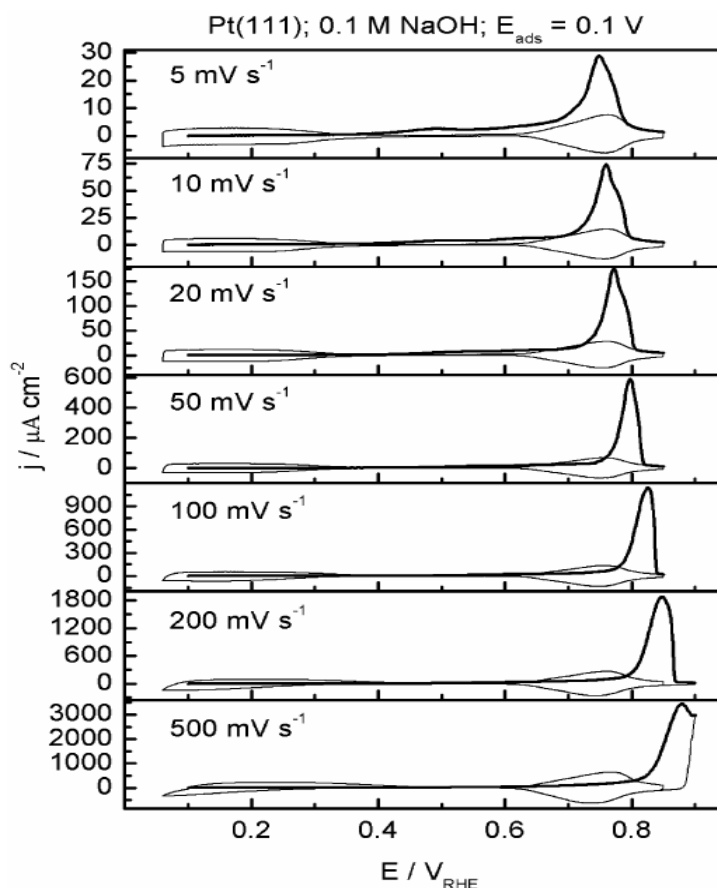


Figure 3-41. CO oxidation on Pt(111) in alkaline solution at various sweep rate. Cited from fig.4 of [27].

3.7 The stepped Pt surfaces modified by Ru and Sn

3.7.1 α' for CO oxidation on Ru step decorated Pt(665)

The CV for Ru deposition on Pt(665), denoted as Ru/Pt(665), is displayed in Figure 3-42. During the potential cycling, the H adsorption peak at 0.12 V decreases gradually, demonstrating that Ru is firstly deposited on the step sites, as also reported by other researchers [28, 29]. After the step is fully covered with Ru, i.e., the peak corresponding to H adsorption on step sites vanishes, the electrode was taken to another cell for further investigations.

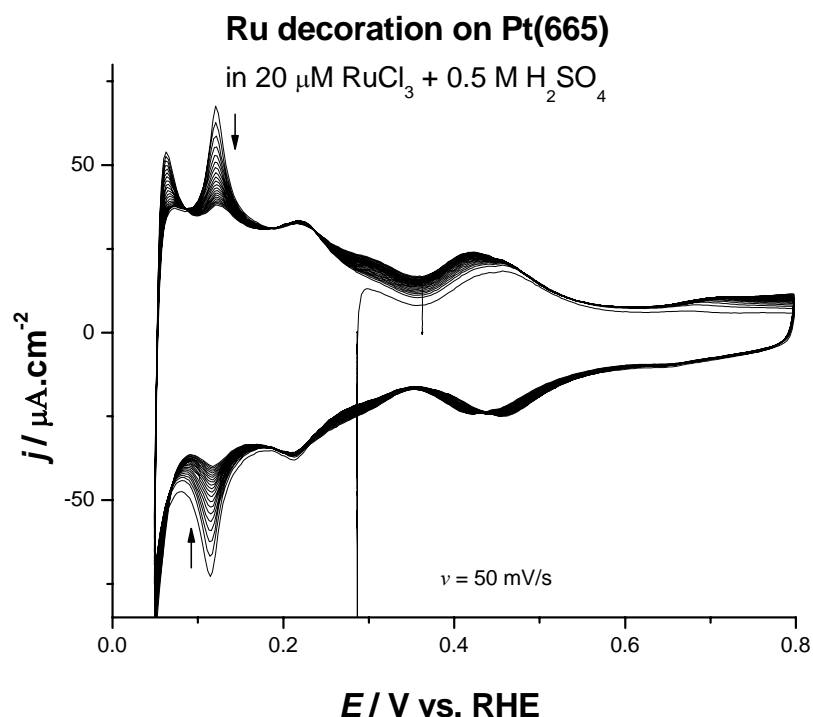


Figure 3-42. CV of Ru decoration on Pt(665). Solution: 20 μM RuCl_3 + 0.5 M H_2SO_4 .

The same procedure was carried out for CO adsorption and oxidation as described previously. The dc current, the real part of the ac current (corrected for slow ion adsorption) and the apparent transfer coefficient for CO oxidation are displayed in Figure 3-43. For the dc current, a sharp peak followed by a hump is observed, in which the peak corresponds to the oxidation of CO_{ad} adjacent to Ru atoms and the hump is the current for CO oxidation at terrace sites far from the steps, as explained by Samjeské et al [30]. The shape of the real part of the ac current is comparable to the dc current in the first peak but too large at more positive potentials due to the slow adsorption of oxygen species and anions. The apparent charge transfer coefficient is displayed in the blue curve and gives a value of 0.7 around the peak, corresponding to a Tafel slope of 84.5 mV.dec^{-1} . The value of α' between 0 and 1 suggests that either the first step, the adsorption of OH, is the rds, or the OH coverage is independent on potential and the second step, the formation of CO_2 is the rds. As suggested by Samjeske et al [30], CO oxidation on Ru/Pt(665) follows the bifunctional mechanism: Pt atoms are the active sites for CO adsorption and Ru atoms act as the active sites for OH adsorption; the reaction occurs between CO and OH at adjacent sites. The adsorption enthalpy in the neighborhood of Ru is increased due to the electronic influence of Ru, as visualized in Figure 3-44. The oxidation potential for adsorbed CO not adjacent to Ru is also lower than at Ru-free electrodes, which is due to the mobility of CO or OH.

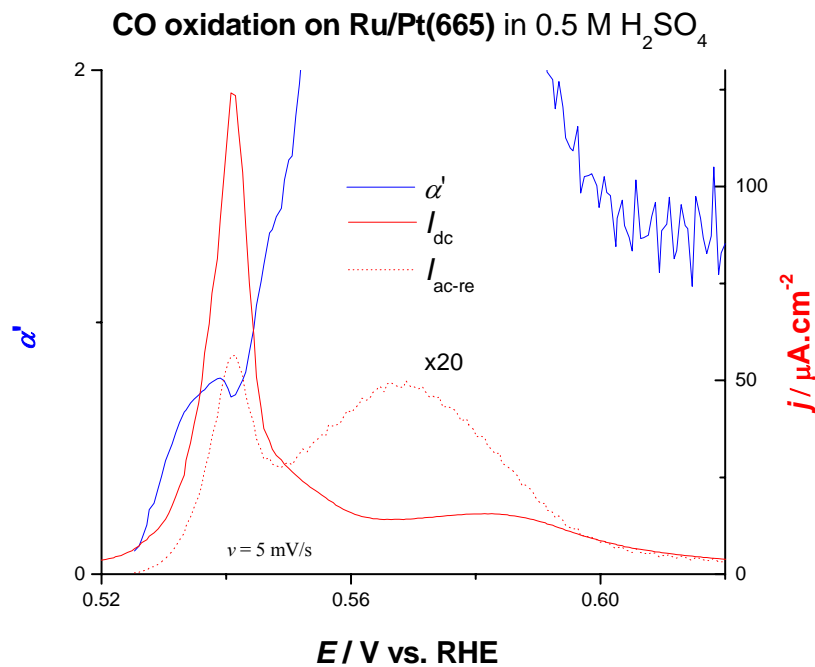


Figure 3-43 The dc current (red), real part of ac current (red dotted, corrected) and the apparent charge transfer coefficient (blue) of CO oxidation on Ru decorated Pt (665). Solution: 0.5 M H₂SO₄. $u_{ac} = 3$ mV.

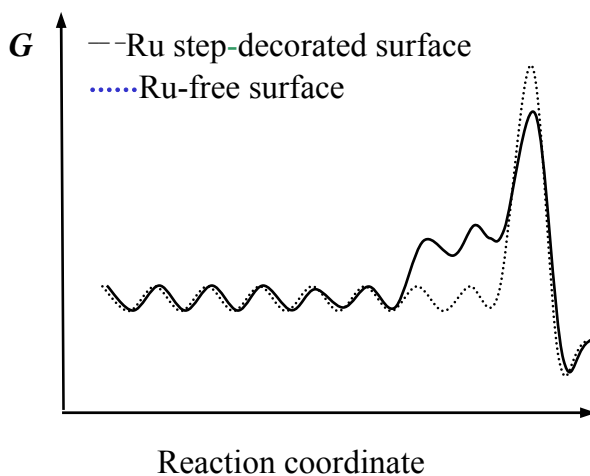


Figure 3-44 Influence of Ru step decoration on activation energy for CO_{ad} oxidation with respect to the reaction coordinate (schematically). (—) Ru-decorated step; (.....) Ru-free surface.

3.7.2 α' for CO oxidation on Sn step decorated Pt(332)

The CV during diffusion limited deposition of sub-monolayer amounts of Sn on Pt (332), is shown in Figure 3-45. From the increasing suppression of the peak for H adsorption at (110) step sites, it is concluded that the Sn deposition on step sites occurs prior to that on terrace sites. After the step sites are fully blocked by Sn, the electrode is transferred into another cell for the CO oxidation experiment.

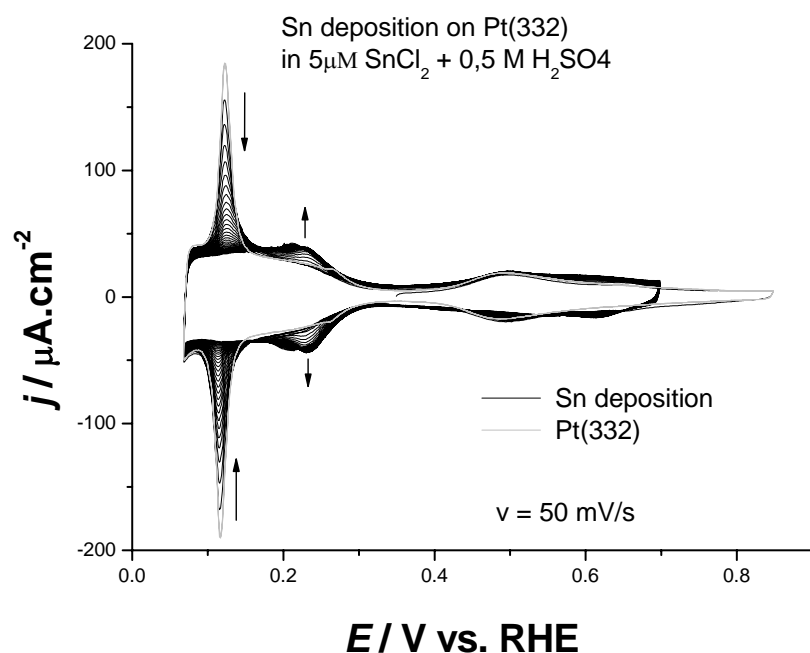


Figure 3-45. CV for Sn decoration on Pt(332). Solution: 5 μM SnCl_2 + 0.5 M H_2SO_4 .

After the CO adsorbed on the electrode at 0.07 V is in saturation and the solution is exchanged with CO-free sulphuric acid, the CV for CO oxidation on Sn/Pt(332) was recorded, as displayed in Figure 3-46. Two separated peaks are observed for CO oxidation: one peak at 0.35 V and the other located around 0.64 V. The lowering of the oxidation potential and the shift of a large amount of CO into the “high coverage state” (oxidized at low potential) were believed to be due to the repulsive reaction between CO and Sn [31, 32]. According to the explanation by Massong et al, electronic effect from Sn will result in strong compression of the CO molecules on the terraces; the first peak is attributed to the oxidation of CO in a decompressing process and the second one is the oxidation of the residual decompressed CO. For the real part of the ac current, the peak around 0.35 V is mainly caused by the Faradaic current of CO oxidation, while the peak at 0.64V is extremely high, which is due to the adsorption of ions and oxidation of some Sn. The apparent transfer coefficient was calculated according to equation (3-8). The real part of the ac current is slightly modified in the calculation. Since the imaginary part of the ac current is always more than 10 times larger than the real part, it's reasonable to subtract the phase shift before CO oxidation in all the potential range and calculate the real part of the ac current caused by CO oxidation according to the adjusted phase. α' is displayed in the blue line, from which we can see that the coefficient at the first peak is about 1, corresponding to a Tafel slope of $60 \text{ mV}\cdot\text{dec}^{-1}$, in accordance with an Eley-Rideal mechanism [31] and a number of electrons of two in the rds.. For the 2nd peak of CO oxidation, no reasonable coefficient can be obtained since Sn oxidation and strong adsorption of other species are involved.

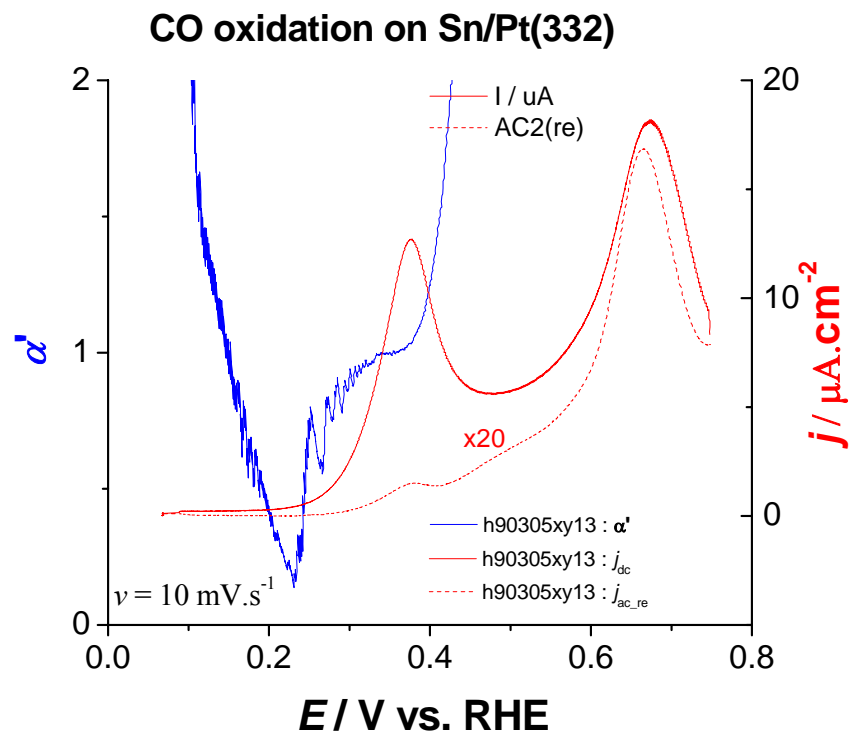


Figure 3-46. The dc current (red), real part of ac current (red dotted, adjusted), and apparent transfer coefficient for CO oxidation on Pt (332) with steps decorated by Sn. Solution: 0.5 M H_2SO_4 . $u_{ac} = 3$ mV.

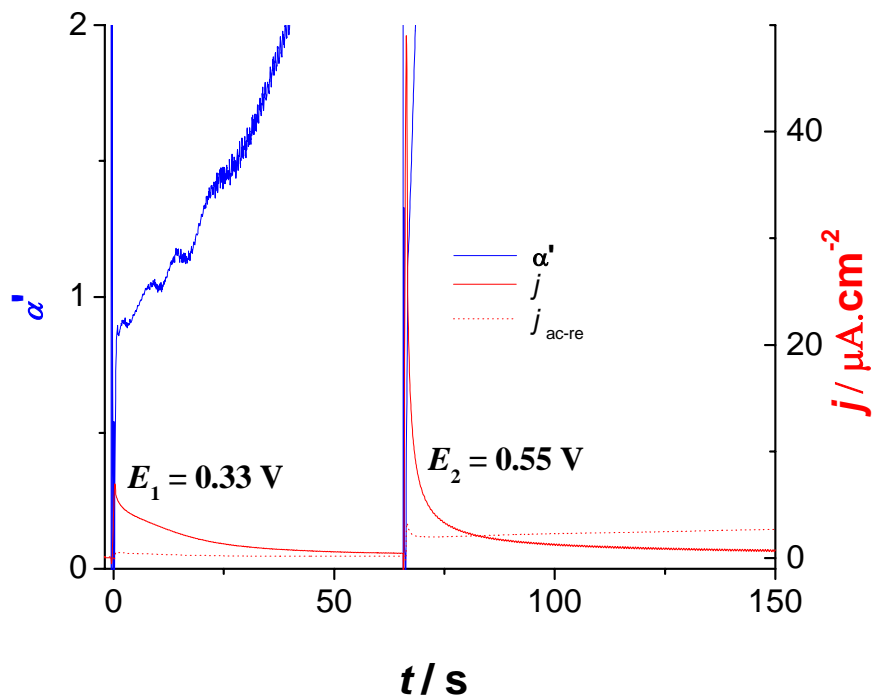


Figure 3-47. CO oxidation and the apparent transfer coefficient on Sn decorated Pt(332). Solution: 0.5 M H_2SO_4 . $u_{ac} = 3$ mV. $f = 18.2$ Hz.

The current transient for CO oxidation on Sn/Pt(332) at successive step potentials of 0.33V and 0.55 V successively is displayed in the red curve of Figure 3-47. Different from the features on pure platinum, the current transient follows a power decay at each step potential. The apparent charge transfer coefficient is measured around 1 at the beginning of CO oxidation at 0.33 V and no reasonable coefficient value can be measured out of this region or at 0.55V due to slow adsorption of other ions. From the current transient, the mechanism for CO oxidation on Sn/Pt(332) is different from that on pure Pt or Ru desorated Pt, as explained by Wang [32] and Massong [31].

3.8 Summary

1. The apparent transfer coefficient for CO oxidation on Pt(poly), Pt(111), Pt(665) and Pt(332) was successfully measured by imposing ac voltage in potential sweep or step experiments. This method made it possible to measure α' or Tafel slope at a fixed potential or coverage in one measurement.
2. α' of CO oxidation on the four Pt electrode was measured to change gradually from about 1.5 to 0.5 with the increase of the step potential, which disproved the assertion that α' value is 1 and a chemical step is the rds. This is the first time to reliably observe the transition of α' or of a Tafel slope. This contributes much to the understanding of the mechanism for this reaction.
3. α' was measured for CO oxidation on Ru step-decorated Pt(665) to be around 0.5 for oxidation of CO adjacent to step sites. α' for CO oxidation on Sn decorated Pt(332) was also measured to be around 1 in the first current peak. These measurements will be of help for the understanding of the mechanism for CO oxidation on Ru and Sn decorated surface.

1. Koper, M.T.M., et al., *Monte Carlo simulations of a simple model for the electrocatalytic CO oxidation on platinum*. Journal of Chemical Physics, 1998. **109**: p. 6051-6062.
2. Cuesta, A., et al., *Potential dependence of the saturation CO coverage of Pt electrodes: The origin of the pre-peak in CO-stripping voltammograms. Part 3: Pt(poly)*. Journal of Electroanalytical Chemistry, 2006. **586**(2): p. 184-195.
3. Markovic, N.M., et al., *Electrooxidation of CO and H₂/CO mixtures on Pt(111) in acid solutions*. Journal of Physical Chemistry B, 1999. **103**: p. 487-495.
4. Lopez-Cudero, A., A. Cuesta, and C. Gutierrez, *Potential dependence of the saturation CO coverage of Pt electrodes: The origin of the pre-peak in CO-stripping voltammograms. Part 1: Pt(1 1 1)*. Journal of Electroanalytical Chemistry, 2005. **579**(1): p. 1-12.
5. Lopez-Cudero, A., A. Cuesta, and C. Gutierrez, *Potential dependence of the saturation CO coverage of Pt electrodes: The origin of the pre-peak in CO-stripping voltammograms. Part 2: Pt(1 0 0)*. Journal of Electroanalytical Chemistry, 2006. **586**(2): p. 204-216.
6. Lebedeva, N.P., et al., *Mechanism and kinetics of the electrochemical CO adlayer oxidation on Pt(111)*. Journal of Electroanalytical Chemistry, 2002. **524**: p. 242-251.
7. Lebedeva, N.P., et al., *Role of Crystalline Defects in Electrocatalysis: Mechanism and Kinetics of CO*

- Adlayer Oxidation on Stepped Platinum Electrodes*. Journal of Physical Chemistry B, 2002. **106**(50): p. 12938-12947.
8. McCallum, C. and D. Pletcher, *An investigation of the mechanism of the oxidation of carbon monoxide adsorbed onto a smooth Pt electrode in aqueous acid*. Journal of Electroanalytical Chemistry, 1976. **70**: p. 277-290.
 9. Kucernak, A.R. and G.J. Offer, *The role of adsorbed hydroxyl species in the electrocatalytic carbon monoxide oxidation reaction on platinum*. Physical Chemistry Chemical Physics, 2008. **10**(25): p. 3699-3711.
 10. Santos, E., E.P.M. Leiva, and W. Vielstich, *CO-adsorbate on Pt(111) single crystal surfaces*. Electrochimica Acta, 1991. **36**(3/4): p. 555-561.
 11. Love, B. and J. Lipkowski. *Effect of surface crystallography on electrocatalytic oxidation of Carbon monoxide on Platinum electrodes*. in *ACS Symposium Series*. 1988: Amer. Chemical Soc., 1155 16th St, NW, Washington, DC 20036.
 12. Bergelin, M., et al., *Oxidation of CO adlayers on Pt(111) at low potentials: an impinging jet study in H₂SO₄ electrolyte with mathematical modeling of the current transients*. Journal of Electroanalytical Chemistry, 1999. **467**: p. 74-84.
 13. Garcia-Araez, N., et al. *Thermodynamic analysis of (bi)sulphate adsorption on a Pt(111) electrode as a function of pH*. 2008: Pergamon-Elsevier Science Ltd.
 14. Funtikov, A.M., et al., *An in-Situ Stm Study of Anion Adsorption on Pt(111) from Sulfuric-Acid-Solutions*. Surface Science, 1995. **324**(1): p. L343-L348.
 15. Palaikis, L., et al., *Surface electrochemistry of carbon monoxide adsorbed from electrolytic solutions at single crystal surfaces of Pt(111) and Pt(100)*. Surface Science, 1988. **199**: p. 183-198.
 16. Herrero, E., et al., *Temperature dependence of CO chemisorption and its oxidative desorption on the Pt(111) electrode*. Langmuir, 2000. **16**(11): p. 4779-4783.
 17. Lebedeva, N.P., et al., *Role of crystalline defects in electrocatalysis: CO adsorption and oxidation on stepped platinum electrodes as studied by in situ infrared spectroscopy*. Journal of Physical Chemistry B, 2002. **106**(38): p. 9863-9872.
 18. Inkaew, P. and C. Korzeniewski, *Kinetic studies of adsorbed CO electrochemical oxidation on Pt(335) at full and sub-saturation coverages*. Physical Chemistry Chemical Physics, 2008. **10**(25): p. 3655-3661.
 19. Lebedeva, N.P., et al., *CO oxidation on stepped Pt[n(111)x(111)] electrodes*. Journal of Electroanalytical Chemistry, 2000. **487**(1): p. 37 - 44.
 20. Lebedeva, N.P., et al., *The effect of the cooling atmosphere in the preparation of flame-annealed Pt(111) electrodes on CO adlayer oxidation*. Electrochemistry Communications, 2000. **2**(7): p. 487-490.
 21. Vidal-Iglesias, F.J., et al., *CO monolayer oxidation on stepped Pt(S) [(n - 1)(1 0 0) × (1 1 0)] surfaces*. Electrochimica Acta, 2009. **54**(19): p. 4459-4466.
 22. Zhu, Y.M., H. Uchida, and M. Watanabe, *Oxidation of carbon monoxide at a platinum film electrode studied by Fourier transform infrared spectroscopy with attenuated total reflection technique*. Langmuir, 1999. **15**(25): p. 8757-8764.
 23. Villegas, I. and M.J. Weaver, *Carbon monoxide adlayer structures on platinum (111) electrodes: A synergy between in-situ scanning tunneling microscopy and infrared spectroscopy*. Journal of Chemical Physics, 1994. **101**(2): p. 1648-1660.
 24. Oda, I., J. Inukai, and M. Ito, *Compression Structures of Carbon-Monoxide on a Pt(111) Electrode Surface Studied by Insitu Scanning Tunneling Microscopy*. Chemical Physics Letters, 1993. **203**(2-3): p. 99-103.
 25. Akemann, W., K.A. Friedrich, and U. Stimming, *Potential-dependence of CO adlayer structures on Pt(111) electrodes in acid solution: Evidence for a site selective charge transfer*. Journal of Chemical Physics, 2000. **113**(16): p. 6864-6874.
 26. Spendlow, J.S., et al., *Mechanism of CO oxidation on Pt(111) in alkaline media*. Journal of Physical Chemistry B, 2006. **110**(19): p. 9545-9555.
 27. Garcia, G. and M.T.M. Koper, *Stripping voltammetry of carbon monoxide oxidation on stepped platinum single-crystal electrodes in alkaline solution*. Physical Chemistry Chemical Physics, 2008. **10**(25): p. 3802-3811.
 28. Massong, H., *Elektrochemische CO-Oxidation an Pt(111)- und Pt(332)-Einkristalloberflächen modifiziert durch Ruthenium-, Zinn- und Bismut-UPD und Kupfer- Untersuchungen mit der Differentiellen Elektrochemischen Massen-Spektrometrie (DEMS)*, in *Department of Physical and Theoretical Chemistry*. 2004, Bonn University: Bonn. p. 212.
 29. Del Colle, V., et al., *Ethanol electrooxidation onto stepped surfaces modified by Ru deposition: electrochemical and spectroscopic studies*. Physical Chemistry Chemical Physics, 2008. **10**(25): p. 3766-3773.
 30. Samjeské, G., X.-Y. Xiao, and H. Baltruschat, *Ru decoration of stepped Pt single crystals and the role of the terrace width on the electrocatalytic CO oxidation*. Langmuir, 2002. **18**(12): p. 4659-4666.

31. Massong, H., et al., *On the influence of tin and bismuth UPD on Pt(111) and Pt(332) on the oxidation of CO*. *Electrochimica Acta*, 1998. **44**(8-9): p. 1379-1388.
32. Wang, K.L., et al., *On the reaction pathway for methanol and carbon monoxide electrooxidation on Pt-Sn alloy versus Pt-Ru alloy surfaces*. *Electrochimica Acta*, 1996. **41**(No.16): p. 2587-2593.

4 The surface volume excess of hydrogen adsorption on polycrystalline Pt and the effect of cations

Adsorption of hydrogen at Pt electrode plays a key role in many electrocatalytic reactions, be it in dehydrogenation reactions, which are the first stage of alcohol oxidations [1], be it in hydrogenation of double or triple bonds, as the hydrogenation of ethene [2]. Adsorption of hydrogen is very sensitive to surface orientation and cleanliness; cyclic voltammetry in the hydrogen region therefore is an often used tool for the characterisation of single crystal electrodes.[3-6] Also the rate of hydrogen adsorption depends on the crystal orientation: it is fastest on Pt(111) both in alkaline and acidic solutions.[7-10]

From this adsorbed hydrogen, which manifests itself as a pseudocapacitive charge at potentials well above the equilibrium potential of hydrogen evolution, an adsorbed hydrogen has to be distinguished which is the intermediate during hydrogen evolution. Whereas the first type of adsorbed hydrogen cannot be observed by vibrational spectroscopies, the second can.[11-13]

Despite of its importance, little is known on the adsorbed hydrogen, in particular on the “first” type. It is often assumed that on Pt (111) this is a hydrogen atom in threefold hollow sites, which would explain its invisibility by IR spectroscopy because of the small dynamic dipole moment.

The volume of adsorption for the hydrogen adsorption reaction has already been determined using a new dynamic pressure modulation technique in our group.[14] Whereas usually for the determination of pressure dependences of chemical reaction rates measurements in the pressure range of up to 1000 bar (10^8 Pa) are performed, using our method activation and adsorption volumes can be determined by a pressure modulation within an amplitude of 1 bar. Changes of the volume in the adsorbed state or on the activated complex are largely determined by the charge density due to electrostriction, and therefore the volume of adsorption should give some information on the charge densities. The volume of adsorbates also could play a role in the interaction between AFM tips and the surface, because above a certain force (and thus pressure) exerted by the tip onto the surface adsorbates might be displaced. This could lead to an additional energy dissipation and thus friction.[15, 16]

The volume of adsorption is closely related to the surface volume excess, and, strictly speaking, only the latter can be directly measured.

4.1 Volume change for $\text{Fe}(\text{CN})_6^{3-} + \text{e}^- \leftrightarrow \text{Fe}(\text{CN})_6^{4-}$: a test experiment

4.1.1 Principles for measuring reaction volume by the method of Pressure modulation

The setup is tested with by measuring the reaction volume of $\text{Fe}(\text{CN})_6^{3-} + \text{e}^- \leftrightarrow \text{Fe}(\text{CN})_6^{4-}$, which is well investigated by many researchers [17-20].

According to the Gibbs function, we can get

$$\frac{\partial \Delta G^R}{\partial p} = \Delta V^R \quad (4-1)$$

For an electrochemical reaction,

$$\Delta G^R = -nFE \quad (4-2)$$

Then

$$\Delta V^R = -nF \frac{dE}{dp} \quad (4-3)$$

Since the potential is under the control of the potentiostat, so

$$E_{\text{WE}} - E_{\text{RE}} = \Delta E = \text{const} \quad (4-4)$$

$$\frac{dE_{\text{WE}}}{dp} = \frac{dE_{\text{RE}}}{dp} \quad (4-5)$$

For the current arising from pressure modulation ($p = p_A \cdot \sin(\omega t)$),

$$i_{\text{PM}} = \frac{dq}{dt} = \frac{CdE}{dt} = \frac{CdE}{dp} \frac{dp}{dt} = C \cdot \left(\frac{dE}{dp} \right) \cdot p_A \omega \cos(\omega t) \quad (4-6)$$

Since the phase for i is shifted by -90° compared with the pressure, $\cos(\omega t)$ can be replaced with a phasor notation j , where $j = \sqrt{-1}$.

$$\left(\frac{dE}{dp} \right) = \frac{\vec{i}_{\text{PM}}}{C \cdot p_A \omega j} \quad (4-7)$$

If the small $\vec{i}_{\text{PM}} \cdot R$ drop from solution is taken into account, and then \vec{i}_{PM} should be replaced by $\vec{i}_{\text{PM}} / \sin(\omega t)$ and the equation should be changed to the following

$$\left(\frac{dE}{dp} \right) = \frac{\vec{i}_{\text{PM}}}{C \cdot p_A j \omega \sin \varphi} = \frac{i_A}{C \cdot p_A \omega \sin \varphi} \quad (4-8)$$

Where i_A is the amplitude of the current from pressure modulation. Substitute the differential in equation (4-3) with equation (4-8), then we get

$$\Delta V^R = -\frac{nFi_A}{p_A C \omega \sin \varphi} \quad (4-9)$$

4.1.2 Results and discussion

The typical cyclic voltammogram of the reaction $\text{Fe}(\text{CN})_6^{3-} + e^- \leftrightarrow \text{Fe}(\text{CN})_6^{4-}$ is displayed in Figure 4-1(a), in which a pair of reversible peaks are attributed to the oxidation and reduction of iron. The capacitance was also measured by ac voltammetry and is displayed in Figure 4-1(b), in which almost the same values are obtained in for all the frequencies measured. The amplitude and phase of the ac current generated from pressure modulation at frequencies of 35.2, 94.2, 165.2, 215 and 336 Hz are displayed in Figure 4-1(c) and (d). Taking the amplitude and phase at -0.5 V in cathodic scan and the average capacitance (3.2 μF) measured at the same potential, the reaction volumes were thus calculated according to equation (4-9) and listed in Table 4-1. The average of the reaction volume is measured to be 28.7 $\text{cm}^3 \cdot \text{mol}^{-1}$ with the root-mean-square deviation of 0.6 $\text{cm}^3 \cdot \text{mol}^{-1}$, which agrees well with those in literature: 35 $\text{cm}^3 \cdot \text{mol}^{-1}$ by Sato et al [17], 29.7 $\text{cm}^3 \cdot \text{mol}^{-1}$ by Doine et al. [18], 29.8 ± 1.6 by Kitamura JI et al. [19], 30 $\text{cm}^3 \cdot \text{mol}^{-1}$ by Bajaj HC et al. [20] and average value 31.5 $\text{cm}^3 \cdot \text{mol}^{-1}$ by Loewe et al [14].

The value measured here is slightly lower than the volume change predicted from the contribution of pure electrostriction, i.e., 30.1 $\text{cm}^3 \cdot \text{mol}^{-1}$, calculated on the basis of $\Delta V_{\text{electr}} = 4.3\Delta(z^2)$ with $\Delta(z^2)$ refers to the “local” change in charge [20]. The results of this measurement demonstrated the reliability of this setup.

Table 4-1. reaction volume of $\text{Fe}(\text{CN})_6^{3-/4-}$ ($\text{Fe}(\text{CN})_6^{4-} \rightarrow \text{Fe}(\text{CN})_6^{3-}$) measured at various frequencies. All the original data are taken at -0.5V.

f/Hz	I/nA	$\varphi/^\circ$	\tilde{V}/V	$P/10^5\text{ Pa}$	$\Delta V_R/\text{cm}^3 \cdot \text{mol}^{-1}$
35.2	22.9	84.5	1.664	1.090	28.9
94.2	57.8	79.3	1.639	1.073	28.0
165.2	100.5	72	1.597	1.046	29.5
215	124.9	71.4	1.555	1.018	29.0
336	171.4	69.5	1.420	0.930	28.2

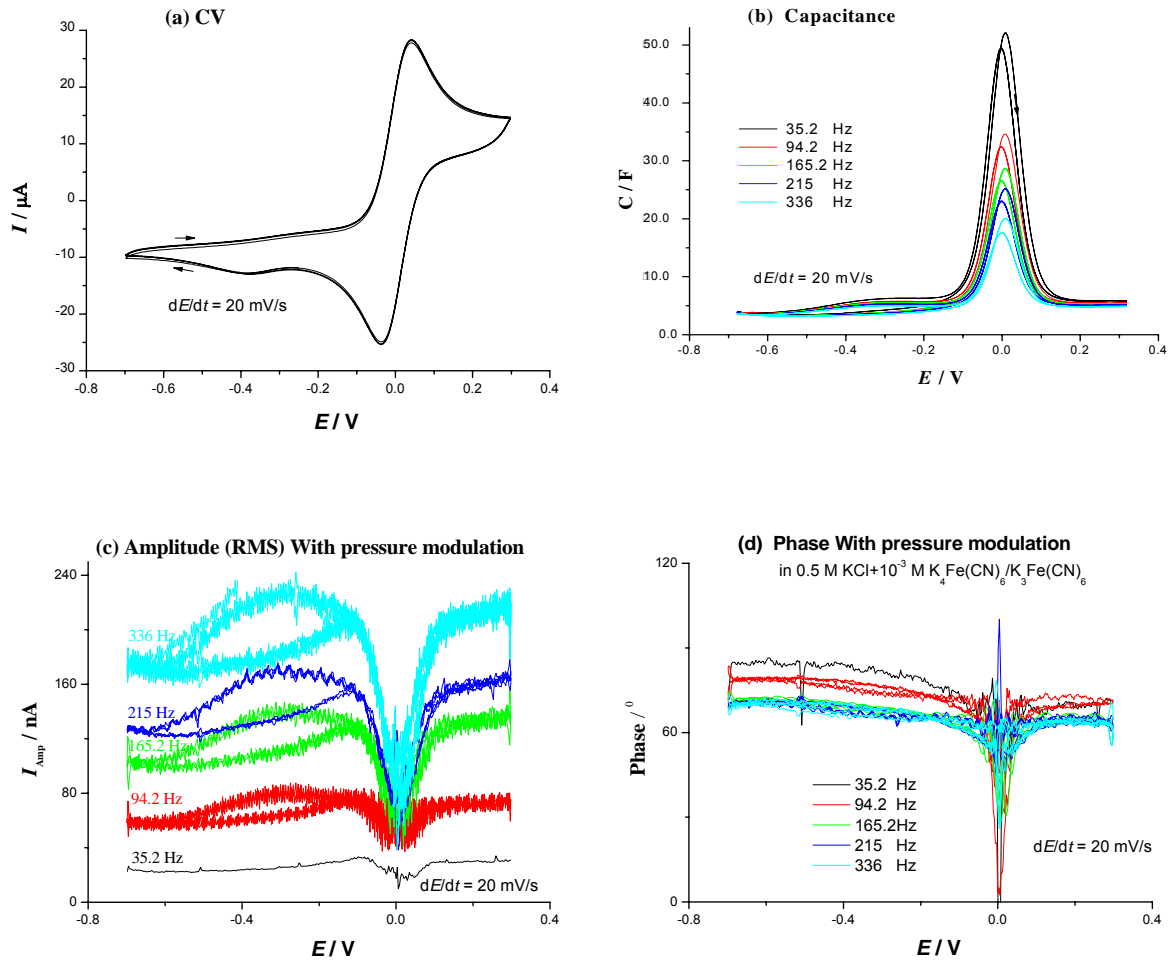


Figure 4-1. CV (a), capacitance (b), and amplitude (c) and phase (d) of ac current induced by pressure modulation. Electrode: Pt wire. Solution: 0.5 M KCl + 1mM $K_4Fe(CN)_6 / K_3Fe(CN)_6$. $dE/dt = 20 \text{ mV}\cdot\text{s}^{-1}$.

4.2 Principles and calculations for surface volume excess measurements

4.2.1 Principles

According to Hills et al [21], the basic electrocapillary equation can be expressed as

$$-d\gamma = \Gamma_s dT - \Gamma_V dp + \sum_i \Gamma_i d\mu_i + qdE \quad (4-10)$$

Here γ is interfacial tension of electrode. Γ_s , Γ_V and Γ_i are surface excess of entropy, volume and amount of species i , respectively. T is system temperature, p pressure, μ chemical potential and q surface charge. According to Schwarz's theorem,

$$\left(\frac{\partial \Gamma_v}{\partial E}\right)_{T, \mu_i, p} = -\left(\frac{\partial q}{\partial p}\right)_{T, \mu_i, E} \quad (4-11)$$

Since q is a function of p and μ_i , which is a function of p , its total dependence on pressure is given by

$$\left(\frac{\partial q}{\partial p}\right)_{T, c_i} = \left(\frac{\partial q}{\partial p}\right)_{T, E, \mu_i} + \sum_i \left(\frac{\partial q}{\partial \mu_i}\right)_{T, E, p} \cdot \left(\frac{\partial \mu_i}{\partial p}\right)_{c_i} \quad (4-12)$$

Here,

$$\left(\frac{\partial \mu_i}{\partial p}\right)_{c_i} = v_i \quad (4-13)$$

v_i is the partial molar volume of species i .

Another cross differentiation of equation (4-10) yields:

$$\left(\frac{\partial q}{\partial \mu_i}\right)_{T, E, p} = \left(\frac{\partial \Gamma_i}{\partial E}\right)_{T, \mu_i, p} \quad (4-14)$$

Combination of equations of (4-11)~ (4-14) yields:

$$\left(\frac{\partial \Gamma_v}{\partial E}\right)_{T, \mu_i, p} = -\left(\frac{\partial q}{\partial p}\right)_{T, E, c_i} + \sum_i \left(\frac{\partial \Gamma_i}{\partial E}\right)_{T, \mu_i, p} v_i \quad (4-15)$$

$$\text{or } d\Gamma_v = -\left(\frac{\partial q}{\partial p}\right)_{T, E, c_i} dE + \sum_i v_i d\Gamma_i \quad (4-16)$$

Here the first term on the right side can be measured as follows: a sinusoidal pressure $p = p_A \cdot \sin(\omega t)$ is applied to the system, then the charge and its derivative with time, the current, will also oscillate with the same frequency and we have:

$$\left(\frac{\partial q}{\partial p}\right)_T = \frac{\partial q / \partial t}{\partial p / \partial t} = \frac{i}{p_A \omega \cos(\omega t)} \quad (4-17)$$

In phasor notation:

$$\left(\frac{\partial q}{\partial p}\right)_T = \frac{\vec{i}_{PM}}{p_A \omega \cdot j} \quad (j = \sqrt{-1}) \quad (4-18)$$

Since this expression should give a real value, the current should be phase shifted by 90° with respect to the pressure. Therefore, from the amplitude of the oscillating current caused by the pressure modulation the potential dependence of the surface volume excess can be obtained. Here \vec{I}_i is obtained by integrating the adsorption current.

In practice, one has to take into account the potential drop at the electrolyte resistance and the pressure dependence of the reference electrode. Firstly, the effect of the electrolyte resistance will be treated. The total impedance Z can be interpreted as a resistance (R), which comes from the solution between reference and working electrode, and the capacitance (C), which originates mostly from adsorption and to a small part from double layer charging, in series, i.e., $Z=Z_C+R$. It should be noted that the E in the above equations refers to the potential across the capacitance (E_C), which is a function of pressure. Then equation (4-12) should be modified as the following:

$$\left(\frac{\partial q}{\partial p}\right)_T = \left(\frac{\partial q}{\partial p}\right)_{T,E,\mu_i} + \left(\frac{\partial q}{\partial E_C}\right)_{T,\mu_i,p} \cdot \left(\frac{\partial E}{\partial p}\right) + \sum_i \left(\frac{\partial q}{\partial \mu_i}\right)_{T,E,p} \cdot \left(\frac{\partial \mu_i}{\partial p}\right)_{c_i} \quad (4-19)$$

$$\text{Here } \left(\frac{\partial q}{\partial E_C}\right)_{T,\mu_i,p} = C \quad (4-20)$$

Since $E_Z=E_C+i \cdot R$ and E_Z is constant under the control of a potentiostat,

$$\left(\frac{\partial E_C}{\partial p}\right) = \frac{\partial E_C / \partial t}{\partial p / \partial t} \quad (4-21)$$

$$\frac{dE_C}{dt} = -R \cdot \frac{di}{dt} = -R \cdot \frac{d(i_{dc} + \vec{i}_{PM} \sin(\omega t))}{dt} = -R \vec{i}_{PM} \omega j \quad (4-22)$$

$$\text{So, } \left(\frac{\partial E_C}{\partial p}\right) = \frac{-R \vec{i}_{PM} \omega j}{\vec{p}_A \omega j} = \frac{-R \vec{i}_{PM}}{\vec{p}_A} \quad (4-23)$$

Substitute the differentials in equation (4-19) with equations (4-12)~(4-23),

$$\begin{aligned} \left(\frac{\partial \Gamma_v}{\partial E_C}\right)_{T,\mu_i,p} &= -\frac{\vec{i}_{PM}}{p_A \omega \cdot j} + C \cdot \frac{-R \vec{i}_{PM}}{p_A} + \sum_i \left(\frac{\partial \Gamma_i}{\partial E_C}\right)_{T,\mu_i,p} v_i \\ &= -\frac{\vec{i}_{PM}}{p_A} \left(\frac{1}{\omega \cdot j} + RC\right) + \sum_i \left(\frac{\partial \Gamma_i}{\partial E_C}\right)_{T,\mu_i,p} v_i \\ &= -\frac{\vec{i}_{PM}}{p_A} \cdot \vec{Z} \cdot C + \sum_i \left(\frac{\partial \Gamma_i}{\partial E_C}\right)_{T,\mu_i,p} v_i \end{aligned} \quad (4-24)$$

$$\text{With } \vec{Z} = R + \frac{1}{j\omega C}.$$

The impedance \vec{Z} can be measured with ac voltammetry, with \vec{u}_{ac} and \vec{i}_{ac} are denoted as ac voltage input and the ac current generated thereafter. Then we can obtain the following:

$$\vec{Z} = \frac{\vec{u}_{ac}}{\vec{i}_{ac}} \quad (4-25)$$

If only one species such as hydrogen is involved in the adsorption process,

$$dq = nFd\Gamma_i = CdE_C \quad (4-26)$$

$$\frac{dE_C}{d\Gamma_i} = \frac{nF}{C} \quad (4-27)$$

Here n is the electron number exchanged in reaction and F the Faradic constant. C is the adsorption capacitance and the double layer capacity is neglected.

$$\frac{\partial \Gamma_V}{\partial \Gamma_i} = -\frac{nF\vec{i}_{PM} \cdot \vec{Z}}{p_A} + \sum_i v_i \quad (4-28)$$

Multiplying equations (4-24) with (4-28),

$$\Delta v_{ad} = \frac{d\Gamma_V}{d\Gamma_i} - v_i = -\frac{nF}{p_A} \cdot \vec{Z} \cdot \vec{i}_{PM} = -\frac{nF}{p_A} \cdot \vec{u}_{ac} \cdot \vec{i}_{PM} \quad (4-29)$$

This equation gives the molar adsorption volume. The quantity $d\Gamma_V/d\Gamma_i$ is the partial molar volume of the adsorbate. Both \vec{i}_{PM} and \vec{i}_{ac} contain a real and imaginary component and can therefore be separated with $\vec{i}_{ac} = X + Yj$ and $\vec{i}_{PM} = x + yj$. Then the equation (4-29) can be written as:

$$\frac{d\Gamma_V}{d\Gamma_i} - v_i = -\frac{nF}{p_A} \cdot \vec{u}_{ac} \cdot \frac{(xX + yY) + j(Xy - xY)}{X^2 + Y^2} \quad (4-30)$$

Only the real part is meaningful since the left side in the equation (4-30) should be real value and the imaginary part should be zero if \vec{i}_{PM} and \vec{i}_{ac} have the same phase shift with respect to the pressure modulation or the ac potential, respectively. From equation (4-30), the surface volume excess in reaction process can be achieved combining the pressure modulation method and the ac voltammetry.

4.2.2 Corrections for the pressure dependence of the reference electrode

For the reference electrode of Ag/AgCl, the potential is determined by the ratio of the oxidant and reductant in the interface and also changed according to the sinusoidal vibrational pressure. The half reaction process can be described as the following:



According to the equation related to the change of Gibbs function (ΔG),

$$d\Delta G = -nF \cdot dE_{RE} = -\Delta SdT + \Delta V_{RE}dp \quad (4-31)$$

Here ΔS is the entropy change, ΔV_{RE} the volume change of the half reaction in reference electrode. If T is

constant,

$$dE_{\text{RE}} = \frac{\Delta V_{\text{RE}} dp}{-nF} \quad (4-32)$$

$$\Delta E_{\text{RE}} = \frac{\Delta V_{\text{RE}} p_A}{-nF} \quad (4-33)$$

The volume change for the half reaction of our reference electrode can be obtained by the following calculation:

$$\Delta V_{\text{RE}} = \nu_{\text{Cl}^-} + \nu_{\text{Ag}} - \nu_{\text{AgCl}} \quad (4-34)$$

The equivalent circuit of the reference electrode under pressure modulation can be represented as diagram in Figure 4-2.

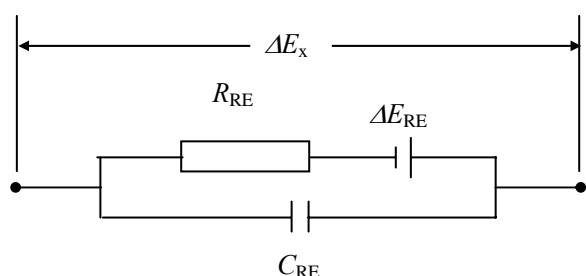


Figure 4-2. Diagram for Ag/AgCl reference electrode under pressure modulation.

The voltage generated by pressure modulation leads to a charging of the double layer capacitance of the reference electrode through its charge transfer resistance. The total pressure induced potential vibration is thus reduced by the internal $i \cdot R$ drop. (Note that there is no external current flow.) In an independent measurement under similar conditions to that of pressure modulation but using Ag/AgCl as working electrode, the phase angle φ of the impedance is measured to be -70° at around 30 Hz. If the impedance is considered to be composed of resistance and capacitance in parallel, as shown in the diagram, the phase shift is given by $\cot |\varphi| = \omega RC$. From the identity of the internal current through R and C we get:

$$\Delta \vec{E}_x = \frac{\Delta \vec{E}_{\text{RE}}}{1 + j\omega CR} = \frac{1}{1 + j(\cot |\varphi|)} \cdot \frac{\Delta V_{\text{RE}} p_A}{-nF} \quad (4-35)$$

To obtain ΔV_{RE} , the molar volume of Ag (ν_{Ag}) and AgCl (ν_{AgCl}) can be calculated from the molecular mass divided by their bulk densities and gives value of 10.3 and 25.8 $\text{cm}^3 \cdot \text{mol}^{-1}$ respectively [22, 23]. The partial molar volume of Cl^- (ν_{Cl^-}) can be calculated from that of HCl (ν_{HCl}) and H^+ (ν_{H^+}) at the same ionic strength I assuming that the deviation of ν_i from ν_i^0 , the partial molar volume in infinitely diluting solution, depends mainly on the ionic strength [24, 25]. Here ν_{HCl} can be derived from density-composition measurement [26], which are 18.9 and 18.6 $\text{cm}^3 \cdot \text{mol}^{-1}$ at the same ionic strength as H_2SO_4 with concentration of 0.6 M ($I = 0.6$ M) and 0.1 M ($I = 0.1$ M), respectively. ν_{H^+} is the sum of $\nu_{\text{H}^+}^0$ (widely accepted to be $-5.4 \text{ cm}^3 \cdot \text{mol}^{-1}$

[27, 28]) and the correction according to ionic strengths calculated from extended Debye-Hückel equation[24, 25], which is 0.5 and 0.3 $\text{cm}^3 \cdot \text{mol}^{-1}$, respectively. Thus v_{Cl^-} is calculated to be 23.8 and 23.7 $\text{cm}^3 \cdot \text{mol}^{-1}$ at an ionic strength of 0.6 M and 0.1 M, separately, as listed in Table 4-2. It is worth to note that, the conventional partial molar volumes of ions are relative values based on the assumption of $v_{\text{H}^+}^0 = 0$ at all temperatures. In this thesis, “absolute” values are used for all the ions, e.g., $v_{\text{H}^+}^0 = -5.4 \text{ cm}^3 \cdot \text{mol}^{-1}$.

$$v_{\text{H}^+} = v_{\text{H}^+}^0 + \Delta v_{\text{H}^+} \quad (4-36)$$

$$v_{\text{Cl}^-} = v_{\text{HCl}} - v_{\text{H}^+} \quad (4-37)$$

And ΔV_{RE} is calculated to be 8.3 and 8.2 $\text{cm}^3 \cdot \text{mol}^{-1}$.

Table 4-2 Partial molar volume of H^+ , HCl and Cl^- at different ionic strength. Unit: $\text{cm}^3 \cdot \text{mol}^{-1}$.

Species \ I / mol/kg	0	0.1	0.6	1.4
H^+	-5.4 [27, 28]	-5.1 [24, 25]	-4.9 [24, 25]	-4.7 [24, 25]
HCl	17.8 [29]	18.6 [26]	18.9 [26]	19.3 [26]
Cl^- ($v_{\text{Cl}^-} = v_{\text{HCl}} - v_{\text{H}^+}$)	23.2	23.7	23.8	24
Ag	10.3 [22, 23]			
AgCl	25.8 [22, 23]			

If the contribution from reference electrode due to pressure modulation is taken into account, then the experiment value i_{PM} is given by the following:

$$\vec{i}_{\text{PM}} = \frac{\Delta \vec{E}_{\text{WE}}}{\vec{Z}} - \frac{\Delta \vec{E}_{\text{x}}}{\vec{Z}} \quad (4-38)$$

Then the equation (4-29) should be modified to the following:

$$\left(\frac{d\Gamma_{\text{v}}}{d\Gamma_{\text{i}}} - v_{\text{i}} \right) = -\frac{nF}{p_A} \cdot \vec{Z} \cdot \frac{\Delta \vec{E}_{\text{WE}}}{\vec{Z}} \quad (4-39)$$

Substitute the equations (4-34), (4-35) and (4-38) into (4-39), then

$$\begin{aligned} \left(\frac{d\Gamma_{\text{v}}}{d\Gamma_{\text{i}}} - v_{\text{i}} \right) &= -\frac{nF}{p_A} \cdot \vec{Z} \cdot \vec{i}_{\text{PM}} + \frac{\Delta V_{\text{RE}}}{1 + j(\cot|\phi|)} \\ &= -\frac{nF}{p_A} \cdot \vec{Z} \cdot \vec{i}_{\text{PM}} + (7.3 - 2.6j) \text{ cm}^3 \cdot \text{mol}^{-1} \end{aligned} \quad (4-40)$$

It should be noted that, if the phase shift of the impedance of the RE is neglected, the above equation can be simplified as:

$$\Delta V_{\text{ad}} - \Delta V_{\text{RE}} = v_{\text{H}_{\text{ad}}} - v_{\text{H}^+} - (v_{\text{Ag}} + v_{\text{HCl}} - v_{\text{H}^+} - v_{\text{AgCl}}) = -nF(dE/dp) \quad (4-41)$$

From equation (4-40), we can see that the phase shift of the ac current from pressure modulation to ACCV is partly due to the contribution of the reference electrode.

4.3 Results and discussion

4.3.1 Cyclic voltammetry

A PM-cell with 3 Pt wires of diameter of 0.5 mm and length of 7 mm fused into the glass was employed. Two wires served as working and counter electrodes respectively and the third was tangled with a newly prepared Ag/AgCl wire (0.1 mm in diameter), which was used as reference electrode. The potential for this reference electrode is determined according to Nernst equation. For a Cl⁻ concentration of 1mM,

$$\begin{aligned} E &= E^0 + \frac{RT}{zF} \ln \frac{1}{a_{\text{Cl}^-}} \\ &= 225 + 59.16 \times \lg \frac{1}{0.001} \text{ mV} \\ &= 402 \text{ mV} \end{aligned}$$

The cyclic voltammetric curves (Figure 4-3) were recorded for polycrystalline Pt in sulphuric acid and different cation-containing sulphate solution after degassing by applying vacuum and with applied prepressure. In the solution of 0.6 M H₂SO₄ + 1 mM HCl, the CV showed some different features due to the presence of Cl⁻ as compared with those in pure sulphuric acid: a pair of peaks (-0.22V) corresponding to hydrogen ad/desorption at the (100) facet are negatively shifted in potential; a pair of shoulders (-0.13 V) positive of hydrogen peaks correspond to specific adsorption of Cl⁻; the onset of oxygen adsorption is also shifted by a 200 mV in a positive direction. A low concentration chloride had to be added because of the Ag/AgCl reference electrode, which is the best choice tested so far in the pressure modulation system. The charges for hydrogen ad/desorption were integrated and averaged to be 47.59 μC, from which the surface area is calculated to be 0.227 cm².

The CV for Pt in cation (Li⁺, K⁺ and Cs⁺) containing solution shares similar features to those in sulfuric acid except for some small differences. The onset potential for hydrogen evolution in cation-containing solution is shifted by 110 mV to lower potential as compared to 0.6 M H₂SO₄, which is due to higher pH (2.32) in such a buffer solution. The difference of peak height of hydrogen ad/desorption between the cation-containing and cation-free solution is due to the different conductivity which is highly dependent on the concentration of H⁺.

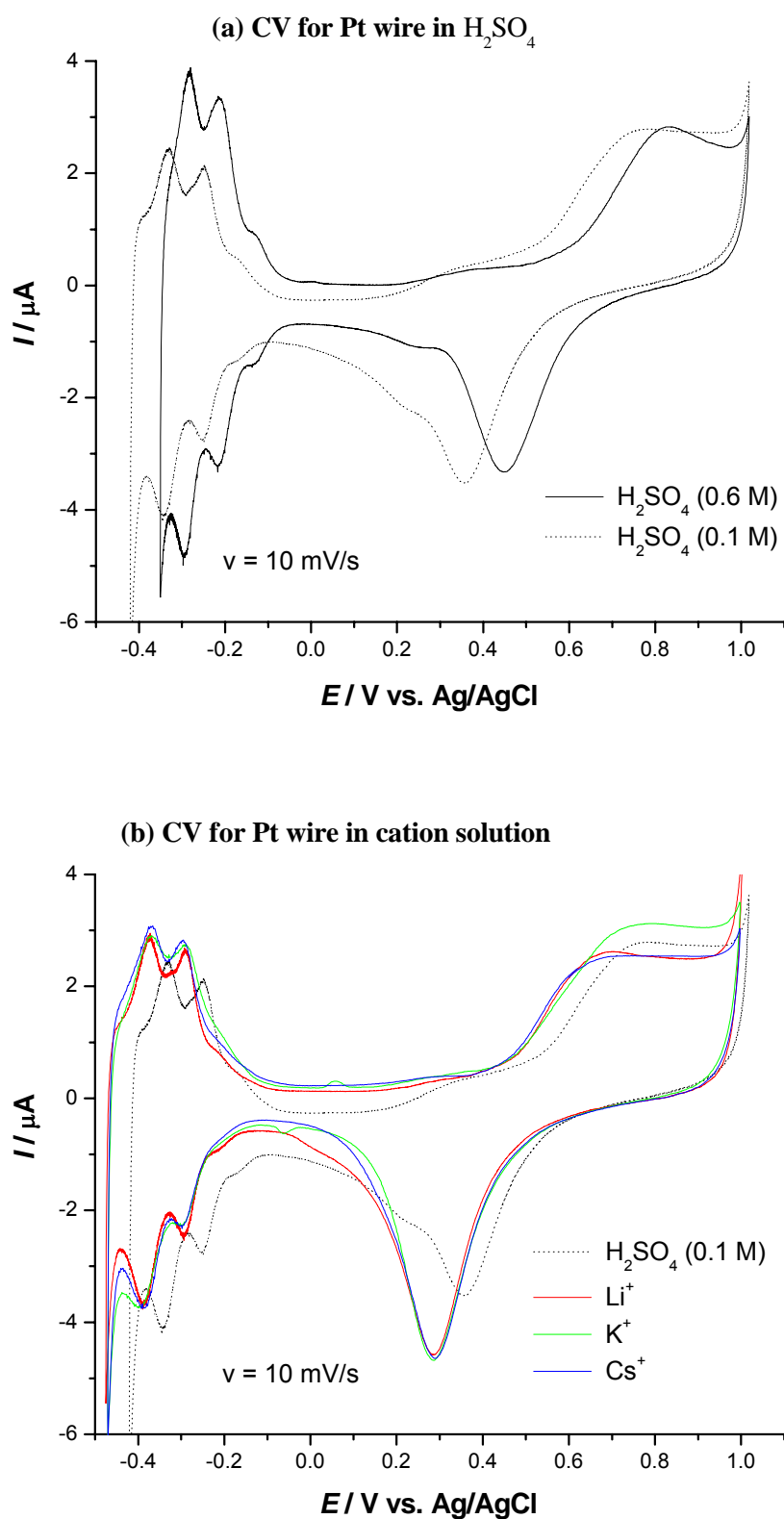


Figure 4-3. CV of polycrystalline Pt: (a) in x M H₂SO₄ + 1 mM HCl with $x = 0.6$ (black) or 0.1 (black dotted) and (b) in 0.1M H₂SO₄ + 0.5 M R₂SO₄ + 1 mM HCl with R = Li (red), K (green), Cs (blue).

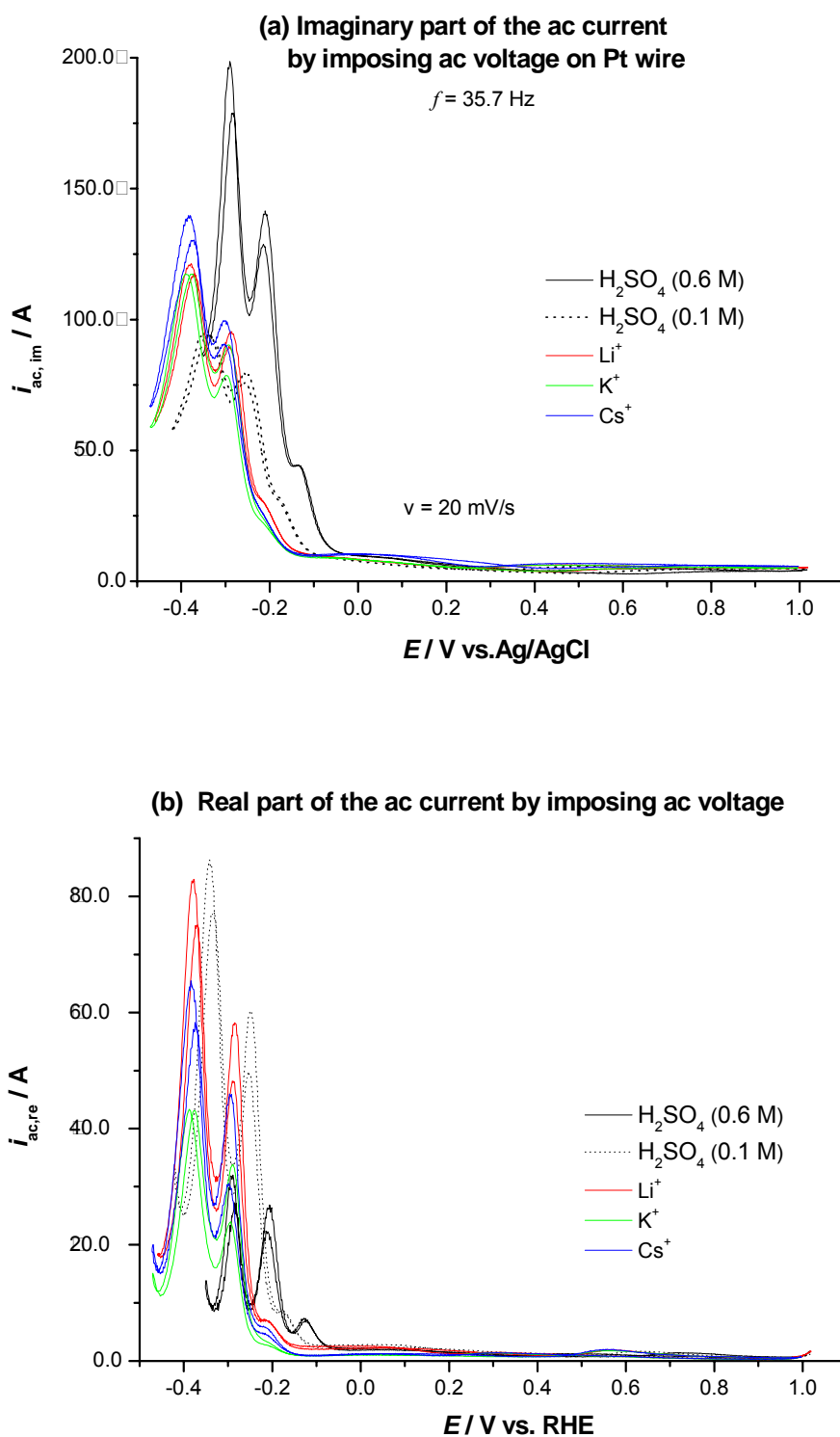


Figure 4-4. The imaginary (a) and real (b) parts of the ac current from superimposing an ac voltage for Pt in $x \text{ M H}_2\text{SO}_4 + 1 \text{ mM HCl}$ with $x = 0.1$ or 0.6 and in $0.1 \text{ M H}_2\text{SO}_4 + 0.5 \text{ M R}_2\text{SO}_4 + 1 \text{ mM HCl}$ with $\text{R} = \text{Li, K, Cs}$. $f = 35.7 \text{ Hz}$, $u_{ac} = 2.3 \text{ mV}$.

4.3.2 The measurement of ac voltammetry

To determine the surface volume excess, the measurement of impedance is important according to equation (4-29). To measure the impedance of the working electrode, an ac voltage of 2.3 mV with a frequency of 35.7 Hz, was superimposed on the cyclic voltammetry. In Figure 4-4a, the imaginary part of the ac current is displayed for the Pt wire in H_2SO_4 (0.6M and 0.1M) and cation containing solution. All peaks in the low potential region correspond to the hydrogen ad/desorption peaks, which show the highest values in 0.6 M H_2SO_4 , followed by cation-containing solution, and the lowest in 0.1 M H_2SO_4 , as the result of electrolyte conductivity. The ac current in the oxygen ad/desorption region is much lower than that in hydrogen ad/desorption region due to lower reversibility to follow the sinusoidal change of the ac voltage. The real part of the ac current is also shown in Figure 4-4b with the similar features as the imaginary part except that the trend for the current height is in a reverse order.

As for comparison, the impedance of the working electrode is also measured and displayed in Figure 4-5. Similar values were obtained for same potential region as in ACCV, which demonstrates that the frequency applied in ACCV is reasonable.

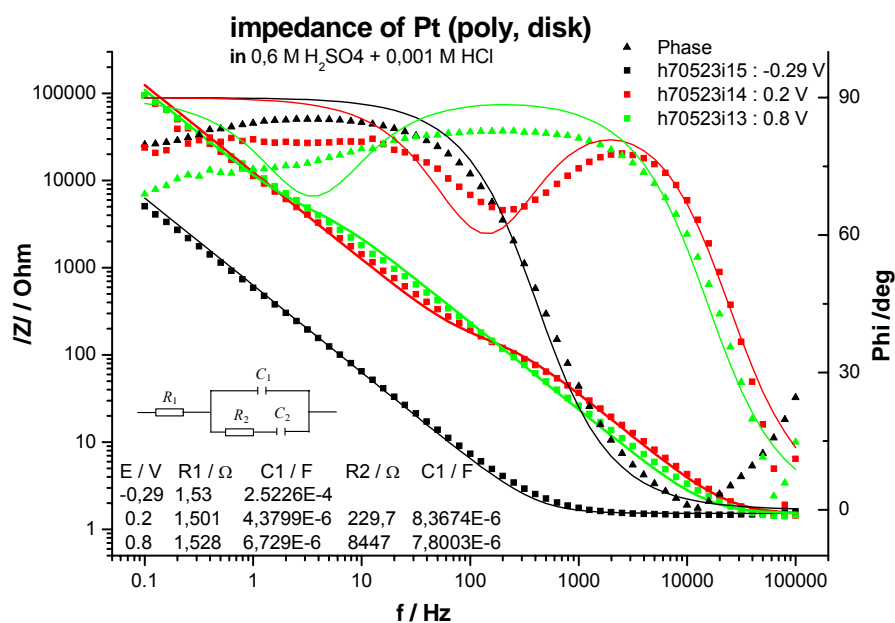


Figure 4-5 Impedance of Pt wire in the PM cell with Ag/AgCl as reference electrode.

4.3.3 The ac current arising from pressure modulation

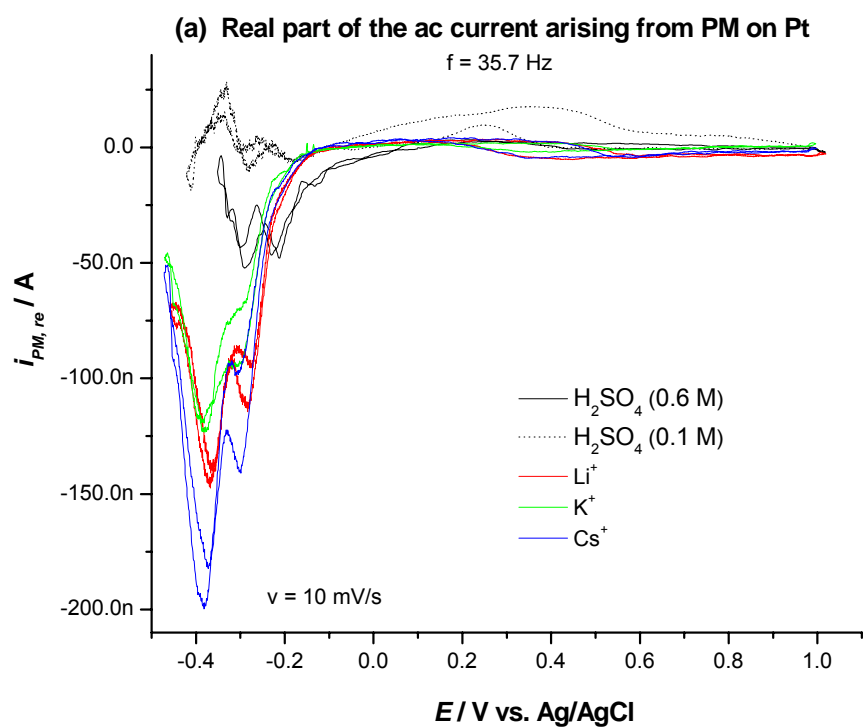
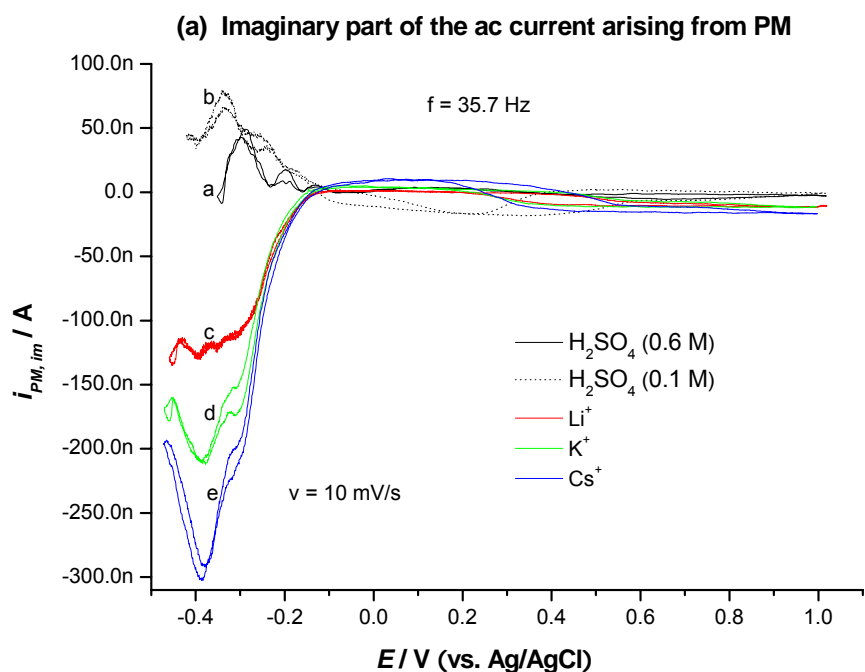
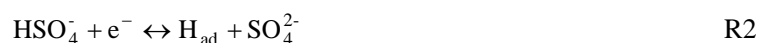


Figure 4-6. The imaginary (a) and real (b) parts of the alternating current caused by pressure modulation in solution $x \text{ M H}_2\text{SO}_4 + 1 \text{ mM HCl}$ ($x=0.6$ and 0.1 for black and black-dotted curve respectively) and $0.5 \text{ M R}_2\text{SO}_4 + 0.1 \text{ M H}_2\text{SO}_4 + 1 \text{ mM HCl}$ with $\text{R} = \text{Li}$ (c, red), K (d, green), Cs (e, blue).

The real and imaginary parts of the ac current induced by pressure modulation with a pressure amplitude of 0.6~0.7 bar at a frequency of 35.7 Hz, the same frequency as ac voltammetry, were recorded as shown in Figure 4-6.

In sulphuric acid only, two pairs of peaks and one pair of shoulders at lower potential are related to the ad/desorption of hydrogen corresponding to those on CV curves. The peak of the imaginary part at lower potential gives values of 45 nA and 71 nA in 0.6 M and 0.1 M sulphuric acid, respectively. In the double layer and oxygen adsorption region, the signal is relatively small since the ad/desorption of oxygen and other species is too slow to follow the tiny potential variation arising from pressure modulation as the ad/desorption of hydrogen do or the change in the surface volume excess may be too small.

In the curves for cation-containing solution, the imaginary part of the ac current is inverted to negative-going direction in hydrogen adsorption region. This signifies a different sign of the adsorption volume. The main reason should be that the adsorbed hydrogen comes from HSO_4^- ($\text{pK}_a = 1.99$) of the buffer solution 0.5 M $\text{R}_2\text{SO}_4 + 0.1\text{M H}_2\text{SO}_4$ instead of H^+ in sulphuric acid, as the following reaction:



Of course it also depends on how fast the ionization reaction for HSO_4^- is compared with the pressure modulation. If the ionization rate is not fast enough, then the adsorbed hydrogen must come from the proton exist in the solution instead of HSO_4^- . In this thesis, all the calculation is based on the assumption that this ionization rate is fast enough. Two pairs of $\text{H}_{\text{ad/de}}$ peaks are still obviously displayed and the pair of small shoulders are submerged in the large hydrogen ad/desorption current. The absolute heights of $\text{H}_{\text{ad/de}}$ peak for imaginary part of the ac current are measured to be 125, 210 and 295 nA at the lowest potential for Li^+ , K^+ and Cs^+ containing solution, rising with the increase of the atomic number of the cation. The dependence of i_{PM} current value on the cation suggested that the metal cation is involved in the adsorption process at hydrogen ad/desorption potential. It should be noted that the volume change is mainly calculated from the imaginary part of the ac current in the measurement of pressure modulation and ACCV.

4.3.4 Molar volume of adsorbed hydrogen on polycrystalline Pt

The half reaction of hydrogen ad/desorption in sulphuric acid can be written as:



In the previous equations, the dependence of the potential of the reference electrode (RE) on pressure has not been taken into account. In the preliminary experiment by Loewe et al [14], a Pt wire was used as a pseudo- reference electrode. Here, due to trace amount of O_2 in the electrolyte the potential is approximately 1 V, i.e., in the onset of oxygen adsorption. In this case, the volume change from the RE can be neglected since the adsorption of oxygen is slow and can't follow the fast pressure modulation. However, according to my own tests, this kind of reference electrode is not stable. Depending on the

conditions, the reference electrode was PtO_x, PtOH, Pt-H and Pt-H₂ or a mixture of two of them with the H and H₂ originating from the H₂ evolved at the counter electrode. The reversibility of the relative reaction to those components is different: the oxidation of platinum or adsorption of oxygen is irreversible; the adsorption of OH is partly reversible; the adsorption of hydrogen is well reversible. Therefore, contradictory results were obtained in the same system with a Pt wire as RE. A good choice for the RE is Ag/AgCl, which is well reversible, and its partial molar volume is easy to obtain. So in the following a newly prepared Ag/AgCl was used as reference electrode, which was tangled on a Pt wire.

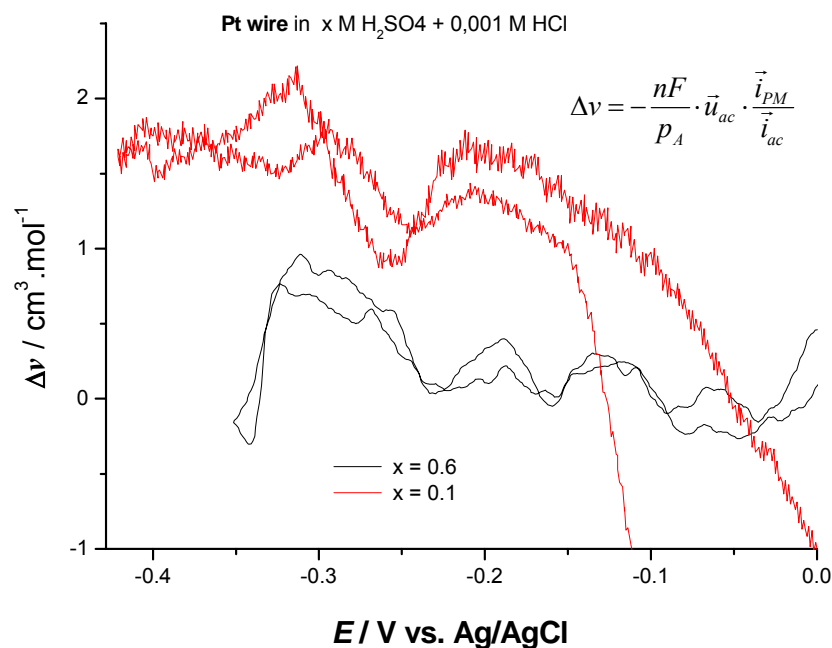


Figure 4-7 Volume change of hydrogen adsorption in 0.6M (black line) and 0.1 M H₂SO₄ (red line) + 1mM HCl.

For the adsorption of hydrogen in sulphuric acid, Figure 4-7 shows the potential dependence of the first term on the right side of equation (4-40). It does not vary much and on average is 0.4 and 1.5 cm³·mol⁻¹. ($d\Gamma_V/dI_i$) for hydrogen adsorption process is thus calculated to be 2.8 and 3.7 cm³·mol⁻¹ in 0.6M and 0.1M H₂SO₄ respectively. The 0.9 cm³·mol⁻¹ difference is partly arises from the calculation of v_{Cl^-} and v_{H^+} . Since it's difficult to obtain a good accuracy for very low concentrations of HCl, the limiting partial molar volume of HCl derived from the density-composition data [26] is 18.5 cm³·mol⁻¹, 0.7 cm³·mol⁻¹ higher than from literature (17.8 cm³·mol⁻¹)[29]. If this and also the experimental error is taken into account, the partial molar volume for adsorbed hydrogen ($d\Gamma_V/dI_{Had}$) is 3.3±1 cm³·mol⁻¹. This value is small but not negligible. It is usually assumed that hydrogen atoms are adsorbed in three-fold hollow sites. There, the contribution to the volume of the interface should be small, if not zero. Part of this volume may also be due to a decreased electrostriction in the double layer.

In a previous work of our group, Loewe et al [14] had found a partial molar volume for adsorbed hydrogen which was close to zero. There, however, it is assumed that in the hydrogen adsorption region a Langmuir isotherm is valid. However, the current approach is more reliable, because it is independent of any particular adsorption isotherm. The fact that the onset of hydrogen adsorption overlaps with anion desorption, as demonstrated by charge displacement experiments by Felio and coworkers [30-32], does not influence the data obtained at more negative potentials due to the differential approach used here.

It is also worth to note about the partial molar volume of electron transferred. If a value of $v_{e^-} = 3 \text{ cm}^3 \cdot \text{mol}^{-1}$ [33] is taken into account for both reference and working electrodes, then the currently measured value of $(d\Gamma_V/d\Gamma_H)$ is slightly positively shifted by $0.3 \text{ cm}^3 \cdot \text{mol}^{-1}$, i.e., $3.6 \text{ cm}^3 \cdot \text{mol}^{-1}$ in average.

4.3.5 The effect of cations on hydrogen adsorption

In the cation-containing solution, the hydrogen atom adsorbed comes from the bisulfate ion of the buffer solution instead of proton, which is as shown in R2. Then the equation (4-40) changes to

$$\left(\frac{d\Gamma_V}{d\Gamma_i} - (v_{\text{HSO}_4^-} - v_{\text{SO}_4^{2-}}) \right) = -\frac{nF}{p_A} \cdot Z \cdot i_{\text{PM}} + (7.3 - 2.6j) \text{ cm}^3 \cdot \text{mol}^{-1} \quad (4-42)$$

$v_{\text{SO}_4^{2-}}$ and $v_{\text{HSO}_4^-}$ could be derived from the density-composition tables⁵ of H_2SO_4 , Na_2SO_4 , NaCl and HCl at the same ionic strength of 1.4 M and v_{H^+} is corrected from the extended Debye-Hückel equation [24] to be $-4.7 \text{ cm}^3 \cdot \text{mol}^{-1}$.

$$v_{\text{HSO}_4^-} = v_{\text{H}_2\text{SO}_4} - v_{\text{H}^+} = 40.7 - (-4.7) = 45.4 \text{ cm}^3 \cdot \text{mol}^{-1}$$

$$\begin{aligned} v_{\text{SO}_4^{2-}} &= v_{\text{Na}_2\text{SO}_4} - 2v_{\text{Na}^+} \\ &= v_{\text{Na}_2\text{SO}_4} - 2(v_{\text{NaCl}} - v_{\text{HCl}} + v_{\text{H}^+}) \\ &= 23.7 - 2 \times (19.8 - 19.3 + (-4.7)) = 32.1 \text{ cm}^3 \cdot \text{mol}^{-1} \end{aligned}$$

Then, $(v_{\text{HSO}_4^-} - v_{\text{SO}_4^{2-}}) = 45.4 - 32.1 \text{ cm}^3 \cdot \text{mol}^{-1} = 13.3 \text{ cm}^3 \cdot \text{mol}^{-1}$

A list of the partial molar volume of other ions are calculated and shown in Table 4-3 at the ionic strength of 1.4 M according to the density data from [26].

Table 4-3 Partial molar volume calculated at Ionic strength of 1.4 ($\text{mol} \cdot \text{kg}^{-1}$) [26].

Electrolyte or ions	H_2SO_4	Na_2SO_4	HCl	NaCl	LiCl	KCl	CsCl	H^+
$v_i / \text{cm}^3 \cdot \text{mol}^{-1}$	40.7	23.7	19.3	19.8	19.6	30.3	42.1	-4.7
Electrolyte or ions	HSO_4^-	SO_4^{2-}	Cl^-	Na^+	Li^+	K^+	Cs^+	
$v_i / \text{cm}^3 \cdot \text{mol}^{-1}$	45.4	32.1	24	-4.2	-4.4	6.3	18.1	

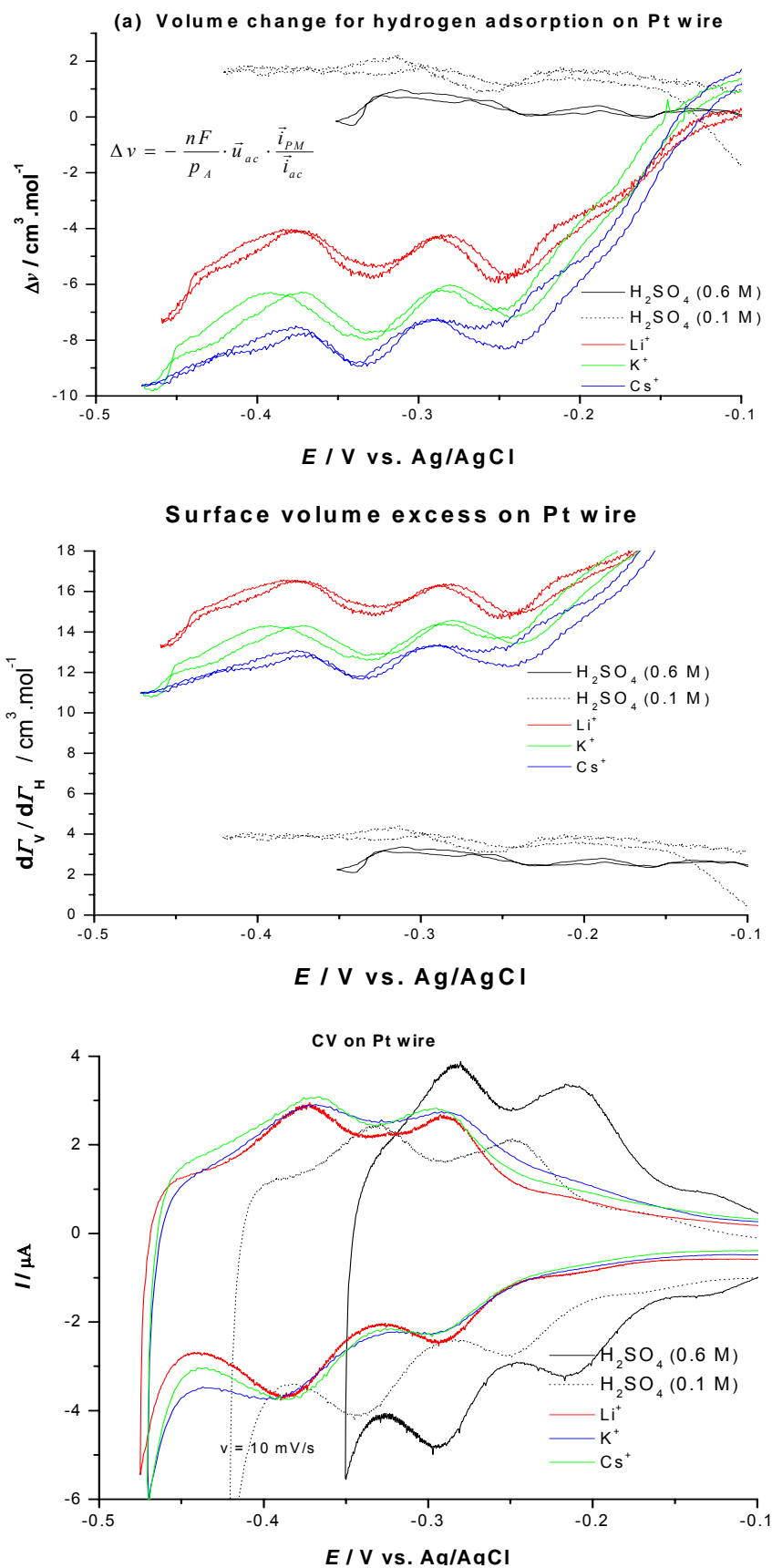


Figure 4-8. Total volume change (a), adsorbate volume (b) and cyclic voltammetry for hydrogen adsorption on polycrystalline Pt in solution 0.1M H_2SO_4 + 0.5 M Me_2SO_4 + 1 mM HCl, Me = H, Li, K, Cs.

The total volume changes in the hydrogen adsorption process, i.e., the real part of the first item in right side of equation (4-42), are plotted in Figure 4-8a with average values about -4.9 , -7.0 and $-8.1 \text{ cm}^3 \cdot \text{mol}^{-1}$ for Li^+ , K^+ and Cs^+ containing solution, respectively. These values are also listed in Table 4-4. Thus, $(d\Gamma_V/d\Gamma_H)$ in hydrogen adsorption region are calculated to be 15.5 (Li^+), 13.6 (K^+) and 12.7 (Cs^+) $\text{cm}^3 \cdot \text{mol}^{-1}$, which are 12.2 (Li^+), 10.3 (K^+) and 9.4 (Cs^+) $\text{cm}^3 \cdot \text{mol}^{-1}$ larger than that in sulphuric acid only. These differences are not neglectable since they exceed the error range of $2 \text{ cm}^3 \cdot \text{mol}^{-1}$. Their potential dependence is shown in Figure 4-8b together with the cyclic voltammetry (Figure 4-8c) in this potential range. And also the differences in Li^+ , K^+ and Cs^+ containing solutions are large enough to be taken into account; they demonstrate a strong effect of cations on the hydrogen adsorption process. The imaginary part in the calculation of the volume change, without correction from RE, is also displayed in Figure 4-9. The values are much smaller than the real part, demonstrating the validity of our measurement.

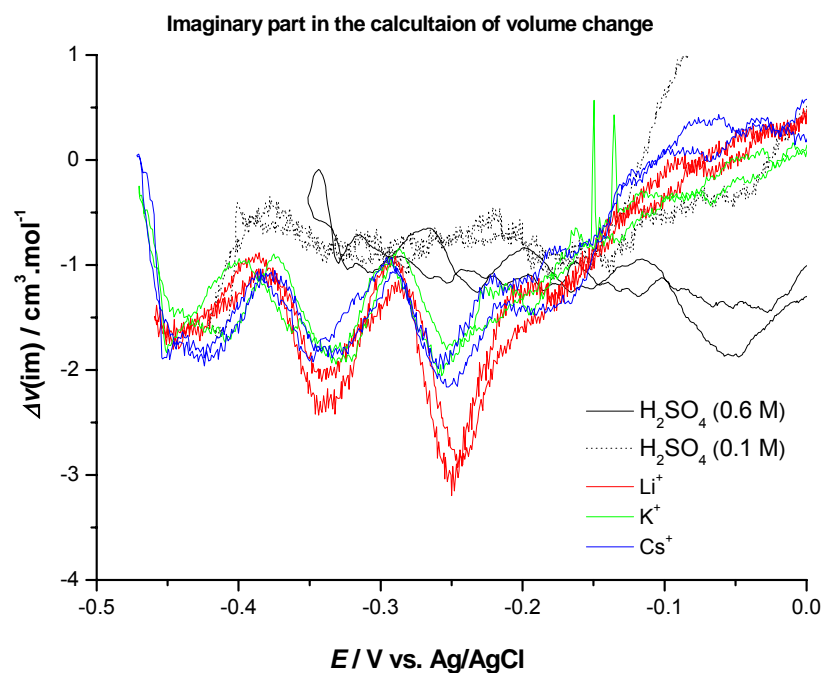


Figure 4-9 The imaginary part calculated for the volume change in H adsorption process.

Special effects of alkali cations were also reported in several papers by Felio et al [30-32], in which the cyclic voltammetry on Pt(111) showed no evident difference in hydrogen ad/desorption features. Nevertheless, remarkable difference is observed at potential higher than that of zero charge (0.32 V), between cation-containing or free solution. Salaita et al also reported the coadsorption of cations (Ca^+ and K^+) in the hydrogen adsorption region in a study of the structure and composition of a Pt (111) surface as a function of pH and electrode potential in aqueous bromide solutions.[34].

Table 4-4. The surface volume excess calculated from cation-free and cation-containing solution in hydrogen adsorption process. (Δv : the total volume change without RE correction. $d\Gamma_V/d\Gamma_H$: surface volume excess per mole hydrogen adsorption with RE correction).

Electrolyte	H ⁺ (0.1M)	H ⁺ (0.6M)	Li ⁺	K ⁺	Cs ⁺
Δv	1.5	0.4	-4.9	-7.0	-8.1
$d\Gamma_V/d\Gamma_H$	3.7	2.8	15.5	13.6	12.7

The notable effect of cations on the adsorption volume or the surface volume excess should be the result of competitive adsorption. These coadsorbed cations either reduce the electrostriction in the double layer or undergo contact adsorption and thus lose part of their solvation shell, as shown in the diagram of Figure 4-10. In literature, it's stated that each water in the solvation shell is shrunk by $2.1 \text{ cm}^3 \cdot \text{mol}^{-1}$ due to electrostriction.[29, 35, 36]. In our case it can be calculated that about 6 (Li⁺), 5 (K⁺), 4-5(Cs⁺) water molecules were freed from the solvation shell during the adsorption of each H. For a more meaningful interpretation, the values of the surface excess of the cations have to be known and the studies using simple crystals will have to be done because of their defined structure and better defined adsorption isotherms.

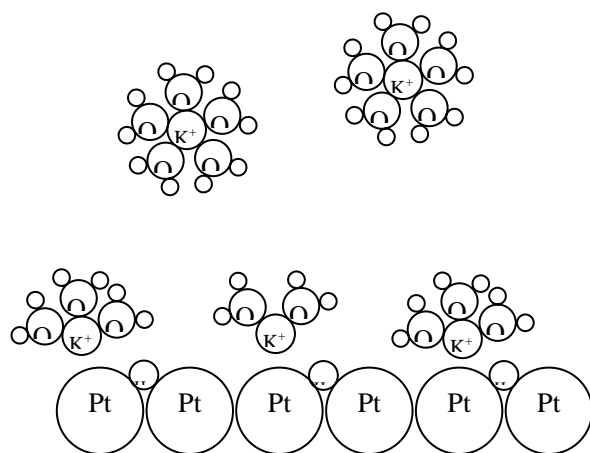


Figure 4-10. Schematic diagram of hydrogen adsorption in the presence of cation.

4.4 Summary

- The reaction volume of $\text{Fe}(\text{CN})_6^{3-} + e^- \leftrightarrow \text{Fe}(\text{CN})_6^{4-}$ is measured to be around $28.7 \text{ cm}^3 \cdot \text{mol}^{-1}$, which is in good agreement with the literature and proved the validity of the pressure modulation setup.
- The volume excess of hydrogen adsorption on polycrystalline Pt was successfully measured to be $3.3 \pm 1 \text{ cm}^3 \cdot \text{mol}^{-1}$ in sulfuric acid combining the method of pressure modulation and ac voltammetry.

- The volume excesses of hydrogen adsorption process in the presence of cations were measured to be 15.5 (Li⁺), 13.6 (K⁺) and 12.7 (Cs⁺) cm³·mol⁻¹, respectively, demonstrating that cations are involved in the hydrogen adsorption process.

1. Lanova, B., H. Wang, and H. Baltruschat, *Methanol Oxidation on Carbon Supported Pt and Ru-Modified Pt Nanoparticles: a Comparison with Single Crystal and Polycrystalline Electrodes*. Fuel Cells, 2006. **6**(3-4): p. 214-222.
2. Müller, U., et al., *Adsorption and hydrogenation of simple alkenes at Pt-group metal electrodes studied by DEMS: influence of the crystal orientation*. Surface Science, 1995. **335**: p. 333-342.
3. Clavilier, J. and D. Armand, *Electrochemical induction of changes in the distribution of hydrogen adsorption states on Pt(100) and Pt(111) surfaces in contact with sulphuric acid solutions*. J ELECTROANAL CHEM, 1986. **199**: p. 187-200.
4. Clavilier, J., et al., *Electrochemical Adsorption Behaviour of Platinum Stepped Surfaces in Sulphuric Acids Solutions*. Journal of Electroanalytical Chemistry, 1986. **205**: p. 267-277.
5. Clavilier, J., et al., *Electrochemical behaviour of the Pt(111)-As system in acidic medium: adsorbed hydrogen and hydrogen reaction*. Journal of Electroanalytical Chemistry, 1990. **294**: p. 193.
6. Furuya, N. and S. Koide, *Hydrogen adsorption on platinum single-crystal surfaces*. Surface Science, 1989. **220**: p. 18-28.
7. Oelgeklaus, R., J. Rose, and H. Baltruschat, *On the rate of hydrogen and iodine adsorption on polycrystalline Pt and Pt(111)*. Journal of Electroanalytical Chemistry, 1994. **376**: p. 127-133.
8. Morin, S., H. Dumont, and B.E. Conway, *Evaluation of the effect of two-dimensional geometry of Pt single-crystal faces on the kinetics of upd of H using impedance spectroscopy*. Journal of Electroanalytical Chemistry, 1996. **412**: p. 39-52.
9. Langkau, T. and H. Baltruschat, *The rate of anion and hydrogen adsorption on Pt(111) and Rh(111)*. Electrochimica Acta, 1998. **44**: p. 909-918.
10. Sibert, E., R. Faure, and R. Durand, *High frequency impedance measurements on Pt(111) in sulphuric and perchloric acids*. Journal of Electroanalytical Chemistry, 2001. **515**(1-2): p. 71-81.
11. Nichols, R.J. and A. Bewick, *SPECTROSCOPIC IDENTIFICATION OF THE ADSORBED INTERMEDIATE IN HYDROGEN EVOLUTION ON PLATINUM*. Journal of Electroanalytical Chemistry, 1988. **243**(2): p. 445-453.
12. Kunimatsu, K., et al., *In situ infrared spectroscopic and electrochemical study of hydrogen electro-oxidation on Pt electrode in sulfuric acid*. Journal of Electroanalytical Chemistry, 2006. **587**(2): p. 299-307.
13. Tadjeddine, A. and A. Peremans, *Vibrational spectroscopy of the electrochemical interface by visible infrared sum frequency generation*. Journal of Electroanalytical Chemistry, 1996. **409**: p. 115-121.
14. Loewe, T. and H. Baltruschat, *Pressure modulation, a new dynamic technique for the electrochemical determination of adsorption, reaction and activation volumes*. Physical Chemistry Chemical Physics, 2005. **7**(2): p. 379-384.
15. Nielinger, M. and H. Baltruschat, *Nanotribology under Electrochemical Conditions: Influence of a Copper (Sub)Monolayer Deposited on Single Crystal Electrodes on Friction Forces Studied with Atomic Force Microscopy*. Physical Chemistry Chemical Physics, 2007. **9**: p. 3965.
16. Hausen, F., et al., *Nanotribology at single crystal electrodes: Influence of ionic adsorbates on friction forces studied with AFM*. Electrochimica Acta, 2008. **53**(21): p. 6058-6063.
17. Sato, M. and T. Yamada, *Effect of high pressure on the rate of electrode reaction of metal complex*. High Pressure Science and Technology, 1980. **2**: p. 812-814.
18. Doine, H., T.W. Whitcombe, and T.W. Swaddle, *Pressure dependence of the electrode potentials of some iron(III/II) and cobalt(III/II) couples in aqueous solution*. Can. J. Chem., 1992. **70**: p. 81-88.
19. John I. Sachinidis, R.D.S., and Peter A. Tregloan, *Measurement of Redox Reaction Volumes for Iron(III/II) Complexes Using High-Pressure Cyclic Staircase Voltammetry. Half-Cell Contributions to Redox Reaction Volumes*. Inorganic Chemistry, 1994. **33**(26): p. 6180-6186.
20. Bajaj, H.C., P.A. Tregloan, and R. van Eldik, *Highly localized charges control electrostriction: Reaction volumes for the reduction of mononuclear and bridged ruthenium complexes*. Inorganic Chemistry, 2004. **43**(4): p. 1429-1435.
21. Hills, G.J. and R. Payne, *Improved method for measuring the double layer capacity at a dropping mercury electrode - APPLICATION TO MEASUREMENTS AT HIGH PRESSURE*. Transactions of the

- Faraday Society, 1965. **61**: p. 316-349.
22. Cruanes, M.T., H.G. Drickamer, and L.R. Faulkner, *Electrochemical measurements at high pressure: solvation and thermodynamics of electron-transfer reactions*. Journal of Physical Chemistry, 1992. **96**: p. 9888-9892.
 23. Sun, J., et al., *Pressure Tuning Voltammetry. Reaction Volumes for Electron Transfer in Cytochrome c and Ruthenium-Modified Cytochromes c*. Journal of the American Chemical Society, 1995. **117**(9): p. 2600-2605.
 24. Borsarelli, C.D. and S.E. Braslavsky, *The partial molar volume of the proton in water determined by laser-induced optoacoustic studies*. Journal of Photochemistry and Photobiology B-Biology, 1998. **43**(3): p. 222-228.
 25. Pitzer, K.S., *Thermodynamics of Electrolytes .1. Theoretical Basis and General Equations*. Journal of Physical Chemistry, 1973. **77**(2): p. 268-277.
 26. Lide, D., *CRC Handbook of Chemistry and Physics*. 80th ed, ed. D. Lide. 1999, Boca Raton: CRC Press.
 27. Zana, R. and E. Yeager, *Ultrasonic Vibration Potentials and Their Use in the Determination of Ionic Partial Molal Volumes*. Journal of Physical Chemistry, 1967. **71**(No. 3): p. 521 - 536.
 28. Leyendekkers, J.V., *Ionic Contributions to Partial Molal Volumes in Aqueous-Solutions*. Journal of the Chemical Society-Faraday Transactions I, 1982. **78**: p. 357-375.
 29. Millero, F.J., *Molal Volumes of Electrolytes*. Chemical Reviews, 1971. **71**(2): p. 147-&.
 30. Feliu, J.M., et al., *Alkali metal cations and pH effects on a splitting of the unusual adsorption states of Pt(111) voltammograms in phosphate buffered solutions*. Journal of Electroanalytical Chemistry, 1993. **345**(1-2): p. 475.
 31. Climent, V., N. Garcia-Araez, and J.M. Feliu, *Influence of alkali cations on the infrared spectra of adsorbed (bi)sulphate on Pt(1 1 1) electrodes*. Electrochemistry Communications, 2006. **8**(10): p. 1577-1582.
 32. Garcia-Araez, N., et al., *Effect of pH and alkaline metal cations on the voltammetry of pt(111) single crystal electrodes in sulfuric acid solution*. ChemPhysChem, 2004. **5**(8): p. 1221-1227.
 33. Heusler, K.E. and L. Gaiser, *Reaktions- und Aktivierungsvolumina der Wasserstoffelektrode*. Berichte der Bunsen-Gesellschaft, 1969. **73**(Nr. 10): p. 1059 - 1068.
 34. Salaita, G.N., et al., *Structure and composition of a platinum(111) surface as a function of pH and electrode potential in aqueous bromide solutions*. Langmuir, 1986. **2**: p. 828-835.
 35. Padova, J., *Solvation Approach to Ion Solvent Interaction*. Journal of Chemical Physics, 1964. **40**(3): p. 691-&.
 36. Padova, J., *Ion-Solvent Interaction .2. Partial Molar Volume and Electrostriction - a Thermodynamic Approach*. Journal of Chemical Physics, 1963. **39**(6): p. 1552-&.

5 . Activation volume for CO oxidation on polycrystalline Platinum

Besides the entropy of activation, the activation volume is one of the fundamental quantities of transition state theory [1] which offers some information on the activated complex. The activation volume has been systematically reviewed in three articles in Chemical Reviews [2-4]. It is of importance in understanding the mechanism for a reaction [5, 6], e.g., in homogeneous electron transfer reactions, negative activation volumes indicate highly charged transition states because of electrostriction. We have recently demonstrated that for reversible adsorption reactions such as hydrogen adsorption, the adsorption volume can be determined with the help of a pressure modulation technique. Here we will demonstrate for the example of CO oxidation, that also activation volumes can be determined in this way.

5.1 Principles

As described in chapter 1, the measurement of the dependence of a rate constant on pressure will result in the activation volume ($\Delta V^\ddagger = -RT(\partial \ln k / \partial p)$). Usually a series of rate constants is measured under various high pressures. In my measurement, instead of using high pressures, a sinusoidally modulated pressure of lower than 1 bar is employed for the investigation of an electrochemical process. For a Faraday process, the current i can be expressed as

$$i = nFkc \quad (5-1)$$

Here n is the number of electron transferred and F is the Faraday constant, c is the concentration factor. For surface reactions following the Eley-Rideal mechanism, the surface coverage θ replaces c or has to be added as a factor (as a second concentration term). For more complicated surface reactions, the coverage dependence of the rate can be expressed as a function of θ , i.e., $f(\theta)$, which replaces θ or c . If c or/and θ is independent of pressure and the reaction is relatively slow compared with the frequency used in pressure modulation, c and θ can be considered as a constant. Then

$$d(\ln i) = d(\ln k) = \frac{-\Delta V^\ddagger}{RT} \cdot dp \quad (5-2)$$

$$\frac{di}{i} = \frac{-\Delta V^\ddagger}{RT} \cdot dp \quad (5-3)$$

Since $p = p_A \cdot \sin(\omega t)$, with $di/dp \approx i_{ac}/p_A$, $d \ln i / dp = i_{ac}/(i_{dc} \cdot p_A)$ and

$$\Delta V^\ddagger = - \frac{i_{ac} \cdot RT}{i_{dc} \cdot p_A} \quad (5-4)$$

Here i_{ac} is the real part of the ac current arising from pressure modulation and measured by lock-in amplifier. This method resembles the ac voltage method applied for the determination of the apparent

transfer coefficient in chapter 3. The same limitations apply: the change of the coverage within one period has to be negligible.

Since the potential of the reference electrode Ag/AgCl is also modulated under the pressure modulation, as described in chapter 4, the influence from reference electrode should be also taken into account. Then we can obtain

$$d(\ln i) = \left(\frac{\partial(\ln i)}{\partial p} \right)_E dp + \left(\frac{\partial(\ln i)}{\partial E} \right)_p d(E_w) \quad (5-5)$$

Here E_w is the potential of the working electrode and E_R the potential of the reference electrode. Since the potential difference $E_w - E_R$ is held constant by the potentiostat, $dE_w = dE_R$. Due to the complexity of Ag/AgCl, here dE_R should be replaced by dE_x , according to the calculation in chapter 4. From equation (5-2)

$$\frac{\partial \ln i}{\partial p} = \frac{-\Delta V^\ddagger}{RT} \quad (5-6)$$

$$\left(\frac{\partial(\ln i)}{\partial E} \right) = \frac{\alpha' nF}{RT} \quad (5-7)$$

Here the apparent transfer coefficient α' is 1.5 at low potentials or low sweep rate for CO oxidation and 0.5 at high potentials, as proved in chapter 3. According to the equation (4-34),

$$\begin{aligned} dE_x &= \frac{\partial E_x}{\partial p} dp \\ &= \frac{1}{1 + j(\cot(70^\circ))} \cdot \frac{\Delta v_{RE}}{-nF} dp \end{aligned} \quad (5-8)$$

The volume change of the reference electrode is

$$\Delta v_R = v_{Ag} + v_{Cl^-} - v_{AgCl} \quad (5-9)$$

Then

$$d(\ln i) = \frac{-\Delta V^\ddagger}{RT} dp - \frac{\alpha'}{RT} \frac{\Delta v_{RE}}{1 + j(\cot(70^\circ))} dp \quad (5-10)$$

$$\begin{aligned} \Delta V^\ddagger &= -\frac{RT d(\ln i)}{dp} - \frac{\alpha' \Delta v_{RE}}{1 + j(\cot(70^\circ))} \\ &= -\frac{i_{ac-re} \cdot RT}{i_{dc} \cdot p_A} - 7.3 \alpha' \text{ cm}^3 \cdot \text{mol}^{-1} \end{aligned} \quad (5-11)$$

Here the imaginary part is neglected.

5.2 Results and discussion

5.2.1 Activation volume for CO oxidation on Pt(poly)

As described in chapter two, a special cell [7] for pressure modulation was employed with 3 electrodes: for both of the working and counter electrodes Pt wire were employed with 0.5 mm in diameter and 7 mm in length, the reference electrode was Ag/AgCl, which was made by entangling Ag wire of 0.1mm on Pt wire and then soaked in 0.1M HCl for 30 minutes. Before the experiment, the solution 0.5 M H₂SO₄ + 0.1 mM HCl inside the cell was degassed by applying vacuum. The removal of most of the air was indicated by the baseline for the CV approaching to zero line. The cleanliness of the electrode surface was checked by recording a CV. Then 2ml 0.5 M H₂SO₄ saturated with CO was injected into the cell. After a few minutes of applying vacuum again, the cell was tightened by the head with the O-ring and a small amount of CO was left in the solution. Then CO was adsorbed on Pt with potential cycling between -0.42V and 0 V until maximum suppression of hydrogen adsorption was achieved. During the oxidation process of CO, a pressure modulation with frequency of 35.7 Hz is imposed. The dc potential and current were recorded with a potentiostat. The ac current arising from pressure modulation was measured simultaneously to the dc current with a lock-in amplifier connected to the current output of the potentiostat. The amplitude of vibrational pressure was measured by a force sensor underneath the cell.

In Figure 5-1a, the voltammetric curve for CO oxidation and the corresponding real part of the ac signal with and without pressure modulation are displayed. In the first positive potential scan, the hydrogen adsorption is suppressed due to the adsorption of CO. The oxidation of CO_{ad} starts at around 0.29 V (versus Ag/AgCl, the same for the following) and the current reaches its maximum at about 0.40 V with a discernible shoulder following. The ac signal under pressure modulation also shows a peak at the same potential with a height of 2.5 nA. Also its shape is similar to that of the dc current, as shown in detail in Figure 5-1b. Only after CO oxidation the ac signal is very noisy. The ac signal in the hydrogen region is caused by the adsorption volume of hydrogen, as described in chapter four. Control measurements without pressure modulation gave no ac signal, as shown in light gray color.

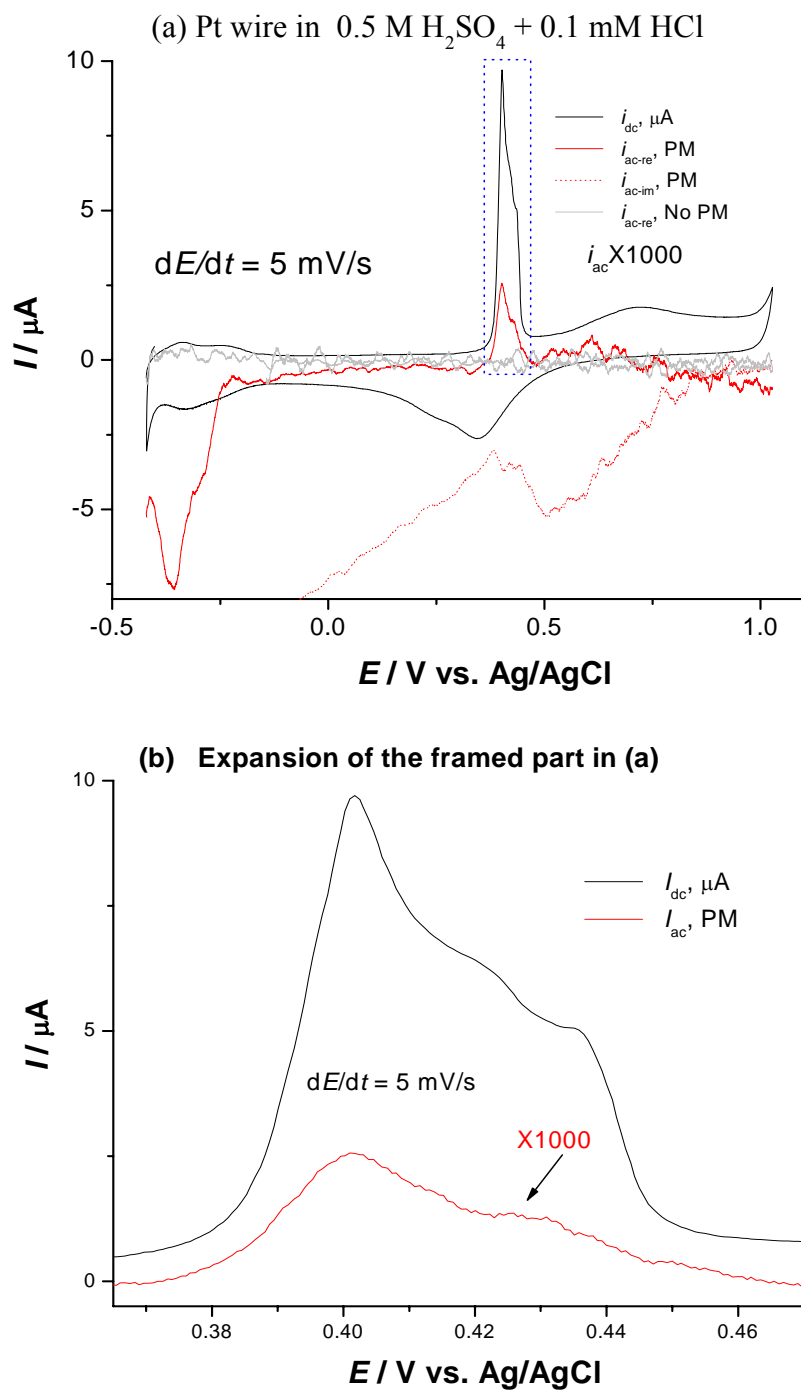


Figure 5-1 Voltammetric curve (black) of CO oxidation, real part (red) and imaginary part (red dotted) of ac current under pressure modulation, real part of ac signal without pressure modulation (light gray) in the CO oxidation process on polycrystalline Pt.

The total volume change in the activation process for CO oxidation thus calculated is shown in Figure 5-2. An average value of about $-6.5 \text{ cm}^3 \cdot \text{mol}^{-1}$ is obtained in the measurement in a potential sweep experiment at $5 \text{ mV} \cdot \text{s}^{-1}$ and at $10 \text{ mV} \cdot \text{s}^{-1}$. Correcting for the volume change in the Ag/AgCl reference electrode due to

pressure modulation, which is calculated to be $-10.9 \text{ cm}^3 \cdot \text{mol}^{-1}$ taking apparent transfer coefficient of 1.5, the activation volume for CO oxidation is calculated to be $-17.4 \text{ cm}^3 \cdot \text{mol}^{-1}$. Here it is worth mentioning that the data are most reliable around the peak because of higher signal.

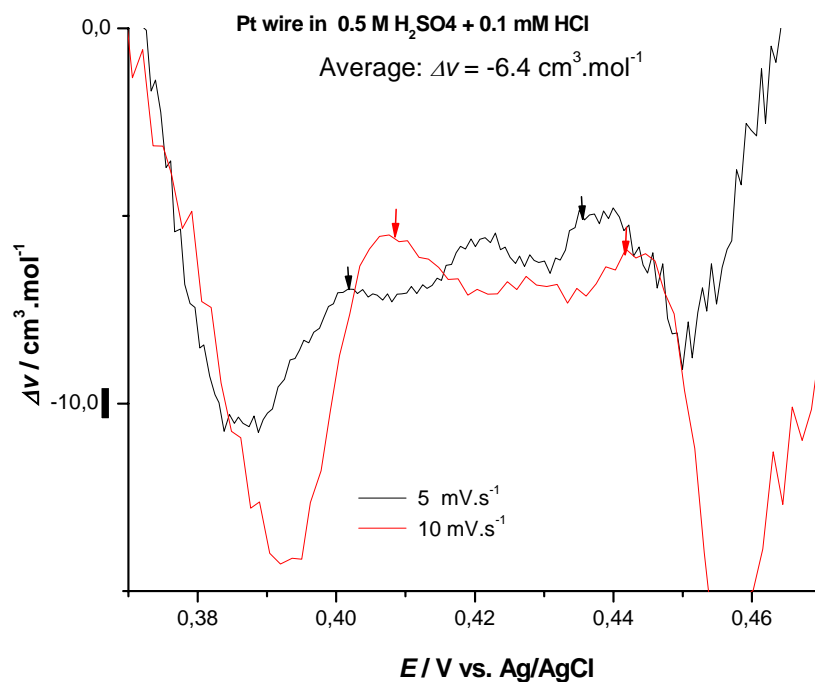
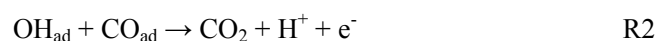


Figure 5-2. Volume change in activation process for CO oxidation on polycrystalline Pt wire in solution 0.5 M H₂SO₄ + 0.1 mM HCl. Black curve, $dE/dt = 5 \text{ mV} \cdot \text{mol}^{-1}$; red curve: $dE/dt = 10 \text{ mV} \cdot \text{mol}^{-1}$.

The activation volume for CO oxidation was also measured in chronoamperometric measurement at constant potentials. The calculated activation volumes are -19.4 , -17.9 and $-18.9 \text{ cm}^3 \cdot \text{mol}^{-1}$ at the current peak for potentials of 0.36 V, 0.38 V and 0.40 V, respectively. All together, the activation volume for CO oxidation on polycrystalline Pt is thus about $-18.2 \text{ cm}^3 \cdot \text{mol}^{-1}$. At such low sweep rates or low potentials, the whole reaction rate is controlled by the 2nd step, the formation of CO₂ from CO_{ad} and OH_{ad}. So the activation volume is also corresponding to the activation process of this step. This negative activation volume points to a highly charged transition state, the volume of which is decreased due to electrostriction.

5.2.2 Explanation for the activation volume

For the mechanism of CO oxidation, it is widely believed that adsorbed hydroxide (or an “activated water” species) is involved in the oxidation process according to the Langmuir Hinshelwood mechanism:



As shown in chapter 3, the apparent transfer coefficient during the oxidation of adsorbed CO was measured using ac voltage method, changing from 1.5 (first reaction in equilibrium) at low potentials to 0.5 at high potentials. This transition occurs, when the sum of the rate constants for the forward reaction (first step: potential dependent OH adsorption, second step: potential dependent oxidation of CO_{ad} with OH_{ad}) exceeds the rate constant for the back-reaction of the first step.

For CO oxidation at low sweep rate and low potentials, the adsorption of hydroxide, R1, thus should be in equilibrium and step R2 should be rate determining step. But even at high potentials the total rate may well be determined by the rate of the 2nd step, as described in chapter three. (At present, since the conditions in the pressure modulation cell are not ideal we cannot exclude an influence of the chloride ions, which are necessary for the reference electrode, on the oxidation potential.) In this case it is reasonable to assume that the transition state is $[\text{H}^+ \cdots \text{O} \cdots \text{CO}]^\ddagger$, according to R3 and the model in Figure 5-3. The negative activation volume found here strongly supports such a positively charged transition state for which the volume is largely reduced with respect to that of reactants.

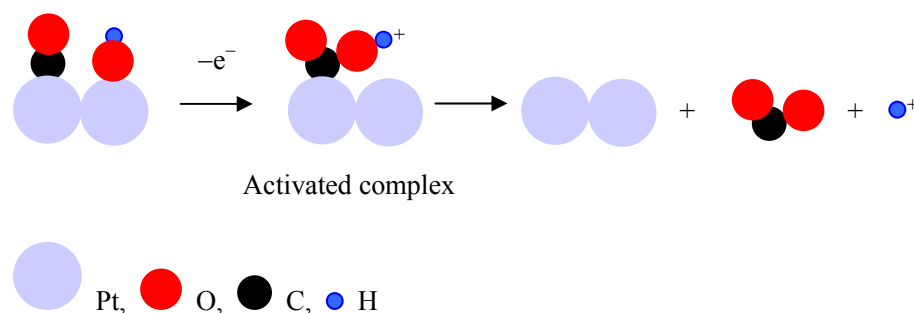
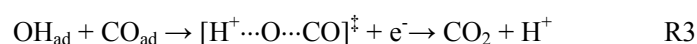


Figure 5-3. Model of the activation process.

To explain experimentally found apparent transfer coefficients of 1, it sometimes has been assumed that a ‘COOH’ species is formed as an intermediate [8-10]. Our above postulated activated complex is not to be confused with such an intermediate, to which of course, it resembles. But as shown in chapter 3 and in the model simulation by Koper et al [11], there is no necessity and no experimental evidence to assume such an more or less stable intermediate.

The above interpretation, however, is preliminary. The determined volume is also influenced by the volume change of the water replacing a CO molecule in the double layer. Furthermore, if the adsorption of the OH species (reaction R1) is fast enough to follow the frequency of the pressure modulation, the corresponding volume change will be contained in the activation volume. This adsorption volume will be largely determined by the partial molar volume of the proton, which is about $-5 \text{ cm}^3 \cdot \text{mol}^{-1}$. Subtracting this value from the experimental activation volume still leads to a negative activation volume of reaction R2 of -15

$\text{cm}^3 \cdot \text{mol}^{-1}$. Further measurements such as determination of the frequency dependence and measurements of the surface volume excess are necessary to better quantify those effects. Moreover, experiments and improvements of our pressure modulation cell are underway which will allow us to perform experiments also using single crystal electrodes.

5.3 Summary

This work can be summarized as the following:

1. It's shown that the activation volume can be measured using the pressure modulation method introduced into our group. Such measurements are particularly helpful in obtaining information on the activated complex.
2. The activation volume for CO oxidation on polycrystalline platinum was measured to be $-18.2 \text{ cm}^3 \cdot \text{mol}^{-1}$ in 0.5 M H_2SO_4 , which demonstrates that the transition state is highly charged and probably corresponds to $[\text{H}^+ \cdots \text{O} \cdots \text{CO}]^\ddagger$.

1. Eyring, H., *The Activated Complex in Chemical Reactions*. J. Chem. Phys., 1935. **3**(2).
2. Asano, T. and J. Lenoble, *Activation and Reaction Volumes in Solution*. Chemical Reviews, 1978. **78**(4): p. 407-489.
3. van Eldik, R., T. Asano, and W.J. Le Noble, *Activation and reaktion volumes in solution*. Chemical Reviews, 1989. **89**: p. 549-688.
4. Drljaca, A., et al., *Activation and Reaction Volumes in Solution*. 3. Chemical Reviews, 1998. **98**: p. 2167 - 2290.
5. Franklin, T.C. and S.A. Mathew, *The Measurement of Volumes of Activation as a Tool for Understanding the Mechanism of Action of Additives in Electrodeposition*. Journal of the Electrochemical Society, 1987. **134**(3): p. 760-761.
6. Whalley, E., *Use of Volumes of Activation for Determining Reaction Mechanisms*. Advances in Physical Organic Chemistry, 1964. **2**: p. 93-162.
7. Loewe, T. and H. Baltruschat, *Pressure modulation, a new dynamic technique for the electrochemical determination of adsorption, reaction and activation volumes*. Physical Chemistry Chemical Physics, 2005. **7**(2): p. 379-384.
8. Santos, E., E.P.M. Leiva, and W. Vielstich, *CO-adsorbate on Pt(111) single crystal surfaces*. Electrochimica Acta, 1991. **36**(3/4): p. 555-561.
9. Lebedeva, N.P., et al., *Mechanism and kinetics of the electrochemical CO adlayer oxidation on Pt(111)*. Journal of Electroanalytical Chemistry, 2002. **524**: p. 242-251.
10. Lebedeva, N.P., et al., *Role of Crystalline Defects in Electrocatalysis: Mechanism and Kinetics of CO Adlayer Oxidation on Stepped Platinum Electrodes*. Journal of Physical Chemistry B, 2002. **106**(50): p. 12938-12947.
11. Koper, M.T.M., et al., *Monte Carlo simulations of a simple model for the electrocatalytic CO oxidation on platinum*. Journal of Chemical Physics, 1998. **109**: p. 6051-6062.

Conclusions

In this thesis I developed an ac method for the determination of the apparent charge transfer coefficient, particularly for surface reactions; the pressure modulation method was combined with ac voltammetry for the measurement of the molar adsorption volume. The pressure modulation method was further used for the first time to measure an activation volume. From these measurements, the following conclusions were obtained:

1. I successfully determined the apparent charge transfer coefficient for CO oxidation on polycrystalline platinum, Pt single crystals (Pt(111), Pt(665) and Pt(332)), Ru and Sn decorated Pt single crystals by potential modulation method; the results can be summarized as the following:

a) The potential modulation method has been shown to be effective in determining α' or the Tafel slope quasi continuously with potential or coverage change in one experiment, which is more reliable than the traditional method in which only a single α' or Tafel slope can be determined through a series experiments over a large range of potentials or currents. This method can easily distinguish any change in α' or Tafel slope with potential change, which is difficult for the traditional method.

b) The α' for the oxidation of adsorbed CO on Pt(poly), Pt(111), Pt(665) and Pt(332) were measured to change from 1.5 to 0.5 with increasing potential in potential step experiment, in accordance with the simulation by Koper et al. Other results obtained with the traditional method yielding a single α' (constant Tafel slope) were thus rejected.

c) The α' for CO oxidation on Ru decorated Pt(665) is obtained to be around 0.5, which agrees well with the widely accepted bifunctional effects in Langmuir-Hinshelwood mechanism. The α' for CO oxidation on Sn decorated Pt(332) is determined to be around 1, in accordance with an Eley-Rideal mechanism and a number of electrons of two in the rds.

2. The molar adsorption volume for hydrogen adsorption was measured and the effect of cations thereupon was further investigated:

a) The molar volume of adsorbed hydrogen was successfully determined combining pressure modulation and ac voltammetry to be $3.3 \pm 1 \text{ cm}^3 \cdot \text{mol}^{-1}$.

b) Alkali metal cations were found to have an influence on the adsorption volume for hydrogen. In cation containing electrolyte, the apparent volumes are increased by 12.2 (Li^+), 10.3 (K^+) and 9.4 (Cs^+) $\text{cm}^3 \cdot \text{mol}^{-1}$, respectively. This measurement will contribute to the fundamental understanding of the structure of adsorbed hydrogen, as well as on the role of cations in the interfacial region.

3. The pressure modulation method was applied to the measurement of the activation volume for CO oxidation on polycrystalline Pt, leading to the following conclusions:

a) Activation volumes can be successfully measured by the pressure modulation method.

b) The activation volume for CO oxidation on polycrystalline Pt was determined to be about $-18 \text{ cm}^3 \cdot \text{mol}^{-1}$, in both measurements with potential sweep at low rates or potential step at low potentials, which demonstrates that the transition state is highly charged and probably corresponds to $[\text{H}^+ \cdots \text{O} \cdots \text{CO}]^\ddagger$.

These investigations largely help in the understanding of the mechanism of CO oxidation and the interfacial structure in the hydrogen adsorption region on Pt.

Acknowledgements

I thank Prof. Dr. Helmut Baltruschat for his academic and financial support as my supervisor during my PhD study, for the chance to work in his research group and learn from others, and for his kind help on my living in Bonn. I am grateful to Prof. Dr. Klaus Wandelt as the second Referee for my thesis.

I thank my present and former colleagues for their help on struggling against the difficulties both in experiment and living. I enjoyed the time working with Fernando, Nicolay, Ali, Micheal, Rainer, Siegfried, Ehab, Nicky, Bara, Tina, Rainhard, Ipek, Ahmet, Ana, Mehdi, Izet, Sabine and Jan. I also enjoyed the sports with Nicolay and Ali. I will always remember those moments we shared together. I specially appreciate all sorts of help and support from Fernando, the help in experiment and German language from Micheal and Rainer, the helpful suggestion from Siegfried, the help from Nicky in the experiments at the beginning of my work.

I should also thank my Chinese friends I've made in Bonn, especially those from Rhine Academic Forum. In those hard days, the communication with them helped me much in understanding the German culture and research system, and in getting through the frustrating time.

I thank my family very much. It's the support of my parents that hold me to go as far as now. The support of my wife and the joy of my lovely son have brought me much energy, which is very important for me to continue the journey. My brother and sister also offered me much help and always keep an eye on my progress.

Publications and Conference presentations

Publications

1. **Hanchun Wang**, Helmut Baltruschat, The determination of activation volume for CO oxidation on Pt by pressure modulation (Accepted on *Chemphyschem*, 2010)
2. **Hanchun Wang**, Helmut Baltruschat, Siegfried Ernst, Determination of apparent symmetry factor and rate determining step for CO oxidation on Pt(poly), Pt(111), Pt(665) and Pt(332), *Phys. Chem. Chem. Phys.*, 2010, **12**, 2190 – 2197
3. **Hanchun Wang**, Helmut Baltruschat, The surface volume excess of hydrogen adsorption on polycrystalline Pt and the effect of cation (to be submitted)
4. **Hanchun Wang**, Helmut Baltruschat, The determination of apparent transfer coefficient for CO oxidation on Ru decorated Pt(665) and Sn decorated Pt(332) (in preparation)

Oral presentations

1. “Potential and pressure Modulation to study the processes of CO Oxidation and H adsorption”, 60th ISE annual meeting, Sep 19, 2009, Beijing (China).
2. “Determination of rate determining step and activation volume for CO oxidation”, meeting of GDCh on Electrochemistry, Oct. 07, 2008, Giessen (Germany).
3. “Determination of rate determining step and activation volume for CO oxidation”, AGEF – Euregio Workshop on Interfacial Electrochemistry, Jun.03, 2008, Kerkrade (Holland).
4. “The surface volume excess of hydrogen adsorption on polycrystalline Pt and the effect of cation measured by pressure modulation”, 14th national conference on electrochemistry (China), Nov. 04, 2007, Yangzhou (China).
5. “Determination of rate determining step and activation volume for CO oxidation”, annual meeting of GCCCD (Association of Chinese Chemists and Chemical Engineers in Germany), Oct.25, 2008, Berlin (Germany).

Posters

1. “Determination of rate determining step and activation volume for CO oxidation”, 59th ISE annual meeting, Sep. 2008, Seville (Spain)
2. “Determination of rate determining step and activation volume for CO oxidation”, BUNSENTAGUNG 2009-Physical Chemistry, May 2009, Cologne (Germany)
3. “Determination of rate determining step and activation volume for CO oxidation on Pt”, 7th ISE spring meeting, Szczyrk (Poland), Mar., 2009.

Curriculum Vitae for Hanchun WANG

Personal Information

Name	Hanchun Wang
Gender	Male
Nationality	PR China
Year of Birth	1979
Place of Birth	Lichuan, Hubei Province, China
Marital Status	Married

Education

2005-2009	PhD student, majoring in Electrochemistry, Institute of Theoretical and Physical Chemistry, University of Bonn
2001-2004	Master degree in Physical Chemistry, Chemistry Department, Xiamen University
1997-2001	Bachelor's degree in Chemical Engineering and Technology, Department of Applied Chemistry, Harbin Institute of Technology

